4-5-2019 10:00 AM

Considering a Seismically Active Leech River Valley Fault Zone in Southwestern British Columbia

Jacob J. Kukovica
The University of Western Ontario

Supervisor
Molnar, Sheri
The University of Western Ontario Co-Supervisor
Ghofrani, Hadi
The University of Western Ontario

Graduate Program in Geophysics
A thesis submitted in partial fulfillment of the requirements for the degree in Master of Science

Abstract

The transpressional reverse Leech River fault (LRF) extends across the southern tip of Vancouver Island and beneath the city of Victoria, British Columbia, Canada. New paleoseismic studies suggest at least three surface-rupturing earthquakes have exceeded a moment magnitude (**M**) of 6 within a proposed Leech River Valley Fault Zone (LRVFZ) within the last 9,000 years. We examine the impact of an active LRVFZ to predicted earthquake ground motions for Victoria. In a probabilistic formulation considering the likelihood of all earthquake sources, LRVFZ earthquakes will contribute the most to high-frequency ground motions (≥ 10 Hz) in Victoria. The Canadian seismic design ground motions for Victoria increase on average by 4 – 23% at 10 Hz depending on the selection for the magnitude-recurrence rate associated with the LRVFZ. In a deterministic formulation considering rupture complexities for a suite of **M** 7 LRVFZ scenario earthquakes, predicted low-frequency (< 0.5 Hz) ground motions in Victoria vary between 1 cm/s (weak shaking) and 19 cm/s (strong shaking) depending on the scenario. The highest ground motions in Victoria are generated by an eastward-rupturing large magnitude LRVFZ earthquake with maximum slip at shallow depth near the city.

Keywords

Earthquake, Seismic Hazard, Probabilistic Seismic Hazard Analysis, PSHA, Deterministic Seismic Hazard Analysis, wave propagation simulation, Leech River fault, Leech River Valley, Victoria, British Columbia

Co-authorship Statement

The thesis is presented in Integrated Article format and consists of the following two papers that have been submitted to, or prepared for, peer-reviewed journals.

Chapter 2: Preliminary findings were published as a 2018 Risk conference paper in Kukovica et al. (2018). This work is superseded here by Kukovica et al. (2019a).

Kukovica, J., Molnar, S., Ghofrani, H., and Assatourians, K. (2018). Impact from a nearby seismically-active fault to seismic hazard in Victoria, Canada. *WIT Transactions on Engineering Sciences*, **121** 173-181, doi: 10.2495/RISK180151.

Kukovica, J., Ghofrani, H., Molnar, S. and Assatourians, K. (2019a). Probabilistic seismic hazard analysis of Victoria, British Columbia: Considering an active fault zone in the nearby Leech River valley. *Bulletin of the Seismological Society of America,* revisions submitted May 9, 2019.

Probabilistic Seismic Hazard Analysis (PSHA) was performed for Victoria by adding the Leech River Valley Fault Zone (LRVFZ) as an active seismic source. I replicated the current uniform hazard curves for Victoria that are reported in the 2015 National Building Code of Canada using EQHAZ software, with the supervision of Dr. Karen Assatourians. I then determined magnitude-recurrence relations for the LRVFZ based on three different sources; Dr. Hadi Ghofrani helped combine paleoseismic data to generate characteristic distribution functions for the LRVFZ. I then generated a MATLAB

code to represent the LRVFZ based on these magnitude-recurrence relations, and fault geometry, in the EqHaz software suite to perform a PSHA of Victoria.

Chapter 3: Kukovica, J., Molnar, S., and Ghofrani, H. (2019b). Earthquake ground motion simulations for Victoria, British Columbia: Considering an active Leech River Valley fault zone. This manuscript is prepared for the *Bulletin of the Seismological Society of America.*

Three-dimensional (3D) finite difference (FD) simulations were performed for southern Vancouver Island using an anelastic wave propagation (AWP) simulation code (AWP-ODC; version 1.1.2) provided by Dr. Sheri Molnar and obtained from Dr. Kim Olsen. The base elastic physical model representative of the local geology beneath Vancouver Island was provided by Dr. Sheri Molnar. I generated my own MATLAB code to superimpose slip models from the 2010 **M** 7 Darfield, New Zealand and 2010 **M** 7 Haiti earthquake ruptures onto the LRVFZ. I then performed 3D FD simulations for 24 different **M** 7 LRVFZ scenarios to generate ShakeMaps for southern Vancouver Island and extracted synthetic low-frequency waveforms at seven different locations with inferred high seismic risk.

The thesis and integrated articles were completed under the supervision of my co-supervisors, Dr. Sheri Molnar and Dr. Hadi Ghofrani. Both supervisors provided exemplary on-going guidance, suggestions, and improvements to the manuscripts.

Acknowledgments

Financial support for this thesis was provided by an NSERC Collaborative Research and Development (CRD) grant with Chaucer Syndicates.

I am truly grateful for the amazing academic guidance, emotional support, and encouragement provided by my supervisor and co-supervisor; Dr. Sheri Molnar and Dr. Hadi Ghofrani. This project could not have been accomplished without their help and professional skills. I'd also like to give a big thanks to Dr. Karen Assatourians for his help co-authoring my first publication.

Thank you to everyone in the *Good Vibrations and Excitations* lab group; the remaining Kristy Tiampo research group; and all my friends and professors in the Earth Sciences department for making these last two years ones to remember. This department has been more than a family to me for my undergraduate and graduate degrees at Western and it will be hard to leave here. Shout out to the "fun-fund", the "Slither Squad", the Relationship Guys, and Vienna for getting me through the long work days.

To my parents, Janice and Peter, thank you for all your love and support through this journey. If I ever needed someone, I knew I could always turn to you to help me through the exciting highs and stressful lows. To my Papa and Grandma, Joe and Lillian Mokanski, I could not have done this without Papa guiding me through (many) calculus problems, or one of grandma's famous chocolate chip cookies! And lastly, to my loving

girlfriend, Rebecca. You were always an anchor for me when the ground got a little shaky and I know I could always turn to you for love and support.

Table of Contents

List of Tables

List of Figures

List of Abbreviations

3D	Three-Dimensional
AWP-ODC	Anelastic Wave Propagation – Olsen, Day, and Cui
BC	British Columbia
CDF	Characteristic Distribution Function
CPU	Central Processing Unit
DSHA	Deterministic Seismic Hazard Analysis
FD	Finite Difference
GMPE	Ground Motion Prediction Equation
GR	Gutenberg – Richter
GPU	Graphics Processing Unit
LRF	Leech River fault
LRVFZ	Leech River Valley Fault Zone
LiDAR	Light Detection and Ranging
NBCC	National Building Code of Canada
NEHRP	National Earthquake Hazards Reduction Program
NEIC	National Earthquake Information Center
NRCAN	Natural Resources Canada
PGA	Peak Ground Acceleration (m/s^2)
PGV	Peak Ground Velocity (m/s)
PSA	Pseudo Spectral Acceleration (m/s^2)
PSHA	Probabilistic Seismic Hazard Analysis
UHS	Uniform Hazard Spectrum

List of Symbols

a	Gutenberg-Richter a value – long term activity rate; the total seismicity rate of the region
A	Area (contextually in m^2)
b	Gutenberg-Richter b value – the decay rate of exponential distribution; describes the relative size distribution of earthquakes
β	Natural logarithmic representation of catalogue slope (b)
D	Fault slip (m)
ε	Randomness
f_ε	Probability density function for randomness
f_M	Probability density function for moment magnitude
f_R	Probability density function for distance
γ	Frequency of exceedance
L	Fault length (km)
m	Given magnitude above the magnitude of completeness
M	Moment magnitude
M_0	Seismic moment (contextually in N · m or dyne · cm)
M_{Char}	Characteristic magnitude
M_{max}	Maximum magnitude
M_{min}	Minimum magnitude
MMI	Modified Mercalli Intensity
μ	Shear modulus (Pa)
N_0	Number of earthquakes (per year) with magnitude ≥ m = 0
P	Probability of predicted ground motion
Q	Quality factor
r	Distance from source

ρ	Density (kg/m^3)
R_{hypo}	Hypocentral distance (km)
R_{cd}	Closest-distance to the top of the rupture plane (km)
R_{JB}	The Joyner-Boore distance (km) defined as the closest distance to the surface projection of the rupture surface
S	Slip rate (mm/yr)
t	Time (s)
t_R	Rise time (s)
ΔT	Duration of catalogue completeness (years)
v	Activity rate (per year)
$v(t)$	Velocity (m/s) at time t
V_P	Compression-wave velocity (m/s)
V_s	Shear-wave velocity (m/s)
V_{s30}	Time-averaged shear wave velocity in the top 30 m (m/s)
Y	Predicted ground motion
y	Ground motion amplitude

1 Introduction

1.1 Seismicity in Victoria

For the residents of Victoria, British Columbia, Canada, the potential for a large-magnitude earthquake is a very real concern. Located on the southern tip of Vancouver Island, Victoria is situated near the northern limit of the Cascadia subduction zone, where the oceanic Juan de Fuca plate is subducting northeast under the crustal North American plate (Figure 1.1). The west coast of Canada is seismically unique because it is one of the few places in the world where all three types of plate movement occur to produce earthquakes; strike-slip, convergent, and divergent plate boundaries (NRCAN, 2017). Subduction of the oceanic Juan de Fuca (at a rate of about 33 to 41 mm yr^{-1}; Gripp and Gordon, 2002) and Explorer plates underneath continental North America has put significant stress on the Cascadia subduction zone. The oblique subduction of the Juan de Fuca plate has created a seismically active fault zone and volcanic arc; creating additional seismic hazard relative to the movement of forearc blocks (Wells et al., 1998). This active tectonic setting has resulted in damaging, large earthquakes, such as the moment magnitude (**M**) 6.8 Nisqually earthquake of February 28th, 2001 (Filiatrault et al., 2001), the **M** 7.8 Haida Gwaii earthquake of October 27th, 2012, or the stronger **M** 8.1 Queen Charlotte Island earthquake of 1949.

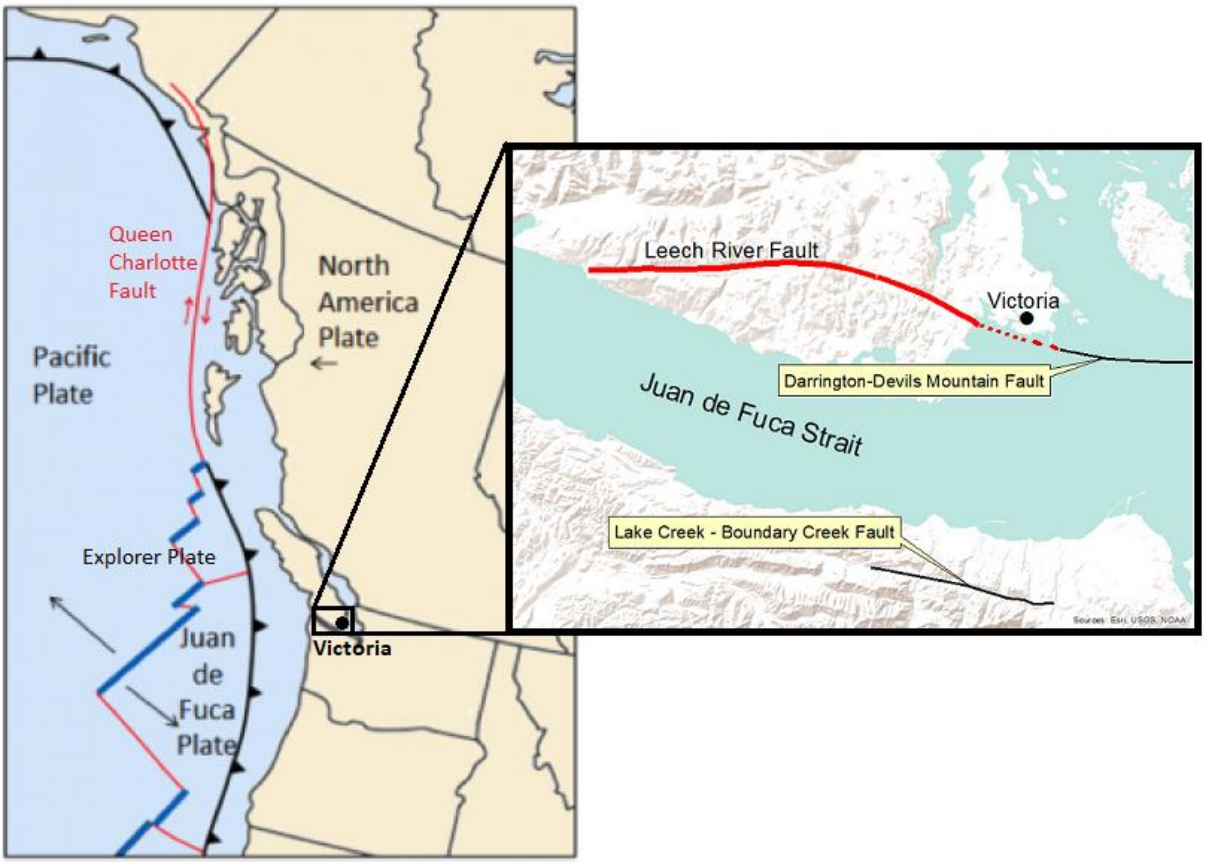

Figure 1.1. Tectonic setting for British Columbia. Arrows show relative plate motions (modified from Earle, 2016). Inset shows the Leech River fault surface expression (solid red line) and extension into the Juan de Fuca Strait (dashed red line) relative to Victoria and nearby active faults according to the 2014 United States Geologic Survey (USGS) (black lines; see Data and Resources).

The Leech River fault (LRF) is a shallow NE dipping terrane bounding fault located on the southern tip of Vancouver Island (Figure 1.1). The fault divides geologic units of Jurassic-Cretaceous schists of the Leech River Complex to the north and Eocene basalts of the Metchosin Formation to the south (Muller, 1977; Fairchild and Cowan, 1982; Rusmore and Cowan, 1985). Underthrusting of the Metchosin formation exhumed the Leech River Complex along the LRF and exposed the Leech River Complex at surface by 35 Ma, when it was then overlain by sediments of the Oligocene Carmanah Group

(Fairchild and Cowan, 1982; Massey, 1986; Clowes et al., 1987; Groome et al., 2003). This event exposed the fault with the sinistral-oblique sense of displacement seen today (Fairchild, 1979; Muller, 1983; Massey, 1986; Groome et al., 2003). The LRF is well imaged on Lithoprobe seismic refraction surveys (e.g. Clowes et al., 1987) and in seismic tomography (e.g. Ramachandran, 2001). Where this fault daylights, a spectacular topographic feature with up to 500 m of relief, the Leech River Valley, cuts across southern Vancouver Island. Recent paleoseismic studies (Morell et al., 2017; 2018) and a microearthquake study (Li et al., 2018) continue to validate that the previously named LRF is not seismically active, but rather suggest there may be a broad deformation zone of high angle transpressional faulting within or near the Leech River Valley that may have been active in Holocene time. In this thesis, we explore the seismic hazard implications of such a fault zone and we refer to it here as the Leech River Valley Fault Zone (LRVFZ). Recent studies of the LRVFZ indicate at least three earthquakes exceeding **M** 6 have occurred within the last ~9 ka (Morell et al., 2017; 2018). In addition, there has been recognition of Quaternary seismic activity just tens of kilometers offshore Victoria in structures of the Juan de Fuca Strait (Barrie and Greene, 2015).

Seismic hazard for a given location is defined as "the potential for dangerous, earthquake related phenomena such as ground shaking, fault rupture, or soil liquefaction" (Reiter, 1990). McGuire (2004) more generally describes seismic hazard as "a property of an earthquake that can cause damage and loss". Seismic hazard analyses

are generalized here to predictions of ground shaking amplitudes. Seismic risk on the other hand is quantitatively expressed as the product of seismic hazard times the vulnerability (Wang, 2011). To understand the difference between seismic hazard and risk, consider a hypothetical example of an active fault. This fault would cut underneath both a heavily built, urban environment with a large population and an open field area with no population or infrastructure. Assuming there are consistent ground conditions throughout both areas and a large-scale earthquake ruptured evenly throughout the entirety of the fault, there would be equal amounts of seismic hazard for both the field and urban regions. However, there would be greater seismic risk associated with the city because of the potential for more human or economic losses.

Previous seismic risk assessments of **M** 6-7 LRF scenarios have been accomplished using HAZUS software (Zaleski, 2014; Ventura and Bebamzadeh, 2016). Zaleski (2014) proposed two deterministic LRF scenarios with a fault dip of 30°: (1) a 13-km length **M** 6 LRF scenario with 0.22 m of average displacement, and (2) a 30-km length **M** 7 LRF scenario with 1 m average displacement. These two LRF earthquake scenarios were developed based on guidance from emergency managers and with consideration to earthquake scenarios with recurrence intervals compatible with planning time horizons. Earthquake ground motions for these two scenarios were calculated using a weighted average of three Ground Motion Prediction Equations (GMPEs) for crustal earthquakes in western North America and captured variable ground conditions using the Victoria

site class map of Monahan et al. (2000). This HAZUS Level 1 risk analysis is limited to direct economic impacts to the residential general building stock, shelter requirements, and debris cleanup for scenarios at 2 am (maximum building occupancy). The two LRF scenarios are predicted to result in $1.8 billion and $5.9 billion Canadian dollars in direct economic losses, respectively. For a Level 2 analysis, structural and non-structural building damage, business inventory loss, relocation cost, business income loss, rental income loss, and wage loss are included. For the **M** 6 and 7 LRF scenarios, Level 2 economic losses increase to $3.5 billion and exceed $11 billion, respectively, in Victoria.

Ventura and Bebamzadeh's (2016) seismic risk analysis used the same **M** 7 LRF scenario of Zaleski (2014). However, ground motions were calculated using western Canada crustal GMPEs developed for the 5th-generation national seismic hazard model (Halchuk et al., 2014) and also included the Victoria site class map of Monahan et al. (2000). This LRF scenario is very damaging with 64% of buildings reaching extensive damage levels. Complete damage (3%) is localized to concrete and masonry buildings of the downtown core. It is expected that water pipelines in Victoria would be reduced to 25% of normal serviceability and sewer pipelines would be lost completely.

The identification of recent seismic activity from the LRVFZ (Morell et al., 2017; 2018) affects seismic activity rates within the southern Vancouver Island region. Currently, the 5th-generation national seismic hazard model, which defines seismic design ground motions in the 2015 NBCC, does not consider the LRVFZ or the LRF as

active faults (Halchuk et al., 2014). Updating seismic design ground motions in the 2020 NBCC to include LRVFZ seismicity is important for future risk and/or resilience assessments. This thesis presents Probabilistic and Deterministic Seismic Hazard Analyses (PSHA) and (DSHA), respectively for Greater Victoria. PSHAs are based on a range of LRVFZ events between **M** ~4 – 7 while DSHAs are based on complex **M** ~7 LRVFZ rupture scenarios that include the ~60 km fault length.

1.2 Seismic Hazard Analyses

Seismic hazard analyses are divided into two main approaches: PSHA and DSHA. PSHA determines the probability of exceeding a particular level of earthquake shaking at a site from all known seismic sources within a given time frame, whereas DSHA predicts earthquake ground motions at a site from a single earthquake occurrence regardless of likelihood.

1.2.1 Probabilistic Seismic Hazard Analyses (PSHA)

PSHA determines the probability of exceedance for a given ground motion amplitude at a site by integrating over all earthquake occurrences, for all associated source zones, and their associated ground motions for a specific temporal period (Cornell, 1968; McGuire, 1995; Wang, 2011). The basis for PSHA requires three main

"inputs" to determine the probability of earthquake shaking within a period of time at a given site (Figure 1.2) (Musson, 1999; 2000).

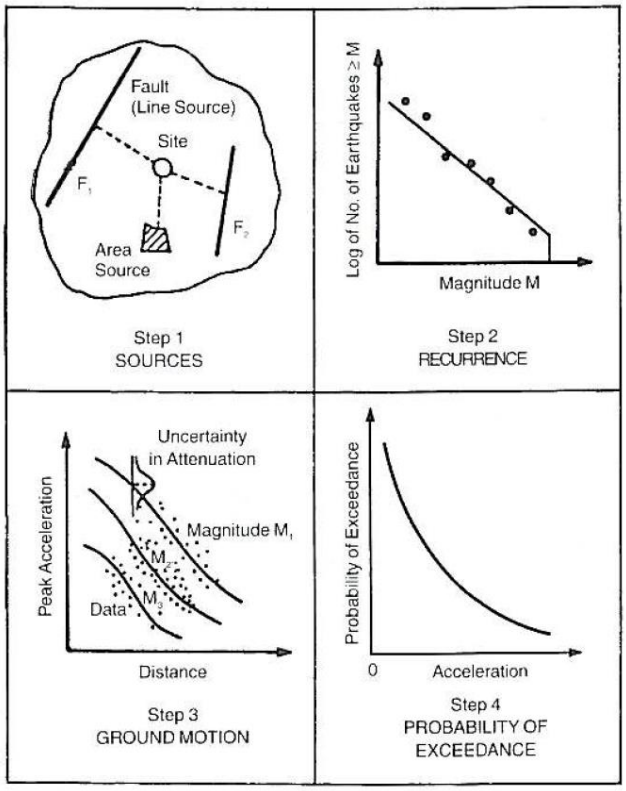

Figure 1.2. The four different steps involved in PSHA. From Tera (1980).

In step 1, to model the occurrence of a region's distributed earthquake activity, seismic sources are spatially based on a region's geologic and tectonic settings into either fault or area source zones. In step 2, the annual rate of occurrence of different earthquake magnitudes is obtained from earthquake statistics associated within each spatial source zone. This is expressed as the Gutenberg-Richter (GR) relationship (Gutenberg and Richer, 1945; 1956) such that

$$\log_{10} N(m) = a - bm, \tag{1.1}$$

where $N(m)$ is the annual rate of earthquakes with a magnitude ≥ m within an assumed duration where the catalogue is complete per magnitude. The values of a and b are constants that relate to the intercept (i.e. activity rate) and slope (i.e. relative number of small magnitude to large magnitude earthquakes) of a source zone, respectively. Seismicity of each source is generally assumed to follow a Poisson distribution (Musson, 2000). Modelling an individual fault or finite volume source zone requires an upper limit for the size of an earthquake governed by the physical properties of the source zone (Youngs and Coppersmith, 1986). This truncates the magnitude distribution below the defined upper bounds of the source zone. To model the GR between a range of minimum and maximum magnitudes, a truncated GR model is used and expanded on in section 2.

In step 3, GMPEs calculate the corresponding ground motions for each scenario of synthetic events determined in step 2 into ground motions with scatter from the predicted median value (epsilon) included. A GMPE is a function that determines the median ground motions at a site based on the magnitude and distance of an earthquake for a specific tectonic setting (Atkinson and Adams, 2013). Typically, a suite of GMPEs are used with various weighting in a logic tree approach to capture epistemic uncertainty in the median ground motion predictions (Atkinson and Adams, 2013). In the 2015 Canadian national seismic hazard maps, a central GMPE was developed with representative upper and lower bounds to express uncertainty about the central GMPE (Atkinson and Adams, 2013). This approach was chosen over a weighted model because

it allows for explicit judgments to be made for magnitude and distance scaling which satisfy important project data constraints, and to provide additional control of central GMPEs with corresponding uncertainty across different regions and event types (Atkinson and Adams, 2013).

In step 4, the frequency of exceedance (γ) is calculated for a given ground motion amplitude (y) at a desired return period through the summation of activity rates for all source zones such that

$$\gamma(Y > y) = \sum_i v_i \iiint f_M(m) f_R(r) f_\varepsilon(\varepsilon) P[Y > y|m, r, \varepsilon] dm\, dr\, d\varepsilon, \quad (1.2)$$

where v_i represents the activity rate v of source i; f_M and f_R represent the probability density functions for moment magnitude and distance, respectively; and the term $P[Y>y|m,r,\sigma]$ represents the probability of the predicted ground motion measure (Y) for a given magnitude (m), distance from source (r), and epsilon (ε) (Cornell, 1968; McGuire, 1995; Halchuk et al., 2014). By applying equation 1.2 for multiple select frequencies, a Uniform Hazard Spectra (UHS) can be generated for a specific return period through plotting ground motion amplitude with frequency. The probability the ground motion measure Y will exceed the value y in t years, assuming that such an event is a Poisson process, is

$$P(Y > y) = 1 - exp\big(-t\gamma(Y > y)\big). \quad (1.3)$$

The PSHA integral in equation 1.2 can be solved in two different approaches: empirically (Milne and Davenport, 1969), where hazard is derived through the relationship between a given ground motion parameter and historical earthquake observations (Wang, 2011); or event-based, where Monte Carlo simulations are performed through random samplings of the probability density functions. The Monte Carlo method involves generating a stochastic earthquake catalog based on source zone seismicity parameters over a certain temporal period and taking the largest event to represent the probability of that magnitude occurring for a given site (Musson, 1999; 2000; Assatourians and Atkinson, 2013).

In summary, PSHA has the great advantage of amalgamating multiple earthquake sources by including the hazard of each event in terms of earthquake size, occurrence frequency, and associated ground motion (McGuire, 1995). PSHA is the basis for seismic design ground motions in building codes. However, large uncertainties can occur in calculations due to insufficient data availability. More data over longer time periods are always a benefit to provide accurate magnitude-recurrence relations, especially when looking at time scales for large magnitudes (Mulargia et al., 2017). This means for certain regions where data is sparse, the occurrence frequency of large magnitude earthquakes is extrapolated from small scale seismicity where data is readily available. This method works for a source zone that follows the GR log-linear trend for magnitude distributions

but may not encapsulate specific characteristic rupture mechanics that could govern the source zone (Mulargia et al., 2017).

1.2.2 Deterministic Seismic Hazard Analyses (DSHA)

DSHA involves calculating ground motions at a site for a given earthquake or set of earthquakes or scenarios, regardless of likelihood (Wang, 2011). Deterministic earthquake scenarios are a special case of the probabilistic approach and can complement PSHA to provide additional insights to the seismic hazard (McGuire, 2004). If peak motions are desired, then a DSHA involves predicting peak (median) motions using empirical GMPEs (only step 3 in Figure 1.2) (Atkinson and Boore, 2006). If earthquake waveforms are desired, then numerical techniques or full wave propagation simulation is performed for the deterministic event(s). In the latter case, complexity of the earthquake source rupture process (source model) is combined with the complexity of the subsurface (physical model) to predict earthquake shaking. A wave propagation simulation is a physics-based solution for the given earthquake source including complexities in the path and site conditions whereas a GMPE predicts the expected ground motion, on average, which statistically captures complexities in source, path, and site effects. The more complex the source, path, and site effects, the more appropriate it is to use physics-based wave propagation simulations compared to GMPEs. However, wave propagation simulations are computationally expensive so have been primarily used to predict motions in sedimentary basin environments from large magnitude

earthquake ruptures (e.g., Olsen 2000; Pitarka et al., 2004; Frankel and Stephenson, 2000; Molnar et al., 2014a; 2014b). In contrast, generating predictions of earthquake shaking for a given earthquake or scenario is accomplished rapidly using GMPEs and is the basis of the United States Geological Survey (USGS) "ShakeMap" product. ShakeMaps display the spatial pattern of predicted motions and are useful products for pre- and post-earthquake planning purposes.

1.2.3 Seismic Hazard Analyses in Canada

Over the last 75 years, five defining seismic hazard models have been produced for Canada, with the latest 5th-generation model produced in 2015 (Allen et al., 2015; Adams et al., 2015). The current 5th-generation seismic hazard model (SHM) includes probabilistic treatment of the Cascadia subduction zone source and other fault sources and estimates mean ground shaking at a 2% probability of exceedance in 50 years hazard level (Allen et al., 2015). This fully probabilistic model is designed for PGA, PGV, and spectral accelerations of 0.2, 0.5, 1.0, 2.0, 5.0, and 10.0 s for a reference site condition (NBCC site class C with a time-averaged shear-wave velocity of the upper 30 meters (V_{S30}) of 450 m/s). Calculations were performed on an extensively modified version of Risk Engineering's (1988) proprietary FRISK88 code (Halchuk et al., 2014). The 6th-generation seismic hazard model will provide the seismic design motions in the 2020 NBCC. This is under current review and will be presented at the upcoming 12th Canadian Conference on Earthquake Engineering in June 2019 (e.g., Halchuk et al., 2019).

1.3 Thesis Aims

The goal of this study is to consider the seismic hazard implications for the city of Victoria due to a seismically active Leech River Valley fault zone. The key questions this research aims to answer are: how much change is expected to predicted ground motions in Victoria due to a seismically active LRVFZ? And what ground motions are expected from large magnitude LRVFZ rupture scenarios? These two questions are answered by performing many PSHAs and DSHAs, respectively, for the Greater Victoria region. An active LRVFZ source zone is incorporated into 8 PSHAs for Victoria considering uncertainty in the fault's seismic activity rate and the appropriate GMPE to predict LRVFZ earthquake motions. The percentage difference in UHS motions for Victoria with respect to the 2015 NBCC motions (5^{th}-generation hazard model) are assessed. A suite of 24 deterministic **M** 7 LRVFZ scenarios are developed from two slip distribution models of empirical **M** ~7 earthquakes elsewhere in the world. Wave propagation simulations of these 24 deterministic **M** 7 LRVFZ rupture scenarios are performed to predict long-period ground motions in southwestern British Columbia. It is hypothesized the addition of the LRVFZ fault source will increase seismic hazard for Greater Victoria because of the proximity to the fault zone. It is also hypothesized that motions will vary greatly based on slip distribution, rupture directionality, and hypocenter location with greatest ground shaking occurring in close proximity to the fault, the hypocenter, or in areas atop low velocity lithologies.

1.4 Organization of Thesis

This thesis consists of two main chapters that address seismic hazard analyses for Greater Victoria, British Columbia considering an active LRVFZ.

1.4.1 Chapter 2 – PSHA Considering an Active LRVFZ

PSHA is performed for the city of Victoria with consideration of the LRVFZ as an active fault source. This study's PSHA methodology first reproduces the 2015 NBCC ground motions for Victoria to quantify adjustments to the national hazard values from inclusion of an active LRVFZ fault source zone. Following a logic tree approach, a set of plausible alternative seismicity parameters (i.e. minimum magnitude (M_{min}), maximum magnitude (M_{max}), *a*- and *b*-values of GR parameters), and GMPEs are considered to explicitly capture the epistemic uncertainty in PSHA motions. Results from 475, 1000, 2475, and 10,000-year return periods are compared to 2015 NBCC motions to determine if seismic hazard alters for Victoria based on a newly identified active LRVFZ source zone. We examine the distribution of hazard contribution between the different applicable source zones and report percentage change in UHS ground motions with respect to the 2015 NBCC.

1.4.2 Chapter 3 – DSHA Considering an Active LRVFZ

Chapter 3 presents DSHAs for a suite of 24 **M** 7 LRVFZ scenarios performed using three-dimensional finite-difference wave propagation simulations. Development of 24

different, potential earthquake scenarios is accomplished by superimposing two **M** 7 empirical slip models onto the LRVFZ: the 2010 **M** 7 Darfield, New Zealand and the 2010 **M** 7 Haiti events. Uncertainties in earthquake rupture parameters including direction of propagation, slip distribution pattern and hypocentre location are captured within the suite of 24 scenarios to assess ground shaking from simulated large LRVFZ earthquakes. We convert PGV to Modified Mercalli Intensity (MMI) to generate "ShakeMaps" from our 24 deterministic scenarios.

1.4.3 Chapter 4 – Conclusions

Discussion of findings and conclusions from the previous two chapters are presented here. The significance of these two papers, in addition to suggestions for future work, is also discussed.

1.5 Data and Resources

Faults for the 2014 USGS active fault zones were obtained from the USGS Interactive Fault map at https://earthquake.usgs.gov/hazards/qfaults/ (accessed on September 2017). ShakeMaps are a product of the USGS Earthquake Hazards Program with information available at https://earthquake.usgs.gov/data/shakemap/ (accessed on December 2018).

1.6 References

Adams, J., S. Halchuk, T. Allen, and G. Rogers (2015). Canada's 5th generation seismic hazard model, as prepared for the 2015 National Building Code of Canada. *11th Canadian Conference on Earthquake Engineering, Victoria, Canada, Paper 93775.*

Allen, T.I, J. Adams, and S. Halchuk (2015). The seismic hazard model for Canada: Past, present and future, *Proceedings of the 10th Pacific Conference on Earthquake Engineering Building and Earthquake-Resilient Pacific, Paper 100.*

Assatourians, K., and G. Atkinson (2013). EqHaz: An open-source probabilistic seismic-hazard code based on the Monte Carlo simulation approach, *Seismol. Res. Lett.* **84** 516-524. doi: 10.1785/0220120102.

Atkinson, G., and J. Adams (2013). Ground motion prediction equations for application to the 2015 Canadian national seismic hazard maps, *Can. J. Civ. Eng.* **40** 988-998.

Atkinson, G.M., and D. M. Boore (2006). Earthquake ground-motion prediction equations for eastern North America, *Bull. Seis. Soc. Am.* **96(6)** 2181-2205.

Barrie, J. V., and H.G. Greene (2015). Active faulting in the northern Juan de Fuca Strait: Implications for Victoria, British Columbia, *Geological Survey of Canada, Current Research 2015-6,* 10 p. doi: 10.4095/296564.

Cornell, C.A. (1968). Engineering seismic risk analysis, *Bull. Seismol. Soc. Am*. **58** 1583-1606.

Clowes, R.M., M.T. Brandon, A.G. Green, C.J. Yorath, A. Sutherland Brown, E.R. Kanasewich, and C. Spencer (1987). LITHOPROBE-southern Vancouver Island: Cenozoic subduction complex imaged by deep seismic reflections, *Can. J. Earth Sci.* **24(3)** 1-51.

Earle, S. (2016). Physical Geology. CreateSpace Independent Publishing Platform.

Fairchild, L.H. (1979). The Leech River unit and Leech River fault, southern Vancouver Island *M.Sc. Thesis,* Seattle, University of Washington.

Fairchild, L.H., and D.S. Cowan (1982). Structure, petrology, and tectonic history of the Leech River complex northwest of Victoria, Vancouver Island, *Can. J. Earth Sci.* **19** 1817-1835.

Filiatrault, A., C.M. Uang, B. Folz, C. Chrstopoulos and K. Gatto (2001). Reconnaissance report of the February 28, 2001 Nisqually (Seattle – Olympia) earthquake, *PEER Center and CUREE Report No. SSRP-2001/02.*

Frankel, A.D., and W.J. Stephenson (2000). Three-dimensional simulations of ground motions in the Seattle region for earthquakes in the Seattle fault zone, *Bull. Seismol. Soc. Am.* **90** 1251–1267.

Gripp, A.E., and R.G. Gordon (2002). Young tracks of hotspots and current plate velocities, *Geophys. J. Int.* **150** 321-361.

Groome, W.G., D.J. Thorkelson, R.M. Friedman, J.K. Mortensen, N.W.D. Massey, D.D. Marshall, and P.W. Layer (2003). Magmatic and tectonic history of the Leech River Complex, Vancouver Island, British Columbia: Evidence for ridge-trench intersection and accretion of the Cresent Terrane, *Geol. S. Am. S.* **371** 327-353.

Gutenberg, B., and C.F. Richter (1945). Seismicity of the Earth, *Bull. Geol. Soc. Am*. **56** 603-668.

Gutenberg, B., and C.F. Richter (1956). Earthquake magnitude, intensity, energy and acceleration, *Bull. Seismol. Soc. Am*. **46** 105 – 145.

Halchuk, S., T. Allen, J. Adams, and G. Rogers (2014). Fifth generation seismic hazard model input files as proposed to produce values for the 2015 National Building Code of Canada. *Geological Survey of Canada, Open File 7576*. doi: 10.4095/293907.

Halchuk, S., T. Allen, J. Adams, and T. Onur (2019). Contribution of the Leech River-Devil's Mountain fault system to seismic hazard in Victoria, BC, *12th Canadian Conference on Earthquake Engineering*, Québec City, Quebec, June 17-20 2019, 9p.

Li, G., Y. Liu, C. Regalla, and K.D. Morell (2018). Seismicity relocation and fault structure near the Leech River fault zone, southern Vancouver Island, *J. Geophys. Res. – Sol. Ea.* **123** 2841-2855. doi: https://doi.org/10.1002/2017JB015021.

Massey, N.W.D. (1986). Metchosin Igneous Complex, southern Vancouver Island: Ophiolite stratigraphy developed in an emergent island setting, *Geology* **14(7)** 602-605. doi: https://doi.org/10.1130/0091-7613(1986)14%3C602:MICSVI%3E2.0.CO;2.

McGuire, R. (1995). Probabilistic seismic hazard analysis and design earthquakes: Closing the loop, *Bull. Seismol. Soc. Am*. **85** 1275-1284.

McGuire, R.K. (2004). Seismic hazard and risk analysis, *Earthquake Engineering Research Institute, MNO-10*, 240 pp.

Milne, W.G., and A.G. Davenport (1969). Distribution of earthquake risk in Canada. *Bull. Seismol. Soc. Am.* **59(2)** 729-754.

Monahan, P.A., V.M. Levson, P. Henderson, and A. Sy (2000). Relative liquefaction and amplification of ground motion hazard maps of Greater Victoria, *British Columbia Ministry of Energy and Mines.*

Molnar, S. (2011). Predicting earthquake ground shaking due to 1D soil layering and 3D basin structure in SW British Columbia, Canada. *PhD Thesis*, University of Victoria, Victoria, British Columbia, Canada.

Molnar, S., J.F. Cassidy, K.B. Olsen, S.E. Dosso, and J. He (2014a). Earthquake ground motion and 3D Georgia Basin amplification in southwest British Columbia: Deep Juan de Fuca plate scenario earthquakes, *Bull. Seis. Soc. Am.* **104** 301-320. doi: 10.1785/0120110277.

Molnar, S., J.F. Cassidy, K.B. Olsen, S.E. Dosso, and J. He (2014b). Earthquake ground motion and 3D Georgia Basin amplification in southwest British Columbia: Shallow blind-thrust scenario earthquakes, *Bull. Seis. Soc. Am.* **104** 321-335. doi: 10.1785/0120130116.

Morell, K.D., C. Regalla, L.J. Leonard, C. Amos, and V. Levson (2017). Quaternary rupture of a crustal fault beneath Victoria, British Columbia, Canada, *GSA Today* **27**. doi: 10.1130/GSATG291A.1.

Morell, K., C. Regalla, C. Amos, S. Bennett, L. Leonard, A. Graham, T. Reedy, V. Levson, and A. Telka (2018). Holocene surface rupture history of an active forearc fault redefines seismic hazard in southwestern British Columbia, Canada, *Geophys. Res. Lett.* **45** 11,605–11,611. doi: 10.1029/2018gl078711.

Mulargia, F., P.B. Stark, and R.J. Geller (2017) Why is probabilistic seismic hazard analysis (PSHA) still used? *Phys. Earth Planet. In.* **264** 63-75.

Muller, J.E. (1977). Evolution of the Pacific Margin, Vancouver Island, and adjacent regions. *Can. J. Earth Sci.* **14** 2026-2085.

Muller, J.E. (1983). Geology, Victoria map area, *Geological Survey of Canada Map 1553A*, scale 1:100,000.

Musson, R.M.W. (1999). Determination of design earthquakes in seismic hazard analysis through Monte Carlo simulation, *J. Earthquake Eng*. **3** 463-474.

Musson, R.M.W. (2000). The use of Monte Carlo simulations for seismic hazard assessment in the U.K., *Ann. Geofis*. **43** 1-9.

NRCAN (2017, November 3) *Seismic zones in Western Canada.* Retrieved from: http://www.earthquakescanada.nrcan.gc.ca/zones/westcan-en.php#offshore_W.

Olsen, K.B. (2000). Site amplification in the Los Angeles basin from three dimensional modeling of ground motion, *Bull. Seismol. Soc. Am.* **90** S77–S94.

Pitarka, A., R. Graves, and P. Somerville (2004). Validation of a 3D velocity model of the Puget Sound region based on modeling ground motion from the 28 February 2001 Nisqually earthquake, *Bull. Seismol. Soc. Am.* **94** 1670–1689.

Ramachandran, K. (2001). Velocity structure of S.W. British Columbia and N.W. Washington from 3-D non-linear seismic tomography, *Ph.D. thesis*, Victoria, University of Victoria, B. C., Canada.

Reiter, L. (1999) Earthquake Hazard Analysis (*Columbia University Press, New York*), p 254.

Risk Engineering, Inc. (1988). FRISK88 User's Manual, Version 1.2. For details contact http://www.riskeng.com/

Rusmore, M.E., and D.S. Cowan (1985). Jurassic-Cretaceous rock units along the southern edge of the Wrangellia terrane on Vancouver Island. *Can. J. Earth Sci.* **22** 1223-1232.

TERA Corporation. (1980) Seismic hazard analysis: A methodology for the Eastern United States. *US Nuclear Regulatory Commission Report No. NUREG/CR-1582.*

Ventura, C.E., and A. Bebamzadeh (2016). Executive summary: Citywide seismic vulnerability assessment of the city of Victoria. *VC Structural Dynamics LTD*. p. 43.

Wang, Z. (2011). Seismic hazard assessment: Issues and alternatives, *Pure Appl. Geophys*. **168** 11-25. doi: 10.1007/s00024-010-0148-3.

Wells, R.E., C.S. Weaver, and R.J. Blakely (1998). Fore-arc migration in Cascadia and its neotectonics significance. *Geology* **26(8)** 759-762.

Youngs, R.R., and K.J. Coppersmith (1986). Capturing uncertainty in probabilistic seismic hazard assessments within intraplate tectonic environments, *Proceedings of the Third US national conference on earthquake engineering*, **1** 301-312.

Zaleski, M.P. (2014). Earthquake loss estimates Greater Victoria, British Columbia. *M.Sc. Thesis,* Vancouver, The University of British Columbia, B. C., Canada.

2 Probabilistic Seismic Hazard Analysis of Victoria, British Columbia: Considering an Active Fault Zone in the Nearby Leech River Valley

2.1 Introduction

The LRF (Figure 2.1) is present southeast of Port Renfrew on the west coast of Vancouver Island and extends east to the provincial capital city of Victoria where it continues offshore in the Juan de Fuca Strait and potentially connects with the Darrington-Devils Mountain fault (Johnson et al., 2001). The LRF is a shallow north dipping terrain bounding fault that is well imaged on Lithoprobe seismic refraction surveys (e.g. Clowes et al., 1987) and in seismic tomography (e.g. Ramachandran, 2001). Recent paleoseismic studies (Morell et al., 2017; 2018) and a microearthquake study (Li et al., 2018) continue to validate that the previously named LRF is not seismically active but suggest there may be a broad deformation zone of high angle transpressional faulting within or near the Leech River Valley that may have been active in Holocene time. We explore the seismic hazard implications of such a fault zone and we refer to it here as the Leech River Valley Fault Zone (LRVFZ).

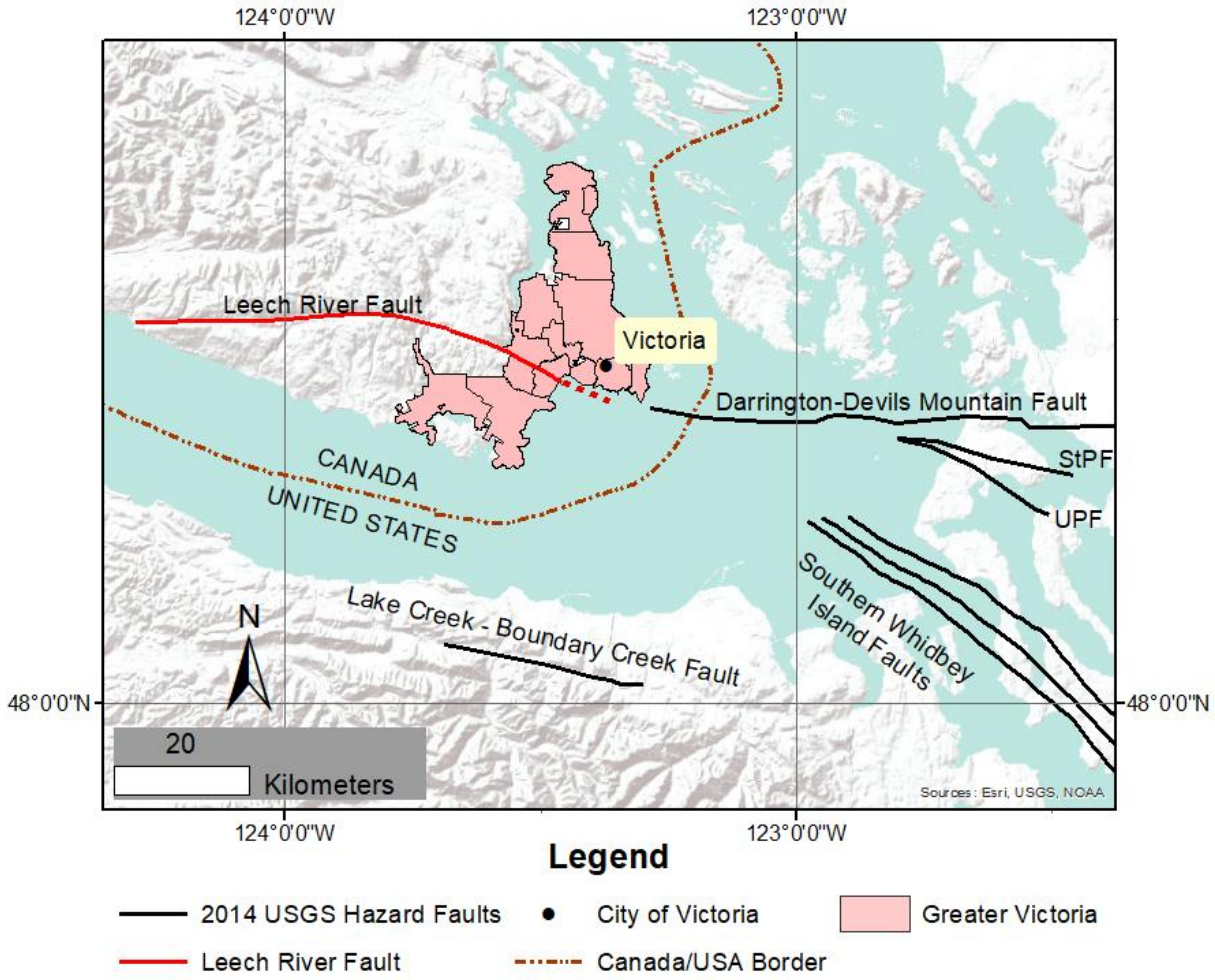

Figure 2.1. Terrain map of the southern tip of Vancouver Island. The LRF surface (solid red line) and its offshore projection (dashed red line) are shown in relation to Greater Victoria. The black lines show fault source zones from the 2014 USGS seismic hazard model. StPF is the Strawberry Point Fault and UPF is the Utsalady Point fault.

Suggestions of Holocene activity within several strands of the LRVFZ has been recently identified (Morell et al., 2017; 2018). The evidence comes from a combination of paleoseismic trenching, Light Detection and Ranging (LiDAR)-based lineament mapping, and geomorphology. Morell et al. (2017) mapped more than 60 steeply dipping, semi-continuous linear scarps, sags, and swales that cut across both bedrock and Quaternary deposits along the LRVFZ. Reconstruction of colluvial fault slip surfaces in

two trenches across a short 200-m lineament detected by LiDAR suggest a total of ~6 m of vertical displacement. They propose two large moment magnitude (**M**) > 6 earthquakes caused this displacement since the last deglaciation event 15,000 years ago. Morell et al. (2018) updated this assessment to three **M** > 6 LRVFZ earthquakes in the last ~9,000 years. Other paleoseismic studies of nearby crustal faults in the region have identified Quaternary fault activity, including the Darrington-Devils Mountain fault zone (Johnson et al., 2001; Barrie and Greene, 2015) and Whidbey Island fault (Sherrod et al., 2008). It is becoming increasingly important to examine how to incorporate these newly identified active faults in southwestern British Columbia, with very little recorded seismicity attributed to the faults themselves, into future seismic hazard assessments.

Vancouver Island is a critically studied part of Canada in terms of earthquake hazard because of its close proximity to the Cascadia subduction zone, where the oceanic Juan de Fuca plate is actively subducting beneath the continental North America plate. The city of Victoria is therefore exposed to the highest seismic hazard for a major city in Canada. For example, the peak horizontal ground acceleration (PGA) in Victoria calculated in the 5th- generation Canadian seismic hazard model, developed for seismic design provisions of the 2015 National Building Code of Canada (NBCC), is 0.58 g at a 2% probability of exceedance in 50 years (Figure 2.2) (Halchuk et al., 2014). This value is eight times greater than the interior of the country.

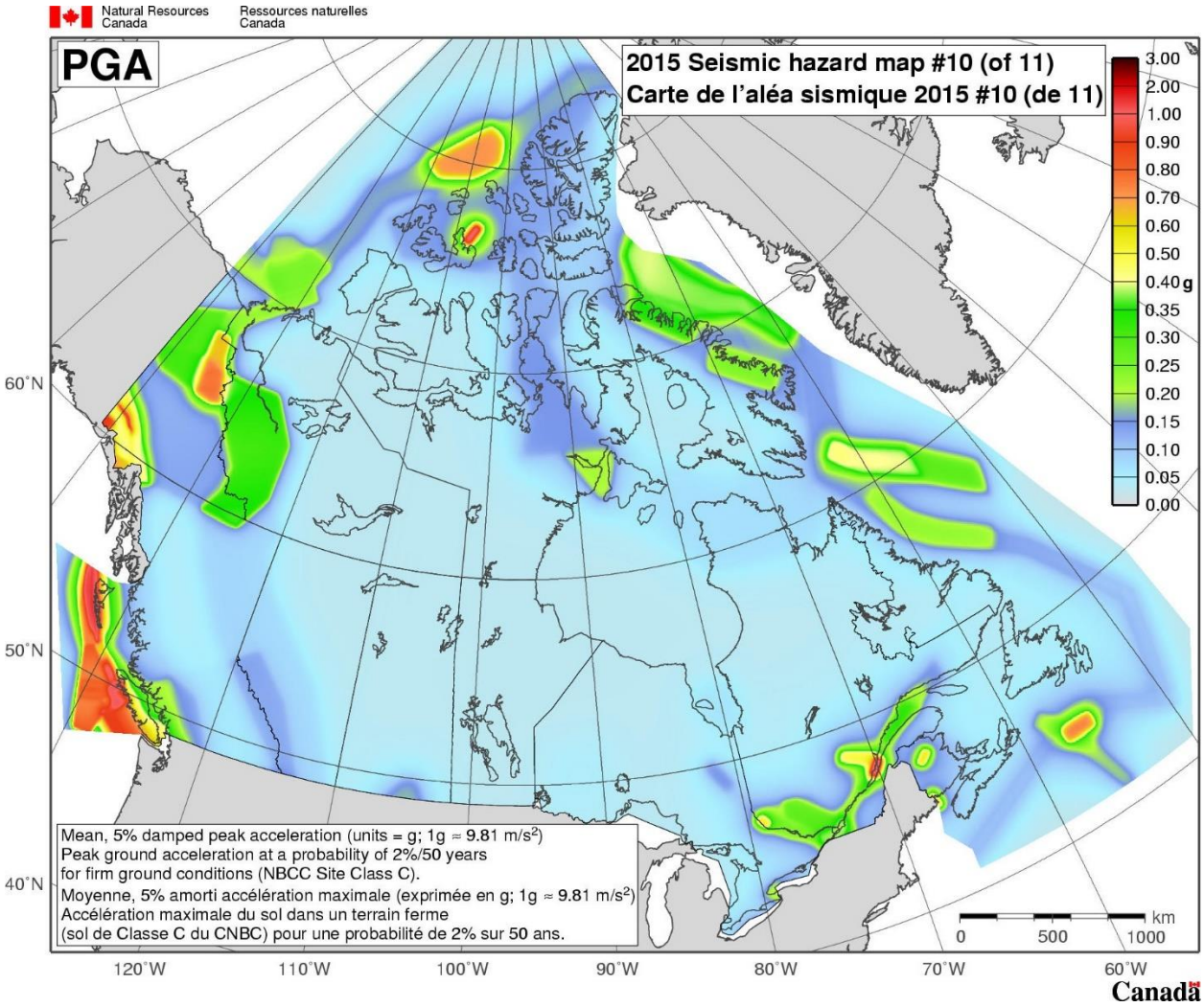

Figure 2.2. 2015 seismic hazard map of Canada for PGA. From NRCAN (see Data and Resources).

The recent evidence that the LRVFZ might be seismically active, having possibly produced up to three **M** > 6 earthquakes in the last 9,000 years (Morell et al., 2017; 2018), adds further to the consideration of seismic hazard in this region. Previously, no recorded seismicity has been attributed to this proposed fault zone (Mulder, 1995; Balfour et al., 2012); however, recent microearthquake relocation analyses (Li et al., 2018) demonstrate linearized seismicity patterns attributed to LRVFZ seismicity. This study performs Probabilistic Seismic Hazard Analyses (PSHA) which include the LRVFZ as an active

seismic fault zone to examine the contribution of this proposed fault source to the seismic hazard of Victoria.

PSHA determines the probability of exceedance for a given ground motion amplitude at a site by integrating over all earthquake occurrences for all source zones and their associated ground motions for a specific temporal period (Cornell, 1968; McGuire, 1995). For a specific site, the related frequency of exceedance (γ) is calculated for a given ground motion amplitude (y) at a desired return period and is achieved through the summation of all activity rates for all source zones in the analysis using equation 1.2. Current available PSHA software includes OpenSHA (Field et al., 2003), OpenQuake (GEM, 2017), EqHaz (Assatourians and Atkinson, 2013), CU-PSHA (Pailoplee and Palasri, 2014), and CRISIS2008 (Ordaz et al., 2013), among others. This study uses the EqHaz software, which uses Monte Carlo simulation (Musson, 1999, 2000) to solve the Cornell-McGuire PSHA methodology presented in section 1.2.1.

We first confirm our PSHA implementation by replicating the 2015 NBCC ground motions at different return periods for Victoria before introducing the LRVFZ as a seismic source. We use the fault zone geometry proposed by Li et al. (2018) and keep it fixed in our PSHA calculations. We note that the fault's possible eastward extent and connection with other nearby splay faults (Morell et al., 2017; 2018), as well as potential seismic activity northward beneath Victoria (Li et al., 2018) have been proposed but are not considered further here. The largest unknowns in our PSHA calculations are therefore

the magnitude-recurrence rate of the LRVFZ and the applicable Ground Motion Prediction Equation (GMPE) for LRVFZ earthquakes. We perform a suite of eight PSHAs considering a range in magnitude-recurrence distributions developed from three different sources of recorded seismicity. The potential Holocene **M >** 6 events (Morell et al., 2017) are used to develop a characteristic magnitude-frequency distribution function for magnitudes greater than **M** > 6. The observed variability in our PSHA calculations captures uncertainty in the LRVFZ's activity rate of the fault zone model and in the applicable GMPEs to calculate fault event ground motions.

2.2 PSHA methodology and validation with 2015 NBCC ground motions

The general workflow of the EqHaz software (Assatourians and Atkinson, 2013) is briefly described here. A synthetic earthquake catalogue is generated via Monte Carlo simulation based on regional seismicity parameters for specific source zones and their geometries. The synthetic earthquake catalogue is calculated by applying magnitude-frequency parameters of an areal source zone or a fault source. The program then creates a grid of points within the source and randomly generates an earthquake event of equal weighting at each grid point. Applicable regional GMPEs are then used to compute a synthetic ground motion catalogue for the site of interest using all events in the synthetic earthquake catalogue. The GMPEs are used with a range of epsilon values to address the

randomness in ground-motion estimations. To obtain a mean hazard curve, EqHaz counts the number of exceedances of specified ground-motion levels in the generated ground-motion catalogue and divides these numbers by the equivalent total duration of the catalogue to find the rate of exceedance of each ground-motion amplitude level (Milne and Davenport, 1969). This refers to steps 3 and 4 of Figure 1.2 and is accomplished via EqHaz2. Rates of exceedance are used to calculate probabilities assuming a Poisson process (Assatourians and Atkinson, 2013). The PSHA can be deaggreated using EqHaz3 (McGuire, 1995; Bazzurro and Cornell, 1999; Harmsen and Frankel, 1999) through binning the strongest ground motion subset of the synthetic ground motion catalogue at different magnitude and distance intervals.

The source zones of the fifth-generation Canadian seismic hazard model (Halchuk et al., 2014) within 500-km of Victoria consist of 11 crustal, two inslab (30-km and 50-km depth) and one interface zones (Figure 2.3). For all source zones, the fifth-generation seismic hazard model parameters are maintained including source zone geometry, magnitude-recurrence parameters and associated GMPEs and uncertainties.

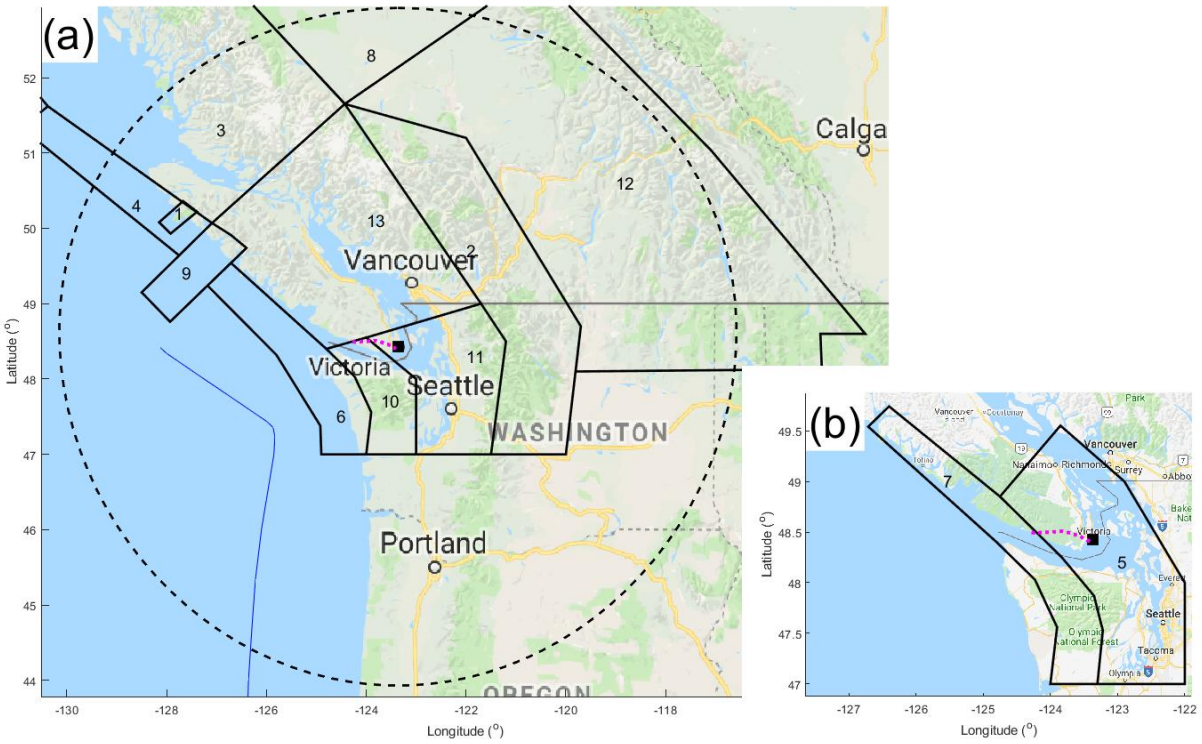

Figure 2.3. Map depicting the 2015 NBCC source zones within a 500 km radius (dashed circle) of Victoria (black square). **(a)** Depicts crustal source zones and **(b)** depicts inslab source zones to a depth of 30 and 50 km. The upper bound of the Cascadia interface source zone (depth of ~5 km) is shown with a thin line to the west (Halchuk et al, 2014). Surface expression of the LRF is shown as a dotted line. 2015 NBCC source zone labels are: 1 – Brooks Peninsula; 2 – Cascade Mountains; 3 – Coastal Mountains Revised; 4 – Explorer Plate Bending; 5 – Georgia Strait/Puget Sound (Deep); 6 – Juan de Fuca Plate Bending, Offshore; 7 – Juan de Fuca Plate Bending, Onshore (Deep); 8 – Northern British Columbia; 9 – Nookta Fault; 10 – Olympic Mountains; 11 – Puget Sound Shallow; 12 – Southern British Columbia; 13 – Vancouver Island Coast Mountains.

Magnitude-frequency statistics are defined by the Gutenberg-Richter relation (Gutenberg and Richter, 1945):

$$\log_{10}\left(\frac{N(m)}{\Delta T}\right) = a - bm, \tag{2.1}$$

where $N(m)$ represents the total number of earthquakes with magnitude ≥ m (assuming completeness for the earthquake catalogue duration), duration of completeness in years (ΔT), with an intercept of a (i.e. activity rate) and slope of b (i.e. the relative number of small to large earthquakes). Magnitude-recurrence parameters, β and N_0, are then defined as

$$\beta = b * \ln(10), \tag{2.2}$$

and

$$N_0 = 10^a. \tag{2.3}$$

Synthetic earthquake catalogues are generated for each of the four source zone types using their determined magnitude-recurrence parameters: crustal, inslab to 30-km depth, inslab to 50-km depth, and interface zones. Maximum moment magnitude (M_{max}) and minimum moment magnitude (M_{min}) for each source zone of the fifth-generation hazard model are used here (Halchuk et al., 2014) and define the magnitude range used in our EqHaz calculations to generate synthetic catalogues. For most of the source zones in the study area, a value of M_{min} 4.8 is typically used (e.g. Halchuk and Adams, 2010; Adams et al., 2015), as smaller events have not generally been observed to cause damage to engineered earthquake-resistant structures (Bommer and Crowley, 2017).

Each synthetic catalogue is simulated for a duration of 1 million years to minimize errors due to sparse sampling. GMPEs developed for each source zone type are

characterized by a lower, central, and upper GMPE relation, which are weighted 16%, 68% and 16%, respectively. Ground motions are calculated from the synthetic catalogues for each source type using the associated GMPE (Figure 2.4) for a reference stiff ground condition with an average shear-wave velocity of the upper 30 meters (V_{S30}) of 450 m/s (NEHRP site class C).

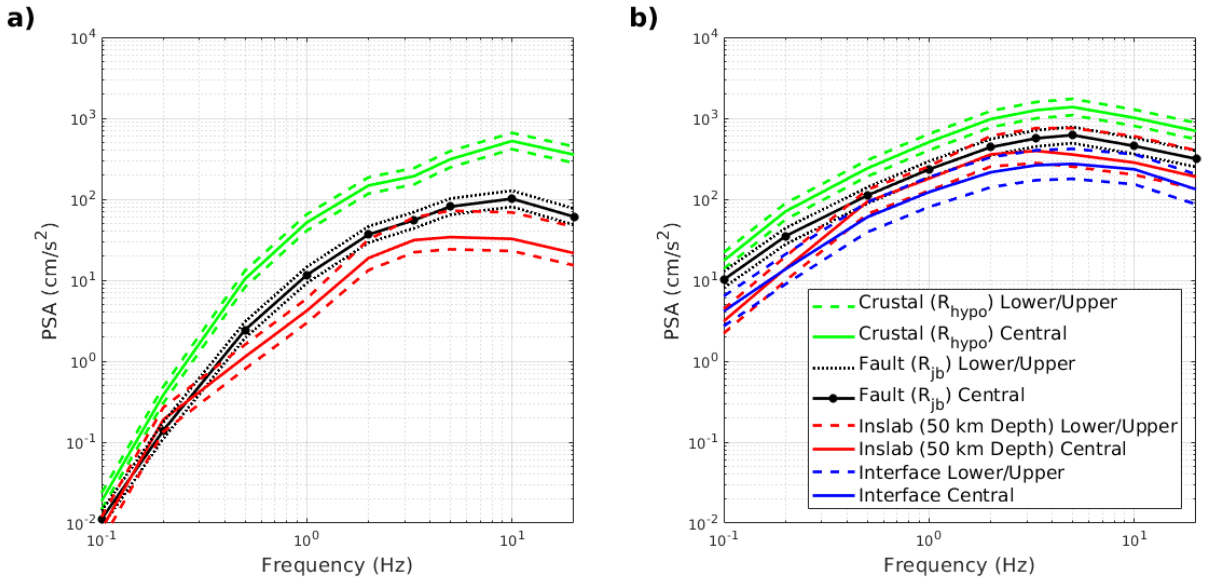

Figure 2.4. Victoria Pseudo-Spectral Acceleration **(**PSA) spectra for **(a) M** 4.5 and **(b) M** 7 earthquakes of select seismic source types. Ground motions are calculated for site class C ground conditions and appropriate distances for Victoria determined from deaggregation. For both magnitudes, the crustal and fault GMPEs site distances are 10 km. Inslab and interface GMPEs site distances are 50 km.

We reproduce 2015 NBCC hazard values for Victoria (see Data and Resources Section) to validate our PSHA implementation prior to introducing the LRVFZ as a fault source. Figure 2.5 shows the uniform hazard spectra (UHS) for Victoria at various return periods: 475 years or 10% probability of exceedance in 50 years (10% in 50 years), 1000

years (5% in 50 years), 2475 years (2% in 50 years), and 10,000 years (0.5% in 50 years). Figure 2.5 demonstrates good agreement between our UHS produced using EqHaz with the 2015 NBCC UHS at different return periods for Victoria. The maximum difference is 11% at 10 Hz for a 2475-yr return period. Hence, confidence in our PSHA implementation is obtained for further analyses and inclusion of the LRVFZ source zone. The NBCC does not record a UHS for a 10,000 year return period and thus is not included in Figure 2.5.

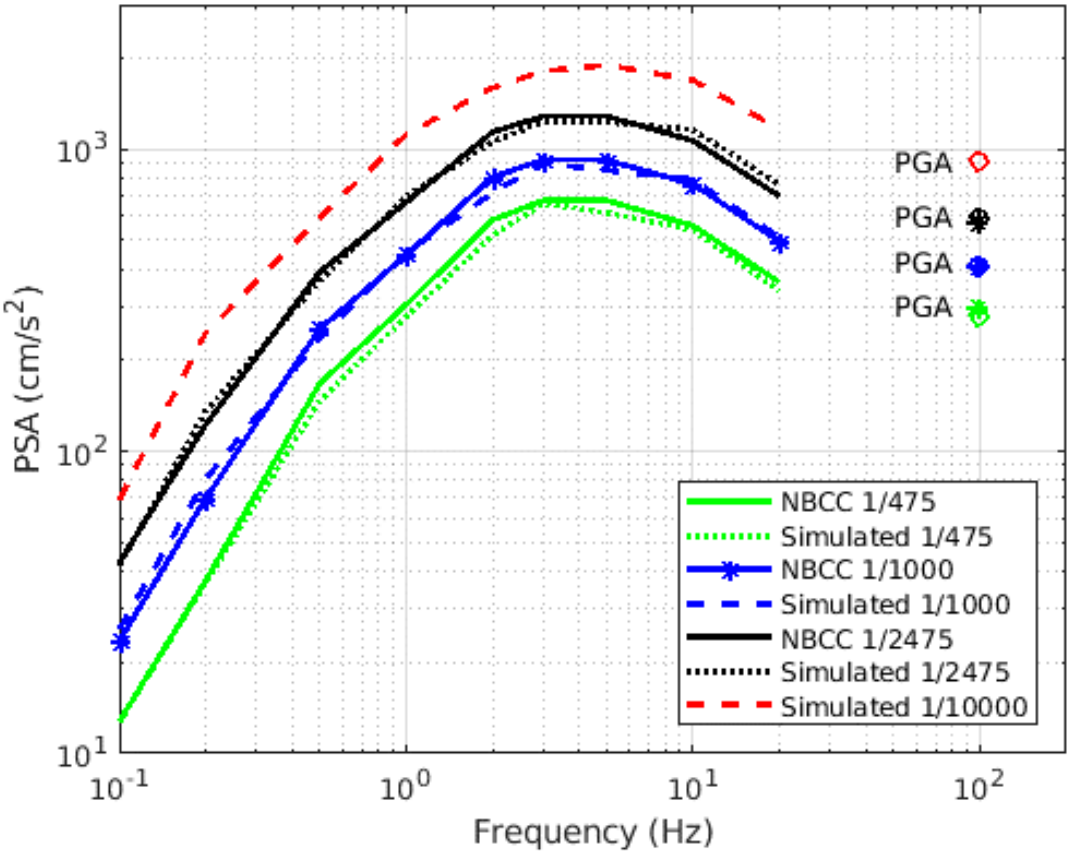

Figure 2.5. Comparison of the Victoria UHS (dashed or dotted lines) calculated at different annual rates of exceedance with the 2015 NBCC UHS (solid lines). Simulated PGA values are represented as an open circle and the 2015 NBCC PGA values are represented by an asterisk.

2.3 Inclusion of the LRVFZ as a fault source zone

In the forearc of the northern Cascadia subduction zone, few planar (linearized) seismicity patterns have been determined (Cassidy et al., 2000; Balfour et al., 2012), which delineate potential active fault seismicity. Morell et al. (2017) mapped > 60 topographic features (scarps, sags and swales) that collectively extend > 60 km in length and span ~1 km in width. Although the topographic features are semi-continuous along strike, it is suggested that the active fault zone extends the entire 60 km length due to similarity of these features along the western ~30 km of the fault to those on the eastern half (Morell et al., 2017). LiDAR imagery and field observations indicated dip slip motion on a steep (70-90° NE), north-dipping reverse fault (Morell et al., 2017). These results are supported by the microseismicity relocation study of Li et al. (2018) which delineate subsurface seismogenic structures within the LRVFZ area. This relatively known fault geometry is used to include an active fault zone into the fifth-generation seismic hazard model. To define the east-west striking LRVFZ geometry, we use a 60-km fault length and 28-km fault width (down dip extent) with a 60° dip NE and 1-km depth to the top of the fault.

To avoid double counting of seismic events in the source model, the seismic activity contribution of the LRVFZ is subtracted from the shallow earthquakes in the areal source that contains the fault. In this way, the (total) seismic moment budget is distributed between the LRVFZ and areal source zone thereby conserving the total moment release.

2.3.1 *Uncertainty in maximum magnitude*

The M_{max} value of the LRVFZ is determined using an empirical relation based on geometric attributes for fault length of a strike-slip fault > 45 km (Leonard, 2010; Leonard, 2012), expressed as

$$M_{max} = c \log L + d, \tag{2.4}$$

where L is the length of the fault (km), and c and d are equal to 1.67 and 4.17, respectively. The M_{max} value of the 60-km LRVFZ length is therefore **M** 7.14 and set as the upper M_{max} value. The M_{max} lower bound is set to **M** 5.8, to encapsulate the **M** > 6 paleoseismic events. The central value of **M** 6.5 is the average between the lower and upper M_{max} bounds. Lower, central, and upper M_{max} values are weighted in each of the PSHA calculations at 35%, 50%, and 15%, respectively. M_{min} was extrapolated to 3.5 to generate a sufficient number of events to avoid errors due to sparse magnitude sampling.

2.3.2 *Uncertainty in earthquake occurrence statistics*

Uncertainty in the magnitude-frequency statistics of the LRVFZ is addressed by generating eight magnitude distribution functions (occurrence rate of various magnitudes) from seismicity catalogues and previous studies using the online Natural Resources Canada (NRCAN) national earthquake catalogue (see Data and Resources). Magnitude-frequency statistics of the LRVFZ are drawn from three different sources: the NRCAN earthquake catalogue, a sub-catalogue of relocated microearthquakes (G. Li and

Y. Liu, pers. comm., 2017) via double-difference hypocenter location techniques (Waldhauser and Ellsworth, 2000), and regional magnitude-frequency statistics obtained from the NRCAN catalogue (Mulder, 1995). In total, eight different magnitude-recurrence distributions are developed here to characterize uncertainty in LRVFZ seismicity in subsequent PSHA calculations.

2.3.3 Magnitude-frequency distributions developed from seismicity catalogues

The NRCAN catalogue is searched to extract earthquakes within 15 kilometers of the fault surface. These 18 $\mathbf{M} \geq 2$ earthquakes are therefore selected as representative of LRVFZ seismicity here. The second sub-catalogue of relocated events consists of 181 $\mathbf{M} \geq 1$ earthquakes which occur in linearized patterns attributed with LRVFZ seismicity (Li et al., 2018). For the NRCAN and Li and Liu catalogues (Table 2.1), the cumulative number of earthquakes greater than and equal to each magnitude bin interval is calculated and divided by the duration (in years) of catalogue completeness. The catalogue completeness durations are taken from the fifth-generation seismic hazard model (S. Halchuk, pers. comm., 2018).

Table 2.1. Magnitude completeness for the NRCAN and Li and Liu catalogues.

Catalogue	Magnitude Range	N	ΔT (Years)
NRCAN	**M** 2.0-2.5	12	42
	M 2.5-3.6	5	48
	M 3.6-4.9	1	78
	M ≥ 6.0	2	15000
Li and Liu	**M** 1.0-2.0	169	10
	M 2.0-2.4	10	22
	M 2.4-3.0	2	48
	M ≥ 6.0	2	15000

To describe fault activity, we develop hybrid magnitude-recurrence models for the LRVFZ (Figure 2.6). For the smaller magnitude earthquakes in the NRCAN or Li and Liu catalogues, an exponential frequency–magnitude relationship (Gutenberg and Richter, 1945; 1956) is developed over the magnitude range of each catalogue. The associating β and N_0 values are provided in Table 2.2.

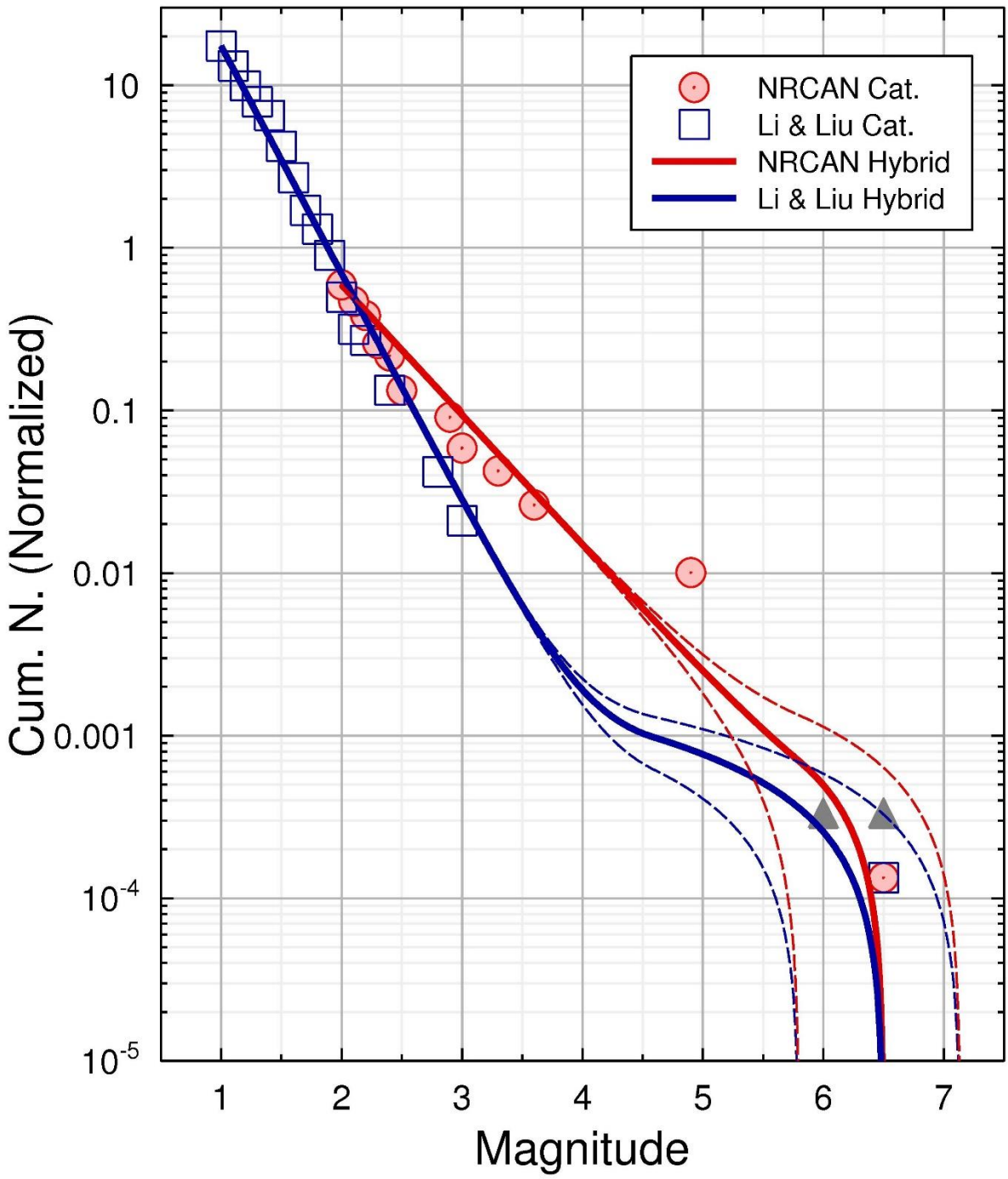

Figure 2.6. Hybrid magnitude-recurrence models developed from the NRCAN and Li and Liu catalogues including two **M** > 6 events in 15,000 years based on Morell et al. (2017). Grey triangles depict three **M** 6 or **M** 6.5 earthquakes within 9,000 years based on Morell et al. (2018).

Table 2.2. Eight sets of magnitude-recurrence parameters for the LRVFZ source zone.

Source	β			N_0			Catalogue Range (M)
	Lower	Central	Upper	Lower	Central	Upper	
(a) NRCAN	1.806	2.007	2.201	72.075	109.850	167.423	$2 \leq \mathbf{M} \leq 4.9$
(b) Li and Liu	2.030	2.255	2.481	147.527	193.375	253.471	$1 \leq \mathbf{M} \leq 3$
(c) Mulder – Vancouver Island (All)	2.213	2.388	2.563	336.394	400.726	477.362	$0 \leq \mathbf{M} \leq 4$
(d) Mulder – Plate Bend (All)	1.913	2.015	2.116	527.205	583.418	645.624	$0 \leq \mathbf{M} \leq 4$
(e) Mulder – Vancouver Island (Shallow)	2.365	2.812	3.258	91.516	143.054	223.614	$0 \leq \mathbf{M} \leq 4$
(f) Mulder – Vancouver Island (Deep)	1.810	1.955	2.100	119.950	134.586	151.356	$0 \leq \mathbf{M} \leq 4$
(g) Mulder – Plate Bend (Shallow)	1.216	1.398	1.580	43.954	50.816	58.749	$0 \leq \mathbf{M} \leq 4$
(h) Mulder – Plate Bend (Deep)	2.105	2.240	2.376	619.441	719.449	835.603	$0 \leq \mathbf{M} \leq 4$

For the larger magnitude paleoseismic events, a characteristic-magnitude model (Schwartz and Coppersmith, 1984; Youngs and Coppersmith, 1985) is developed to allow for the increased likelihood of characteristic fault events. To define the characteristic distribution function at larger magnitudes, we first examined the range in average slip per year for known active faults near the LRVFZ. Based on previous studies of the Devils Mountain fault zone and the Strawberry Point and Utsalady Point faults (Johnson et al., 1999; 2001), the suggested fault slip rate is between 0.7-1.1 mm/yr. Our calculations are performed based on two $\mathbf{M} > 6$ earthquakes within 15,000 years from Morell et al. (2017) (Figure 2.6). Morell et al. (2018) provide new constraints about LRVFZ seismicity, identifying three $\mathbf{M} > 6$ earthquakes within the last 9,000 years (triangles in Figure 2.6) and a LRVFZ slip rate of ≥ 0.2-0.3 mm/yr. These recent findings were taken into consideration and do not significantly change our initial input variables. Figure 2.6 shows

that the reported increase in the number and frequency of paleoseismic events lies within the bounds of our characteristic distribution functions.

There is large uncertainty in calculating the LRVFZ activity rate. Using 0.7-1.1 mm/yr as a representative range in slip rate for the LRVFZ, we then compute the potential activity rate for the LRVFZ between M_{min} and M_{max} in terms of seismic moment. The seismic moment can be expressed as,

$$M_0 = \mu AD, \tag{2.5}$$

where μ is the shear modulus of the crust (dyne/cm^2), A is the area of fault rupture (cm^2), and D is the average displacement (cm) or slip over the rupture surface. The annual rate of buildup of seismic moment is then equal to the time derivative of equation 2.5;

$$\frac{\mathrm{d}M_0}{\mathrm{d}t} = \frac{\mathrm{d}\mu AD}{\mathrm{d}t} = \mu AS, \tag{2.6}$$

where S is the slip rate of the fault (Youngs and Coppersmith, 1985). To convert slip rate to an earthquake activity rate, the long-term rate of seismic moment accumulation is set to equal the long-term rate of seismic moment release. The characteristic recurrence model with $N(M_{min})$ set as the rate of non-characteristic earthquakes, or total number of earthquakes in the magnitude range of M_{min} to M_c, can be written as (Gupta, 2007)

$$N(M) = \begin{cases} N(M_{\min})\dfrac{\exp\left(-\beta(M - M_{\min})\right) - \exp\left(-\beta(M_c - M_{min})\right)}{1 - \exp\left(-\beta(M_c - M_{min})\right)} + \dot{n}(M_c)\Delta M_c; & M_{\min} \le M < M_c \\ \dot{n}(M_c)(M_{\max} - M); & M_c \le M < M_{\max} \end{cases}, \tag{2.7}$$

where $\dot{n}(M_c)$ is the probability density for the occurrence rate of the characteristic earthquakes. This is equal to the rate density at magnitude M', represented by the exponential distribution for magnitudes up to M_c,

$$\dot{n}(M_c) = N(M_{min}) \frac{\beta \exp(-\beta(M' - M_{min})}{1 - \exp(-\beta(M_c - M_{min})} \ . \tag{2.8}$$

The calculated activity rate is used to constrain the rate of potential earthquakes with the characteristic mean **M** of 6.5. Solving equations 2.5 through 2.8 for the NRCAN and Li and Liu catalogs results in the hybrid frequency-magnitude distribution shown in Figure 2.6 and describes the adjustment of the GR curve to higher magnitudes. The hybrid NRCAN magnitude-frequency distribution predicts a higher rate of LRVFZ events with M > 2. Both hybrid models will predict the same number of large characteristic LRVFZ events. The fault activity rate depends on the distribution of earthquake magnitudes that release the seismic energy along the fault. We assumed the LRVFZ is in equilibrium by releasing the seismic moment in many small to moderate magnitude earthquakes as well as in a few large magnitude earthquakes. The relative rate of small-to-moderate earthquakes to large magnitude earthquakes for the LRVFZ is described by our characteristic recurrence models. The rate of earthquakes above a specified minimum magnitude, $N(M_{min})$, is given by the ratio of the seismic moment accumulation rate (equation 2.6) to the mean moment per earthquake with $M > M_{min}$.

2.3.4 *Magnitude-frequency distributions developed from earthquake statistics*

The Mulder (1995) earthquake catalogue, a regional catalogue of the NRCAN catalogue from 1981 to 1991 consists of 2816 **M** ≤ 4.5 regional earthquakes. The earthquake data were broken into four regions based on varying stress regimes and geological composition. For our study, we focused on two regions that contained the LRVFZ and thus were most likely to represent the magnitude-recurrence rate of the fault, Mulder's "Vancouver Island" and "Plate Bend" regions. The earthquake occurrence statistics (*a* and *b* values) were calculated by Mulder (1995) for these two areal source zones: the larger "Vancouver Island" zone with 368 **M** ≤ 4 events over approximately 41,600 km^2, and the smaller "Plate Bend" zone inclusive of southern Vancouver Island and the LRVFZ with 778 **M** ≤ 4 events over approximately 17,800 km^2 (Figure 2.7).

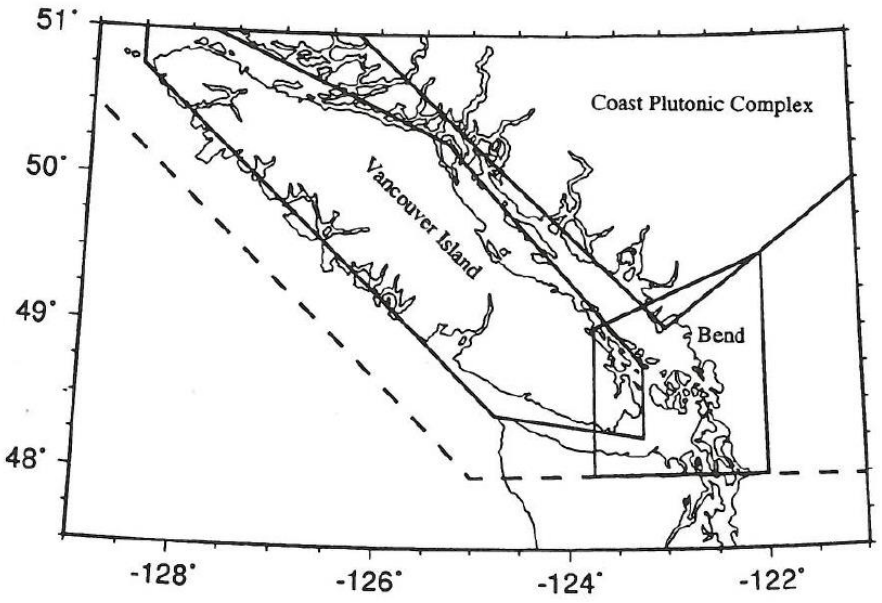

Figure 2.7. Map depicting the "Vancouver Island" and "Plate Bend" source zones. Taken from Mulder (1995).

In total, these two regions consist of 1146 **M** ≤ 4 earthquakes. The crustal seismicity in the region also occurs in a bi-modal depth distribution. Hence, these two areal source zones were divided into three different depth ranges by Mulder (1995): shallow events ≤ 10 km depth, "deep" events > 10 km depth, and all events from 0-30 km depth. We assume the "Plate Bend" event statistics are more representative of the LRVFZ due to spatial proximity, i.e., similarity in stress regime. However, the accuracy of these magnitude-recurrence statistics to represent LRVFZ seismicity cannot be verified. We therefore also utilize the regional "Vancouver Island" magnitude-recurrence statistics determined by Mulder (1995).

We substitute the a and b values calculated by Mulder (1995) from events within these 6 different sub-regions into equations 2.2 and 2.3 to define central β and N_0 values (Table 2.2). Lower and upper bounds for β and N_0 values are set to 10% deviation of the central value. Weighting applied to the lower, central and upper bounds of β and N_0 are 16%, 68%, and 16%, respectively. The Mulder (1995) **M** ≤ 4 recurrence statistics therefore define exponential frequency-magnitude distributions that are essentially extrapolated to the M_{max} in each PSHA calculation. Hybrid models were only applied to the NRCAN and Li and Liu catalogues due to the similar range the GR relations from the Mulder (1995) values (Figure 2.8).

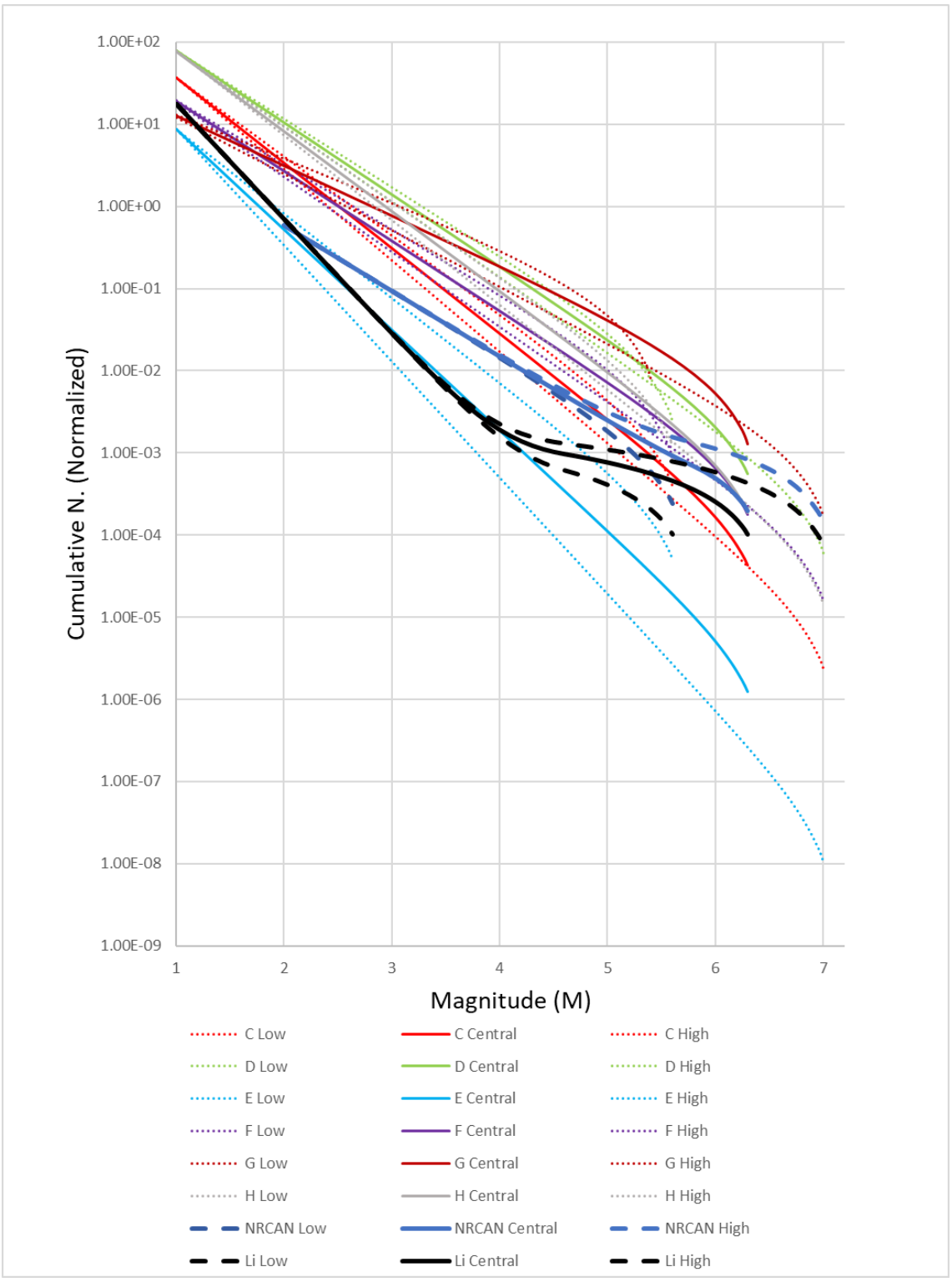

Figure 2.8. Gutenberg-Richter relations for all simulations in comparison to the hybrid models.

2.3.5 Uncertainty in ground motion prediction

A GMPE specific to the LRVFZ is required to estimate ground motion intensities from synthetic LRVFZ events, yet the ground motions associated with various magnitude LRVFZ earthquakes is relatively unknown. In lieu of a GMPE specific to LRVFZ motions, the central, upper, and lower GMM relations for active crustal faults in western Canada are used from the fifth-generation seismic hazard model (Halchuk et al., 2014) to calculate ground motions from the eight sets of synthetic LRVFZ seismicity catalogues. These western Canada fault-appropriate GMPEs are used to calculate ground motions for the Queen Charlotte and Fairweather faults in the 5th-generation seismic hazard model (Halchuk et al., 2014). The central GMPE is based on the modified Boore and Atkinson (2008) GMPE developed from the NGA-West 2 ground motion database. Lower and upper bound GMPEs were developed to express epistemic uncertainty about the central GMPE (Atkinson and Adams, 2013). The central, upper, and lower GMPEs are representing alternative estimates of the median ground-motion amplitudes. These fault-appropriate models were converted from western Canada crustal GMPEs which are based on a point-source distance metric. The distance metric of fault-appropriate GMPE suites is the Joyner-Boore distance (R_{JB}; Joyner and Boore, 1981). A conversion from a point-source distance metric to fault-distance metrics were made using a simple approximation that accounts for average fault size (see Appendix A of Atkinson (2012) for details).

2.4 PSHA for Victoria including the LRVFZ

PSHA calculations are performed for Victoria using each of the eight magnitude-recurrence distributions developed to represent LRVFZ seismicity. Their appropriate β and N_0 values reported in Table 2.2 are used. Uncertainties in the maximum magnitude and fault source GMPE are included in each PSHA. A total of 8 PSHA calculations are therefore performed for Victoria including the LRVFZ as an active fault source to examine the impact (percentage change) to predicted ground motions.

Figure 2.9 shows the contribution of each earthquake source type to the Victoria UHS at a 2475-year return period. At low frequencies (longer periods), the UHS motions are dominated by Cascadia subduction zone interface sources. Above 2.0 Hz, the crustal North American plate sources control the UHS motions. Earthquakes within the subducting Juan de Fuca plate directly below Victoria (50 km depth inslab zone) provide similar ground motion contributions as crustal events at high frequencies and interface events at low frequencies. The 30-km depth inslab source zone for events offshore Vancouver Island contributes the least to motions in Victoria.

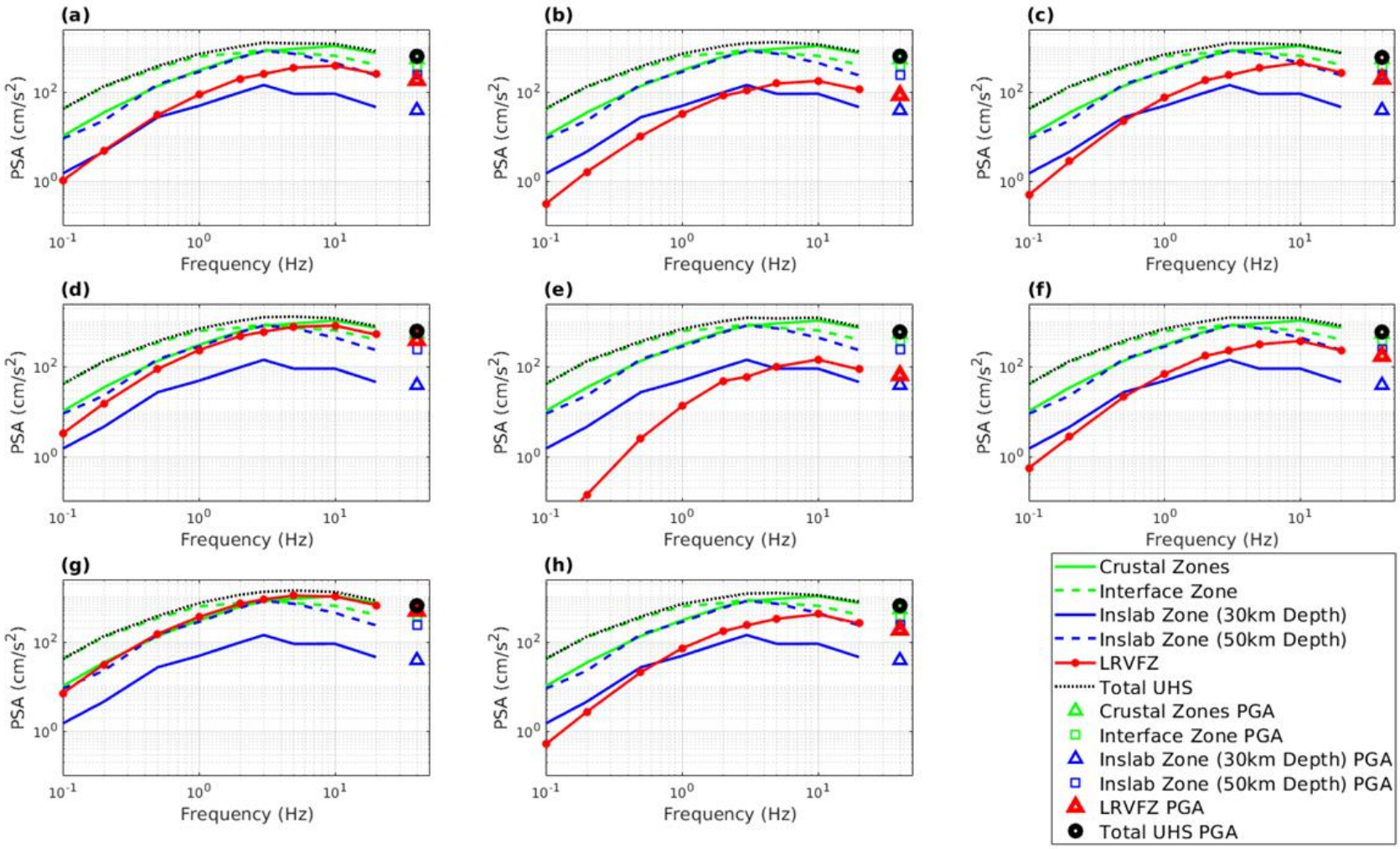

Figure 2.9. Victoria UHS curves at a 2475-year return period from eight PSHA calculations with a different LRVFZ magnitude-recurrence rate (a-h; listed in Table 2.2) showing contribution of each source zone type as well as the total UHS from all source contributions (dotted line).

The contribution of an active LRVFZ source varies based on the fault's magnitude-recurrence rate. Figure 2.9 demonstrates that the LRVFZ zone will contribute to Victoria UHS motions at higher frequencies, similar to interface and crustal source contributions in some cases (subplots a, c, f, h), and has the potential to become the greatest contributor at high frequencies (subplots d, g). These latter two PSHA calculations included LRVFZ seismicity based on earthquake events that occur in the upper 10 km of the crust at the southern tip of Vancouver Island and correspond to low β values (Table 2.2). The LRVFZ contributes the least to the UHS when its simulated seismicity is based on magnitude-frequency statistics from shallow (< 10 km depth) earthquakes of the entire Vancouver Island region (subplot e; largest β value). In other words, magnitude-recurrence rates with lower β values leads to an increase in the number of larger magnitude events, which increases the LRVFZ ground motion contribution.

We further explore the predicted 2% in 50 years UHS ground motions by performing deaggregation of select PSHAs at high frequency (10 Hz). Figure 2.10 shows deaggregation of PSHAs without and with the LRVFZ source zone included. Prior to adding the LRVFZ as a fault source zone (Figure 2.10a), the main contributions of ground motions arise from three distinct sources: **M** ≤ 7.5 crustal earthquakes within 20 km of Victoria, **M** 6 to 7 inslab earthquakes at distances > 40 km from Victoria, and **M** > 8.5 Cascadia interface earthquakes within 40-100 km of Victoria. Deaggregations of PSHA calculations with the hybrid NRCAN and Li and Liu seismicity models (Figures 2.10b

and c, respectively) demonstrate the LRVFZ contribution is generated from occurrences of **M** 6 to 7 earthquakes at 40 km distance and **M** 4.5 to 5 events at closer (≤ 20 km) distances. Figure 2.10d shows the PSHA deaggreation including a shallow "Plate Bend" LRVFZ seismicity model (calculation g in Figure 2.9); the PSHA calculation with the largest LRVFZ contribution. Contribution of large magnitude earthquake occurrences associated with the Cascadia subduction zone and **M** 6 to 7 inslab earthquakes at a 40 km distance appear reduced due to significant increased occurrences of **M** 4.5 to 5 LRVFZ events within 20 km of Victoria.

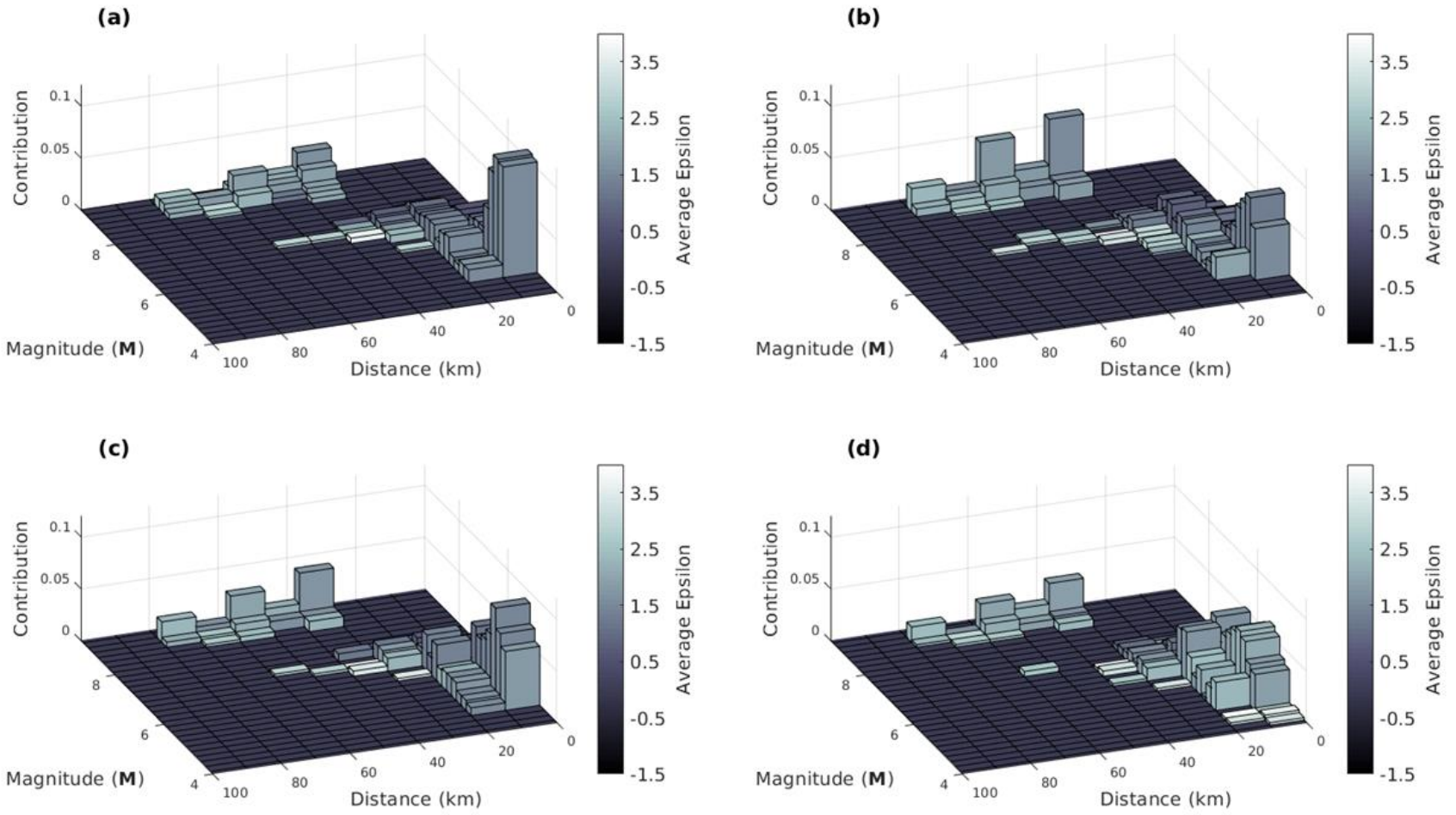

Figure 2.10. PSHA deaggregations at 10 Hz for Victoria at a 2475-year return period **(a)** without an active LRVFZ zone and including an active LRVFZ zone from PSHA **(b)** calculation a, **(c)** calculation b, and **(d)** calculation g in Figs. 2.9 with fault appropriate GMPEs.

The impact of including the LRVFZ as an active fault source zone to the predicted 2015 NBCC UHS ground motions for Victoria is shown in Figure 2.11. Introduction of the LRVFZ source zone causes the greatest increase in UHS motions at high frequencies (≥ 10 Hz) related to the associating magnitude-recurrence rate of the fault. At a 2% probability of exceedance in 50 years, the percentage increase compared to the 2015 NBCC UHS at frequencies ≤ 10 Hz ranges between 1% to 23% for all calculations (Table 2.3).

Table 2.3 reports a 4% to 23% increase in UHS motions at 10 Hz compared to the 2015 NBCC UHS. PSHA calculations a and b which utilized hybrid magnitude-frequency distributions show increases in UHS motions at 10 Hz of 12% and 8%, respectively.

Table 2.3. UHS motions at 2% probability of exceedance in 50 years for Victoria. Percent difference (%) calculated with reference to the 2015 NBCC UHS motion.

Source	Calculation	Fault Specific GM		
		PSA at 5 Hz (cm/s^2)	PSA at 10 Hz (cm/s^2)	PGA (g)
2015 NBCC		1280.85	1064.90	0.58
NRCAN	**a**	1216.20 (5%)	1188.82 (12%)	0.64 (10%)
Li and Liu	**b**	1298.93 (1%)	1154.60 (8%)	0.64 (10%)
Vancouver Island (All)	**c**	1215.12 (5%)	1130.55 (6%)	0.60 (4%)
Plate Bend (All)	**d**	1304.69 (2%)	1194.38 (12%)	0.63 (9%)
Vancouver Island (Shallow)	**e**	1187.90 (7%)	1230.45 (16%)	0.61 (5%)
Vancouver Island (Deep)	**f**	1239.11 (3%)	1208.65 (14%)	0.60 (4%)
Plate Bend (Shallow)	**g**	1416.35 (11%)	1312.28 (23%)	0.66 (14%)
Plate Bend (Deep)	**h**	1244.27 (3%)	1107.63 (4%)	0.66 (14%)
Average		1265.32 (1%)	1190.92 (11%)	0.63 (8%)

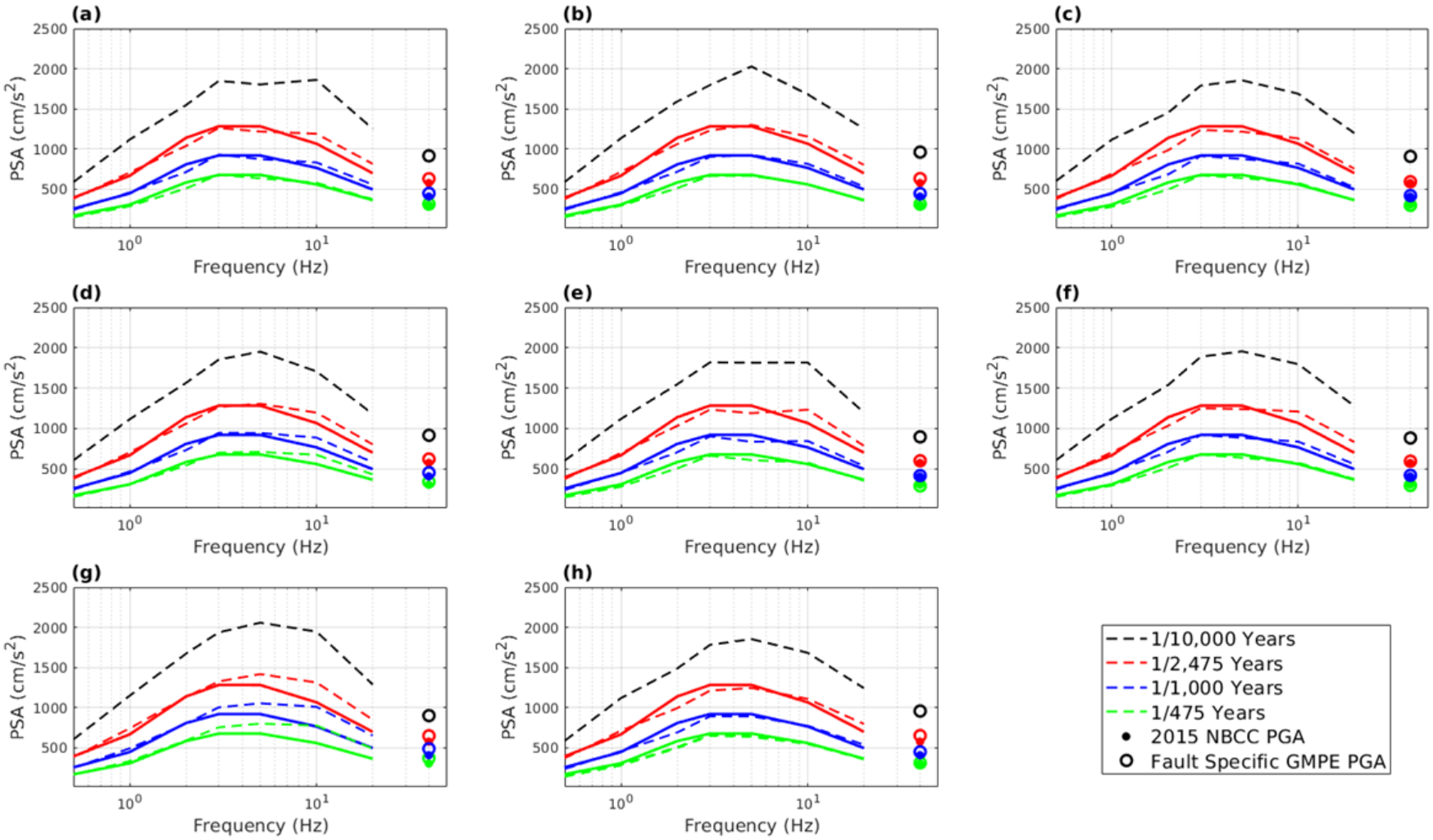

Figure 2.11. Reference 2015 NBCC Victoria UHS (solid lines) compared to calculated Victoria UHS curves from eight PSHA calculations including an active LRVFZ zone (a-h; listed in Table 2.2). Symbols denote PGA values. The 2015 NBCC Victoria UHS at a 10,000 year return period is not available.

The predicted PGA in Victoria at a 2% probability of exceedance in 50 years is an average of 0.63 g (0.02 g one standard deviation) amongst the eight calculations, which is an increase of 9% compared to the 2015 NBCC PGA of 0.58 g. Three hydroelectric dams in southern Vancouver Island are located near the LRVFZ. Seismic hazard assessment for dams requires longer return periods, e.g., 10,000 years. At this longer return period, an active LRVFZ zone may increase motions up to 15% at a 5 Hz frequency and 6% at 10 Hz frequency (Figure 2.11g).

2.5 Discussion and Conclusions

We performed 8 PSHA calculations to examine the seismic hazard impact to Victoria from an active LRVFZ. These PSHA calculations capture variability due to uncertainties in implementing a LRVFZ source zone, including maximum magnitude, earthquake occurrence statistics, and fault appropriate GMPEs. We used a consistent east-west striking ~60-km length and 28-km width fault geometry with 60° N dip and 1 km depth to top of the fault for all 8 PSHA calculations. LRVFZ seismicity parameters are based on magnitude-frequency statistics from three different sources. 8 different sets of magnitude-recurrence distributions are developed or taken from these sources to capture uncertainty in the LRVFZ seismicity rate. A suite of lower, central, and upper fault-appropriate GMPEs were used to convert the eight synthetic LRVFZ seismicity

catalogues into predicted motions based on a fault projection (R_{jb}) distance metric. The LRVFZ has the potential to be a significant seismic source contributor to high-frequency ground motions for Victoria depending on the magnitude-recurrence associated with the fault. The tested variation in LRVFZ *b*-value is 0.6 to 1.2 in this study. When fault seismicity is highly uncertain, as is the case for the LRVFZ, care should be taken in selecting an appropriate b-value for smaller magnitude earthquakes in the characteristic model.

Overall, inclusion of the LRVFZ as an active fault zone causes notable increases in Victoria ground motions at high frequencies compared to the 2015 NBCC ground motions. The 2,475-year return period PSA motions increase by a maximum of 23% (1064.90 cm/s^2 to 1312.28 cm/s^2 at 10 Hz) compared to the 2015 NBCC UHS. Higher frequency ground motions impact shorter buildings with higher resonance frequencies. For example, one-story tall buildings typically resonate at 10 Hz (Meyer, 2006).

The LRVFZ is one of several faults to be recently identified as potentially seismically active in southwestern British Columbia and northwestern Washington State. How best to implement and assess the impact of these newly identified active faults, in which recorded seismicity may or may not be related to the fault itself, is a major challenge for future seismic hazard analysis. In general, the mixing of Gutenberg-Richter recurrence statistics with paleoseismic evidence can improve the statistical representation of a fault (Valentini et al., 2017). Future PSHA works for the LRVFZ would therefore

benefit from continued monitoring and densifying of local seismic networks around the LRVFZ to further constrain its magnitude recurrence rate. Additional paleoseismic studies of the LRVFZ and others in the fault system would be beneficial in constraining fault activity rates in the region. Trenching studies to more accurately identify the causative fault, its previous movements, and thereby its maximum magnitude. Additionally, deterministic seismic hazard analyses of large scenario LRVFZ earthquakes would capture variability in potential ground motions due to uncertainty in the rupture process and characteristics of large LRVFZ (paleo and future) earthquakes.

This study's PSHA calculations are considered exploratory by the authors and do not replace the proposed 2015 NBCC ground motions. Inclusion of the LRVFZ and the Darrington-Devils Mountain fault zone as seismically active is included in the 6th-generation national seismic hazard model for development of the 2020 NBCC design ground motions (Halchuk et al., 2019).

2.6 Data and Resources

2015 NBCC hazard values for Victoria were obtained using NRCAN's seismic hazard calculator at http://www.earthquakescanada.nrcan.gc.ca/hazard-alea/interpolat/index_2015-en.php (last accessed on September 2018). The NRCAN earthquake catalogue used in this study is retrieved from the national earthquake

database at http://www.earthquakescanada.nrcan.gc.ca/stndon/NEDB-BNDS/index-en.php (last accessed on September 2018). The 2015 earthquake hazard map for PGA used in the 2015 NBCC is retrieved from http://www.earthquakescanada.nrcan.gc.ca/hazard-alea/zoning-zonage/NBCC2015maps-en.php (last accessed on December 2018).

2.7 Acknowledgments

Funding provided by Natural Sciences and Engineering Research Council (NSERC) and Chaucer Syndicates. We thank Ge Li and Yajing Liu (McGill University) for providing us with their relocated earthquake catalogue associated with the Leech River Valley fault zone. All figures produced using Mathworks Matlab® software and ESRI ArcGIS.

2.8 References

Adams, J., S. Halchuk, T. Allen, and G. Rogers (2015). Canada's 5th Generation seismic hazard model, as prepared for the 2015 National Building Code of Canada, *11th Canadian Conference on Earthquake Engineering, Victoria, Canada*, Paper 93775.

Assatourians, K., and G. Atkinson (2013). EqHaz: An open-source probabilistic seismic-hazard code based on the Monte Carlo simulation approach, *Seismol. Res. Lett.* **84** 516-524. doi: 10.1785/0220120102.

Atkinson, G. (2012). White paper on development of ground-motion prediction equations for Canadian National Seismic Hazard Maps. www.seismotoolbox.ca (Misc. Resources). Last accessed April 2019.

Atkinson, G., and J. Adams (2013). Ground motion prediction equations for application to the 2015 Canadian national seismic hazard maps, *Can. J. Civ. Eng.* **40** 988-998. doi: dx.doi.org/10.1139/cjce-2012-0544.

Balfour, N.J., J.F. Cassidy, and S.E. Dosso (2012). Identifying active structures using double-difference earthquake relocations in southwest British Columbia and the San Juan Islands, Washington, *Bull. Seismol. Soc. Am.* **102** 639-649. doi: 10.1785/0120110056.

Barrie, J.V., and H.G. Greene (2015). Active faulting in the northern Juan de Fuca Strait: Implications for Victoria, British Columbia, *Geological Survey of Canada, Current Research 2015-6*. doi: 10.4095/296564.

Bazzurro, P., and C.A. Cornell (1999). Disaggregation of seismic hazard, *Bull. Seismol. Soc. Am.* **89** 501-520.

Bommer, J.J., and H. Crowley (2017). The Purpose and definition of the minimum magnitude limit in PSHA calculations, *Seismol. Res. Lett.* **88.** https://doi.org/10.1785/0220170015.

Boore, D.M., and G. Atkinson (2008). Ground motion prediction equations for the average horizontal component of PGA, PGV, and 5%-damped PSA at spectral periods between 0.01 and 10.0 s, *Earthquake Spectra* **24** 99-138.

Cassidy, J.F., G.C. Rogers, and F. Waldhauser (2000). Characterization of active faulting beneath the strait of Georgia, British Columbia. *Bull. Seismol. Soc. Am.* **90(5)**, 1188–1199. doi: https://doi.org/10.1785/0120000044.

Clowes, R.M., M.T. Brandon, A.G. Green, C.J. Yorath, A. Sutherland Brown, E.R. Kanasewich, and C. Spencer (1987). LITHOPROBE-southern Vancouver Island: Cenozoic subduction complex imaged by deep seismic reflections, *Can. J. Earth Sci.* **24(3)** 1-51.

Cornell, C.A. (1968). Engineering seismic risk analysis, *Bull. Seismol. Soc. Am.* **58** 1583-1606.

Field, E.H., T.H. Jordan, and C.A. Cornell (2003). OpenSHA: A Developing Community-Modeling Environment for Seismic Hazard Analysis, *Seismol. Res. Lett.* **74** 406-419.

GEM. (2017) The OpenQuake-engine user manual, *Global Earthquake Model (GEM) Technical Report 2017-11* doi: 10.13117/GEM.OPENQUAKE.MAN.ENGINE.2.8/01.

Gupta, I.D. (2007). Probabilistic seismic hazard analysis method for mapping spectral amplitudes and other design-specific quantities to estimate the earthquake effects on man-made structures, *ISET J. Earthquake Technology*, **44(1)**, 127-167.

Gutenberg, B., and C.F. Richter (1945). Seismicity of the Earth, *Bull. Geol. Soc. Am.* **56** 603-668.

Gutenberg, B., and C.F. Richter (1956). Earthquake magnitude, intensity, energy and acceleration, *Bull. Seismol. Soc. Am.* **46** 105 – 145.

Halchuk, S., and J. Adams (2010). Mmin − Implications of its choice for Canadian seismic hazard and seismic risk, *Proceedings of the 9th U.S. National and 10th Canadian Conference on Earthquake Engineering*, July 25-29, 2010, Toronto, Ontario, Canada, Paper No 439.

Halchuk, S., T. Allen, J. Adams, and G. Rogers (2014). Fifth generation seismic hazard model input files as proposed to produce values for the 2015 National Building Code of Canada, *Geological Survey of Canada, Open File 7576.* doi: 10.4095/293907.

Halchuk, S., T. Allen, J. Adams, T. Onur (2019). Contribution of the Leech River-Devil's Mountain fault system to seismic hazard in Victoria, BC, *12th Canadian Conference on Earthquake Engineering*, Québec City, Quebec, June 17-20 2019, 9p.

Harmsen, S., D. Perkins, and A. Frankel (1999). Deaggregation of probabilistic ground motions in the central and eastern United States, *Bull. Seismol. Soc. Am*. **89** 1-13.

Johnson, S.Y., S.V. Dadisman, J.R. Childs, and W.D. Stanley (1999). Active tectonics of the Seattle fault and central Puget Lowland – Implications for earthquake hazards, *Bull. Seismol. Soc. Am*. **111** 1042-1053.

Johnson, S., S. Dadisman, D. Mosher, R. Blakely, and J. Childs (2001). Active tectonics of the Devil's Mountain Fault and related structures, Northern Puget Lowland and Eastern Strait of Juan de Fuca Region, Pacific Northwest, *U.S. Geol. Surv. Professional Paper 1643*.

Joyner, W.B., and D.M. Boore (1981). Peak horizontal acceleration and velocity from strong-motion records including records from the 1979 Imperial Valley, California, earthquake, *Bull. Seismol. Soc. Am.* **71** 2011-2038.

Leonard, M. (2010). Earthquake fault scaling: Self-consistent relating of rupture length, width, average displacement, and moment release, *Bull. Seismol. Soc. Am.* **100** 1971 - 1988.

Leonard, M. Erratum to Earthquake fault scaling: Self-consistent relating of rupture length, width, average displacement, and moment release, *Bull. Seismol. Soc. Am.* **102** 2797-2797.

Li, G., Y. Liu, C. Regalla, and K.D. Morell (2018). Seismicity relocation and fault structure near the Leech River fault zone, southern Vancouver Island, *J. Geophys. Res. – Sol. Ea.* **123** 2841-2855. doi: https://doi.org/10.1002/2017JB015021.

McGuire, R. (1995). Probabilistic seismic hazard analysis and design earthquakes: Closing the loop, *Bull. Seismol. Soc. Am.* **85** 1275-1284.

Meyer, P.K. (2006). The impact of high frequency/low energy seismic waves on unreinforced masonry. *M. Sc. thesis*, Cambridge, Massachusetts Institute of Technology, Massachusetts, United States of America. pp. 90.

Milne, W.G., and A.G. Davenport (1969). Distribution of earthquake risk in Canada, *Bull. Seismol. Soc. Am.* **59** 729–754.

Morell, K., C. Regalla, L. Leonard, C. Amos, and V. Levson (2017). Quaternary rupture of a crustal fault beneath Victoria, British Columbia, Canada, *GSA Today.* **27** 1-7. doi: 10.1130/GSATG291A.1.

Morell, K., C. Regalla, C. Amos, S. Bennett, L. Leonard, A. Graham, T. Reedy, V. Levson, A. Telka (2018). Holocene surface rupture history of an active forearc fault redefines seismic hazard in southwestern British Columbia, Canada, *Geophysical Research Letters*. doi: 10.1029/2018gl078711.

Mulder, T. L. (1995). Small Earthquakes in Southern British Columbia: 1975-1991. *M. Sc. thesis*, Victoria, University of Victoria, British Columbia, Canada. pp 117.

Musson, R.M.W. (1999). Determination of design earthquakes in seismic hazard analysis through Monte Carlo simulation, *J. Earthquake Eng*. **3** 463-474.

Musson, R.M.W. (2000). The use of Monte Carlo simulations for seismic hazard assessment in the U.K. *Ann. Geofis*. **43** 1-9.

Ordaz, M., F. Martinelli, V. D'Amico, and C. Meletti (2013). CRISIS2008: A flexible tool to perform probabilistic seismic hazard assessment, *Seismol. Res. Lett.* **84** 495-504. doi: 10.1785/0220120067.

Pailoplee, S., and C. Palasri (2014). CU-PSHA: A MATLAB software for probabilistic seismic hazard analysis, *J. Earthq. Tsunami* **8** 1450008-1-1450008-26, doi: 10.1142/S1793431114500080.

Ramachandran, K. (2001). Velocity structure of S.W. British Columbia and N.W. Washington from 3-D non-linear seismic tomography, Ph.D. thesis, Univ. of Victoria, Victoria, B. C., Canada.

Schwartz, D.P., and K.J. Coppersmith (1984). Fault behavior and characteristic earthquakes: Examples from the Wasatch and San Andreas fault zones, *J. Geophys. Res.* **89** 5681 – 5698.

Sherrod, B.L., R.J. Blakely, C.S. Weaver, H.M. Kelsey, E. Barnett, L. Liberty, K.L. Meagher, and K. Pape (2008). Finding concealed active faults: Extending the southern Whidbey Island fault across the Puget Lowland, Washington, *J. Geophys. Res.* **113.** doi: 10.1029/2007JB005060.

Valentini, A., F. Visini, and B. Pace (2017). Integrating faults and past earthquakes into a probabilistic seismic hazard model for peninsular Italy, *Nat. Hazards Earth Syst. Sci.* **17** 2017-2039. doi: https://doi.org/10.5194/nhess-17-2017-2017.

Waldhauser, F., and W.L. Ellsworth (2000). A double-difference earthquake location algorithm: method and application to the northern Hayward Fault, California, *Bull. Seism. Soc. Am.* **90** 1353-1368.

Youngs, R.R., and K.J. Coppersmith (1985). Implications of fault slip rates and earthquake recurrence models to probabilistic seismic hazard estimates, *Bull. Seismol. Soc. Am.* **75** 939-964.

3 Earthquake Ground Motion Simulations for Victoria, British Columbia: Considering an Active Leech River Valley Fault Zone

3.1 Introduction

The LRVFZ (Figure 3.1) is an ~60 km transpressional reverse fault zone that extends along the southern tip of Vancouver Island, British Columbia, Canada. The fault is present near the city of Port Renfrew and extends east under the provincial capital city of Victoria and potentially continues offshore connecting with the Devil's Mountain Fault. It is important to examine how earthquake ground motions generated along this newly identified active fault will affect nearby infrastructure or cities.

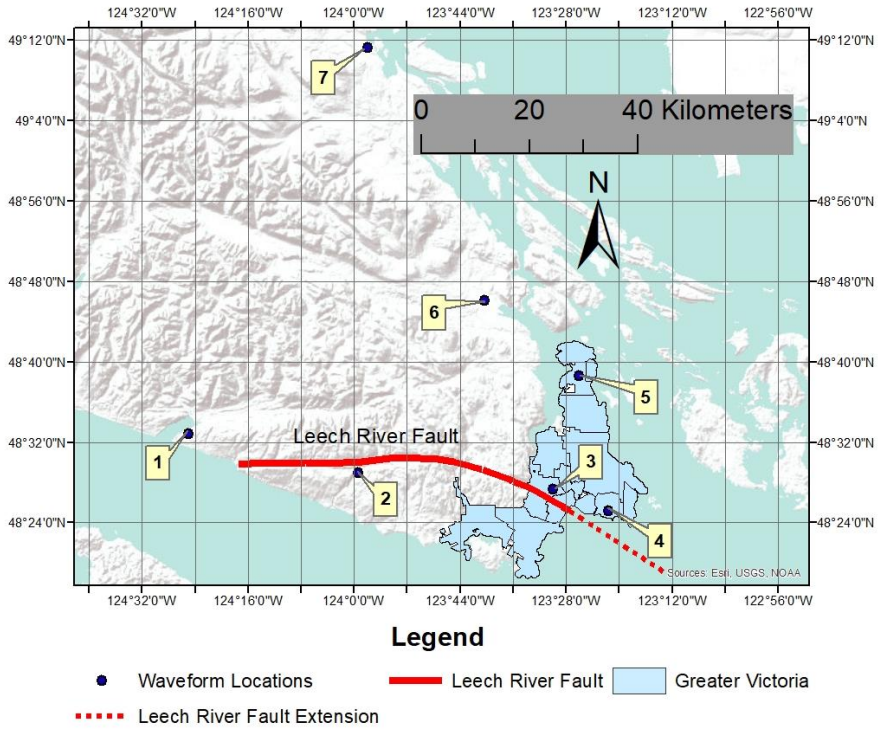

Figure 3.1. Terrain map of the southern tip of Vancouver Island. The LRVFZ surface projection (solid red line) used in ground motion simulations, and its

potential extension beneath Juan de Fuca Strait (red dashed line), shown in relation to Greater Victoria (light blue region). The blue circles mark points of interest where waveforms from ground motion simulations are extracted. The locations are: 1 – Port Renfrew; 2 –Jordan River; 3 – Langford; 4 – Victoria; 5 – Victoria Airport; 6 – Duncan; 7 – Nanaimo.

Vancouver Island is situated on the crustal North America plate where crustal earthquake stress accumulation is caused due to compression (Molnar et al., 2014a). Historical large M ≥ 7 crustal NA plate earthquakes occurred in central Vancouver Island in 1918 and 1946. Moderate **M** 5.5-6 earthquakes have occurred closer to Victoria, beneath the San Juan Islands, Washington, in 1909 and 1920 (Molnar et al., 2014b). The activity rate of **M** 5 crustal earthquakes in southwestern British Columbia is approximately one every 20 years, and a best-estimate maximum magnitude of **M** 7.3 for shallow crustal earthquakes (Adams and Halchuk, 2003). Outside of the three **M** ≥ 6 paleoseismic LRVFZ earthquakes proposed by Morell et al. (2017; 2018), modern seismic networks have not recorded large magnitude LRVFZ earthquakes. Recent paleoseismic studies suggest the LRVFZ has produced three large magnitude > 6 ruptures in the Holocene (Morell et al., 2017, 2018). Including the LRVFZ as a seismic source in PSHA analyses increases PGA in Victoria at a 2,475-year return period by 9% on average (Kukovica et al., 2019a).

3D Finite Difference (FD) wave propagation simulations were performed to quantify the Georgia sedimentary basin effect on long-period ground shaking in Greater Vancouver considering eight realistic scenarios of **M** 6.8 shallow North America plate earthquakes (Molnar et al., 2014b). On average, the maximum peak ground motion was

17.8 cm/s for Greater Vancouver; corresponding to a very strong shaking level or a Modified Mercalli Intensity (MMI) VII (Figure 3.2).

PERCEIVED SHAKING	Not felt	Weak	Light	Moderate	Strong	Very strong	Severe	Violent	Extreme
POTENTIAL DAMAGE	none	none	none	Very light	Light	Moderate	Mod./Heavy	Heavy	Very Heavy
PEAK ACC.(%g)	<0.05	0.3	2.8	6.2	12	22	40	75	>139
PEAK VEL.(cm/s)	*<0.02*	*0.1*	*1.4*	*4.7*	*9.6*	*20*	*41*	*86*	*>178*
INSTRUMENTAL INTENSITY	I	II–III	IV	V	VI	VII	VIII	IX	X+

Figure 3.2. Modified Mercalli Intensity units and corresponding perceived shaking, peak motion type attributes. PGV values represent the minimum value for corresponding instrumental intensity. From Worden and Wald (2016).

Scenario 5 in Molnar et al. (2014b) used a **M** 6.8 rupture with a hypocenter located under Victoria, British Columbia which is similar to LRVFZ scenarios in this thesis. Their scenario is based on a modified 1994 **M** 6.7 Northridge, California earthquake source model with a N270°E strike and 45° dip north, and is comparable to an eastern portion rupture of the LRVFZ. PGV in the southern section of Vancouver Island from this **M** 6.8 scenario ranged from 3.4 to 9.6 cm/s (MMI I to V) with peak ground motions near 20 cm/s at Victoria (MMI VI).

This study performs Deterministic Seismic Hazard Analyses (DSHA) using 3D FD wave propagation simulations to predict low frequency (≤ 0.5 Hz) or long-period (≥ 2 s) ground motions from large **M** 7 LRVFZ earthquake scenarios. Slip distributions for two empirical **M** 7 earthquakes elsewhere in the world are modified to produce a suite of 24 LRVFZ rupture scenarios with varying depth and distribution of maximum slip, direction of rupture propagation (east-to-west vs. west-to-east), and hypocenter location.

The slip distribution models from the 2010 **M** 7 Darfield, South Island, New Zealand earthquake and the 2010 **M** 7 Haiti earthquake are used (see Data and Resources). 3D FD wave propagation simulations provide long-period (≥ 2 s) ground motions at the surface of a regional velocity model of southwestern British Columbia for the 24 deterministic **M** 7 LRVFZ scenario earthquakes. Waveforms are extracted at seven select locations (Figure 3.1) with high populations and/or critical infrastructure in southern Vancouver Island, i.e. locations of higher seismic risk, to examine earthquake shaking of potential large magnitude LRVFZ earthquakes. The PGV metric used for computing a synthetic horizontal waveform is calculated as

$$max_t\left(\sqrt{v_{EW}(t) \times v_{NS}(t)}\right), \tag{3.2}$$

where $v(t)$ represents the synthetic horizontal velocity in the east-west (EW) and north-south (NS) components (Molnar et al., 2014a; 2014b).

3.2 Physical-Structure Model and Finite-Difference Scheme

The base elastic physical model is extracted from the Molnar (2011) southwest British Columbia 3D velocity model (Figure 3.3). This model is a modified version of the larger Pacific Northwest velocity model of Stephenson (2007). The physical structure model incorporates the 3D P- and S-wave velocities (V_P and V_S, respectively) and densities (ρ) to 60-km depth within the Cascadia subduction zone. The model is based on six main

geologic units: continental basin sediments, crust, and mantle; and oceanic sediments, crust, and mantle. Surface topography is not included in the model and the minimum V_S is set to 625 m/s for computational feasibility. Molnar (2011) updated the upper 1 km of the Stephenson (2007) model for the Greater Vancouver or Georgia basin region, which helped reduce overprediction of long-period ground motions in Greater Vancouver from a factor of 2.1 to 1.6. The higher velocities of the metamorphic Leech River Complex and igneous Metchosin Formation (Figure 3.3c and d) are overlain by lower velocity sediments from the Oliogocene Carmanah group near the LRVFZ (Figure 3.3a and b) (Fairchild and Cowan, 1982; Groome et al., 2003).

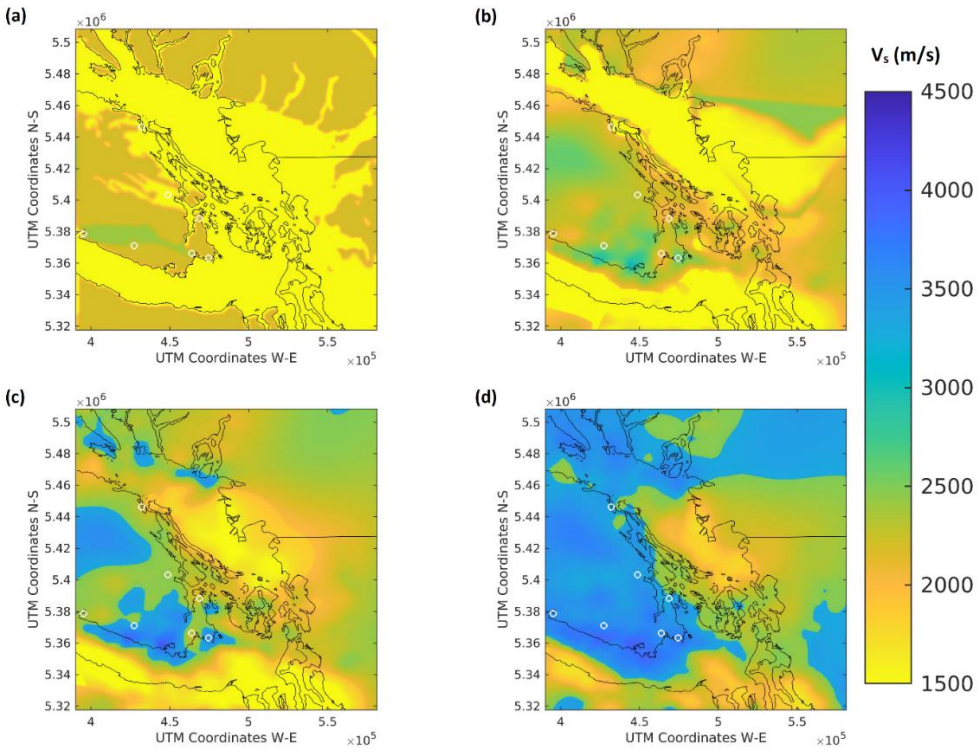

Figure 3.3. Depth slices from the Molnar (2011) modified Pacific Northwest velocity model for V_S at: **(a)** 0 m; **(b)** 500 m; **(c)** 1000 m; and **(d)** 3000 m depth. White circles denote 7 locations described in Figure 3.1.

Velocity depth profiles (Figure 3.4) of each waveform location are extracted from the physical structure (velocity) model. Shear wave velocities range between 1000 m/s and 4000 m/s with velocities increasing to ~2500 m/s to ~3500 m/s in the upper 1-3 km for each location. Victoria is the stiffest of all sites with the highest velocities in the upper 4 km. Velocities at > 10 km depth for all locations are between 3500 m/s to 4000 m/s to the base of the NA plate (~30 km depth).

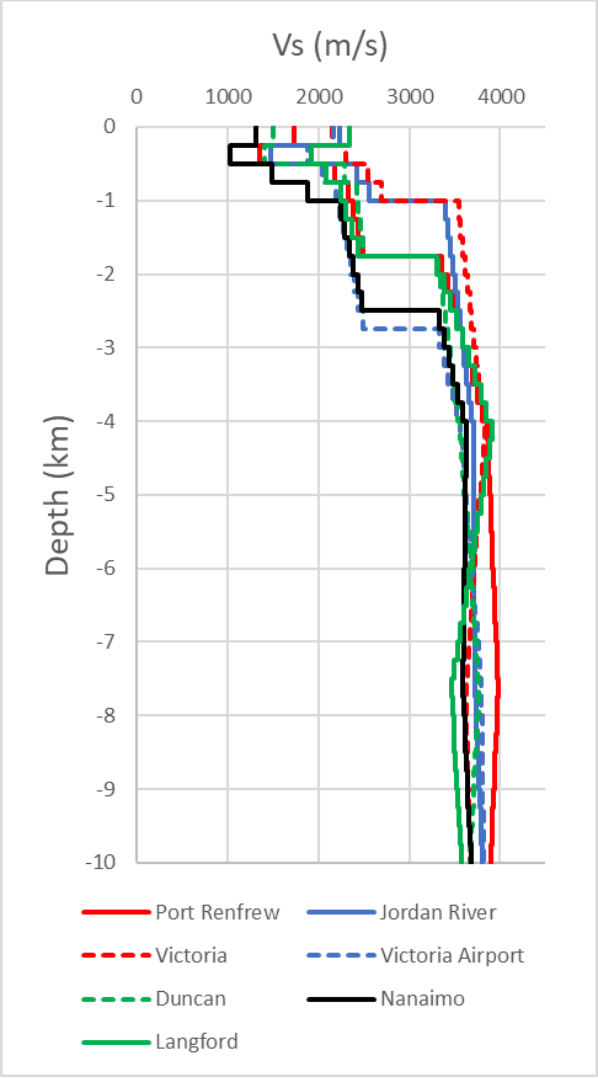

Figure 3.4. Velocity profiles (V_s) from 0 km to 10 km depth for the seven waveform locations expressed in Figure 3.1.

For this study, we extracted a 191 km by 191 km by 30 km portion of the Molnar (2011) Georgia basin velocity model centered over the LRVFZ and Greater Victoria (Table 3.1). The regional physical model used in this study is discretized into a uniform 250-m grid mesh with ~7.5 x 10^7 grid nodes.

Table 3.1: 3D Velocity Model Parameters

Parameter	Regional Model
Spatial discretization	250 m
Temporal discretization	0.015 s
Lowest V_P	1562.50 m/s
Lowest V_S	625.20 m/s
Lowest ρ	1674.36 kg/m^3
Number of grid nodes in the *x* direction	764 (191 km)
Number of grid nodes in the *y* direction	764 (191 km)
Number of grid nodes in the *z* direction	128 (32 km)
Number of time steps (simulation duration)	4668 (70 s)
Numerical averaging	Arithmetic
Boundary conditions	Cerjan
Real time simulation duration	~ 2 hours

3.2.1 Finite-Difference Methodology

The FD wave propagation scheme created by Olsen (1994) uses a physical model for the medium that is discretized into a uniform cubic mesh. The shortest shear wavelength of the grid must be sampled at a rate of 5 nodes per wavelength to minimize the effects of grid dispersion and grid anisotropy (Levander, 1988; Moczo et al., 2000). For computational feasibility, this limits minimum V_s to 625 m/s and caps the maximum

resolvable frequency at 0.5 Hz. Synthetic results that are measured above the resolvable-frequency limit become spectrally deficient which biases ground motion estimates near this cut off frequency (Day et al., 2008). To ensure stability in each simulation, the stability criterion should be less than the maximum resolvable frequency,

$$0.5 > \frac{C_{max} \times DT}{DX}, \tag{3.1}$$

where C_{max} is the highest encountered V_P, DT is the time discretization, and DX is the space discretization. The stability criterion value for all simulations is calculated to be 0.482.

Based on the staggered-grid FD method outlined by Graves (1996), the nodes of each cell can be expressed as wavefield variables and media (Lamé) parameters, with cell lengths defined as half the distance between two adjacent cell centers (Olsen, 1994). This means the equations for wave propagation within 3D, linear, isotropic elastic media are expressed as three velocity components and six stress components (Graves, 1996). In a staggered-grid method of simulation, the system is staggered both spatially and temporally. Therefore, velocities and stresses are updated independently which improves computational efficiency. The seismic source is applied to the FD grid by adding the moment tensor for an earthquake subfault ($-M_{ij}(t)$) divided by the cell volume ($V = dx^3$) to the stress tensor on the fault ($S_{ij}(t)$) at time t, where ij refers to a specific cell in the fault (Olsen, 2000).

The anelastic quality factor (Q) for viscoelasticity is incorporated independently for compression (P) and shear (S) waves with a coarse-grained implementation of memory variables (Day, 1998; Day and Bradley, 2001). Reflections from the boundaries of the model are minimized using absorbing boundary conditions (Clayton and Engquist, 1977) and a zone of highly attenuative material (Cerjan et al., 1985).

The two defining parameters for ground motion prediction are generally Q_S and V_S, as they govern the shear- and surface-wave amplitudes of the strongest ground motions (Brocher, 2007). From previously tested regional Q relations in Molnar et al. (2014a), there was little variation in predicted low-frequency ground motions (Olsen, 2003; Brocher, 2008; Frankel et al., 2009). Therefore, Q relations for stiff sediments in the Pacific Northwest from Frankel et al. (2009) were chosen by Molnar et al. (2014a) to be consistent with regional geology (Table 3.2).

Table 3.2. Q values for 3D visoelastic structure model

High Q_S model (low attenuation)	
$Q_s = 0.1643V_S - 14$	$V_S < 1$ km/s
$Q_s = 0.15V_S$	$V_S > 1$ km/s
$Q_P = 2Q_S$	

The Anelastic Wave Propagation (AWP) wave propagation code of Olsen, Day and Cui (ODC), termed AWP-ODC (version 1.1.2) was compiled for simulations on the "Richter" Lenovo ThinkStation at the University of Western Ontario which has an Octa-core Intel Xeon processor running at 3.50 GHz. Arithmetic numerical averaging (Olsen,

1994) with absorbing boundary conditions for a 20-grid cell padded zone of attenuative material are used in the regional model for the simulations. Arithmetic numerical averaging of ground motions is used due to the presence of water in the model, where V_S is set to 0. Simulations were calibrated on this computer system by first reproducing the results found by Molnar et al. (2014a) for a **M** 6.8 Nisqually shallow crustal earthquake rupture scenario. Original simulated waveforms from Molnar et al. (2014a) were validated against recorded waveforms from the **M** 6.8 Nisqually earthquake.

3.3 Earthquake Source Models

The rupture characteristics of a large LRVFZ earthquake, including rupture length, direction of rupture, locations of maximum slip, etc. are relatively unknown. We develop a suite of 24 deterministic **M** ~7 LRVFZ rupture models to determine the impact to motions in southern Vancouver Island from varying rupture characteristics. These 24 **M** 7 LRVFZ scenarios are based on the slip distribution of two real earthquakes, the 2010 **M** 7 Darfield, New Zealand earthquake and the 2010 **M** 7 Haiti earthquake (Table 3.3 and see Data and Resources section). The slip models of these empirical earthquakes were chosen based on similarities in exposure to Greater Victoria and fault structure to the LRVFZ, respectively. The 2010 **M** 7 Darfield, New Zealand earthquake occurred on a previously unidentified fault approximately 40 km west of the populated city of

Christchurch (Potter et al., 2015). In 2010, Christchurch had a similar population to Greater Victoria of 370,000 residents. No casualties resulted due to the 4:36 AM time of rupture (EERI Report, 2010). Lateral spreading and liquefaction damage in Christchurch greatly contributed to the total estimated losses of $4 billion New Zealand dollars (approximately $3 billion Canadian dollars in November 2010). Damages in Victoria from a nearby earthquake have been suggested to be analogous to a "Darfield-like" rupture due to similarities in infrastructure and predicted loss estimates (Zaleski, 2014; Ventura and Bebamzadeh, 2016; Morell et al., 2017). The 2011 **M** 6.2 aftershock occurred immediately below Christchurch (10 km depth) and resulted in greater structural and liquefaction-related damage and is therefore more widely known but is not simulated here.

The 2010 **M** 7 Haiti earthquake was one of the most destructive earthquakes in recorded history due the large magnitude located near a region with a large population on or below the poverty line, and infrastructure built to low levels of earthquake preparedness (Eberhard et al., 2010). There are vast differences between Haiti's and Greater Victoria's economic status or building codes; however, similarities in paleoseismicity and fault geology can be drawn which make simulating the Haiti event a compelling choice. Haiti's rupture occurred on or near the mapped Enriquillo fault west-southwest of Port-au-Prince; a strike-slip fault system that separates two major geologic units of basaltic rocks to the south, and marine sedimentary rocks to the north

(Eberhard et al., 2010). This fault is one of the principal plate boundary faults between the Caribbean and North American tectonic plates and has been rather dormant (Eberhard et al., 2010). Since the installation of a modern seismic network in 1964, Port-au-Prince has only experienced one earthquake greater than **M** 4, with additional events occurring 100 km to the west (Eberhard et al., 2010). Other reports suggest the main **M** 7 Haiti rupture occurred along the Léogâne fault which lies subparallel to the Enriquillo fault, resulting in a transpressional rupture of the fault (Calais et al., 2010). Except for the LRVFZ separating igneous and metamorphic rocks, the LRVFZ has a similar strike, transpressional fault type, and location within an adjacent crustal system like the Haiti Léogâne fault.

Table 3.3. Modified Earthquake Source Model Characteristics

Parameter	Darfield Model	Haiti Model
Parent slip model	NEIC (Hayes 2010a)	NEIC (Hayes 2010b)
Subfault size	4.0×10^6 m^2 (2000 m × 2000 m)	7.5×10^6 m^2 (3000 m × 2500 m)
Strike (°)	292.5	292.5
Dip (°)	70	70
Rise Time (s)	1.96	2.45
Seismic Moment (N · m)	3.02×10^{19}	5.15×10^{19}
M	6.92	7.07

The LRVFZ is modelled with a 66 km fault length and 30 km down dip width towards the north east. The fault strikes east to west from Port Renfrew for approximately 40 km where it bends south east at Leechtown towards Langford (Figure 3.1).

Computationally, this bend is included and does not impact the AWP-ODC software's ability to calculate ground-motion simulations along the LRVFZ. The source models of Darfield and Haiti are modified (resized) to be within the limits of the LRVFZ rupture model. The 64 km by 28 km Darfield fault plane is discretized into 448 subfaults (Figure 3.5a), and the 66 km by 30 km Haiti fault plane is discretized into 264 subfaults (Figure 3.5b). The discretization is based on the size of the subfaults provided in the parent slip models (see Table 3.3). The slip that is reported in each subfault of the source model is converted to seismic moment (M_0) for the FD simulations through

$$M_0 = \mu DA, \tag{3.4}$$

where μ is equal to the physical model shear modulus along the LRVFZ in Pascal, D is the average slip of each subfault in metres, and A is the area of each subfault in m^2 (Sommerville et al., 1999). The longer Darfield slip model was clipped so the dimensions would fit within the LRVFZ fault plane. Removal of these Darfield 'edge' sub-faults reduced the **M** from 7 to the simulated **M** of 6.9. Darfield has a greater number of smaller subfaults with lower slip values per subfault; however, most of the seismic moment (slip) occurs within the upper 10 km of the original source model. In contrast, Haiti is simulated with higher slip values on larger subfaults with most of the slip concentrated in a particular quadrant to ~20-km depth.

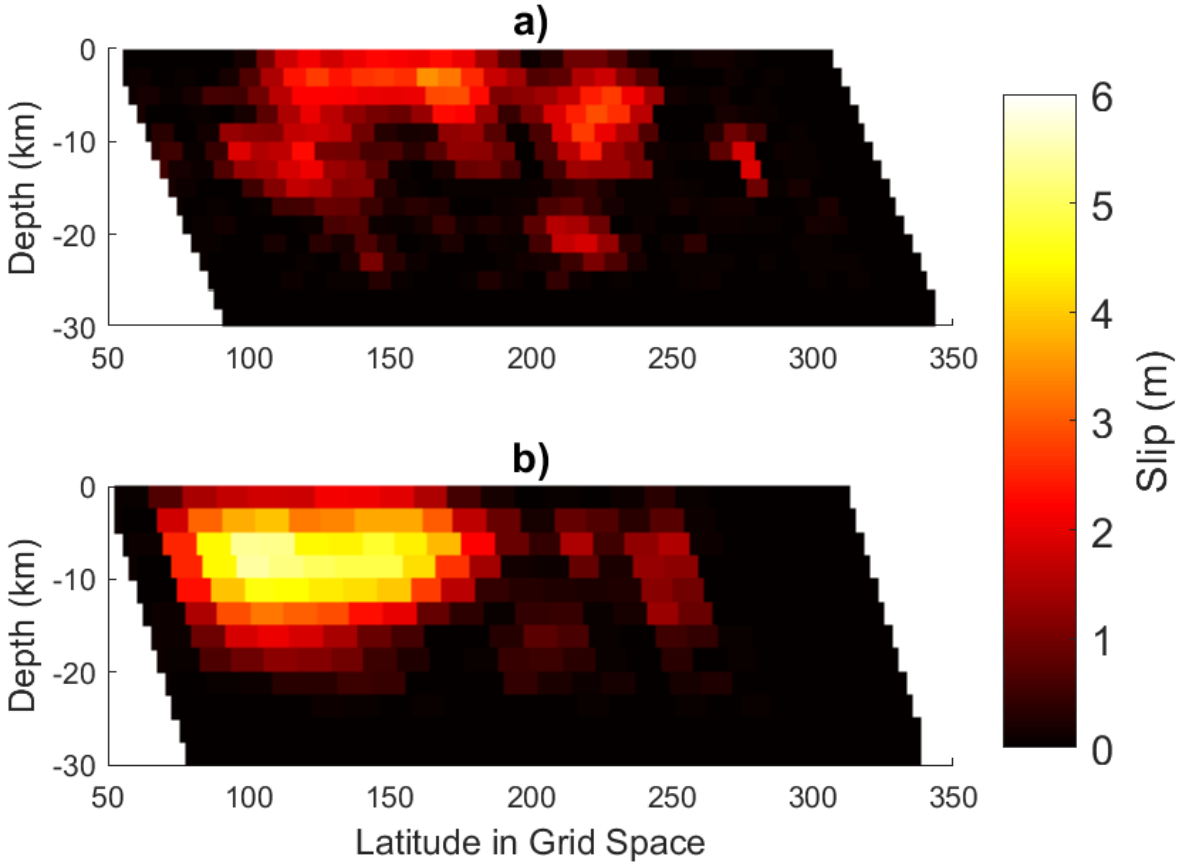

Figure 3.5. LRVFZ scenario slip distribution models of the **(a)** Darfield slip model with 448 subfaults over 64 km by 28 km area and **(b)** Haiti slip model with 264 subfaults over 66 km by 30 km area. Orientation is west to east (north is into the page) with Victoria located at approximately latitude grid point 300.

A moment tensor represents the focal mechanism of an earthquake and mathematically describes how the amplitudes of seismic waves vary as they radiate away from a source through 9 different force couples inclusive of positive or negative forces in the three (x, y, z) directions. The moment tensor rate of each subfault (Figure 3.6) is characterized here by a half-cosine function with a constant rise time of ~2.0-2.5 s (Table 3.3). The rise time (t_R) for each **M** ~7 earthquake scenario was derived through the Sommerville et al. (1999) relation to seismic moment (M_0):

$$t_R = 1.48 \times 10^{-11} \times {M_0}^{0.42}. \quad (3.3)$$

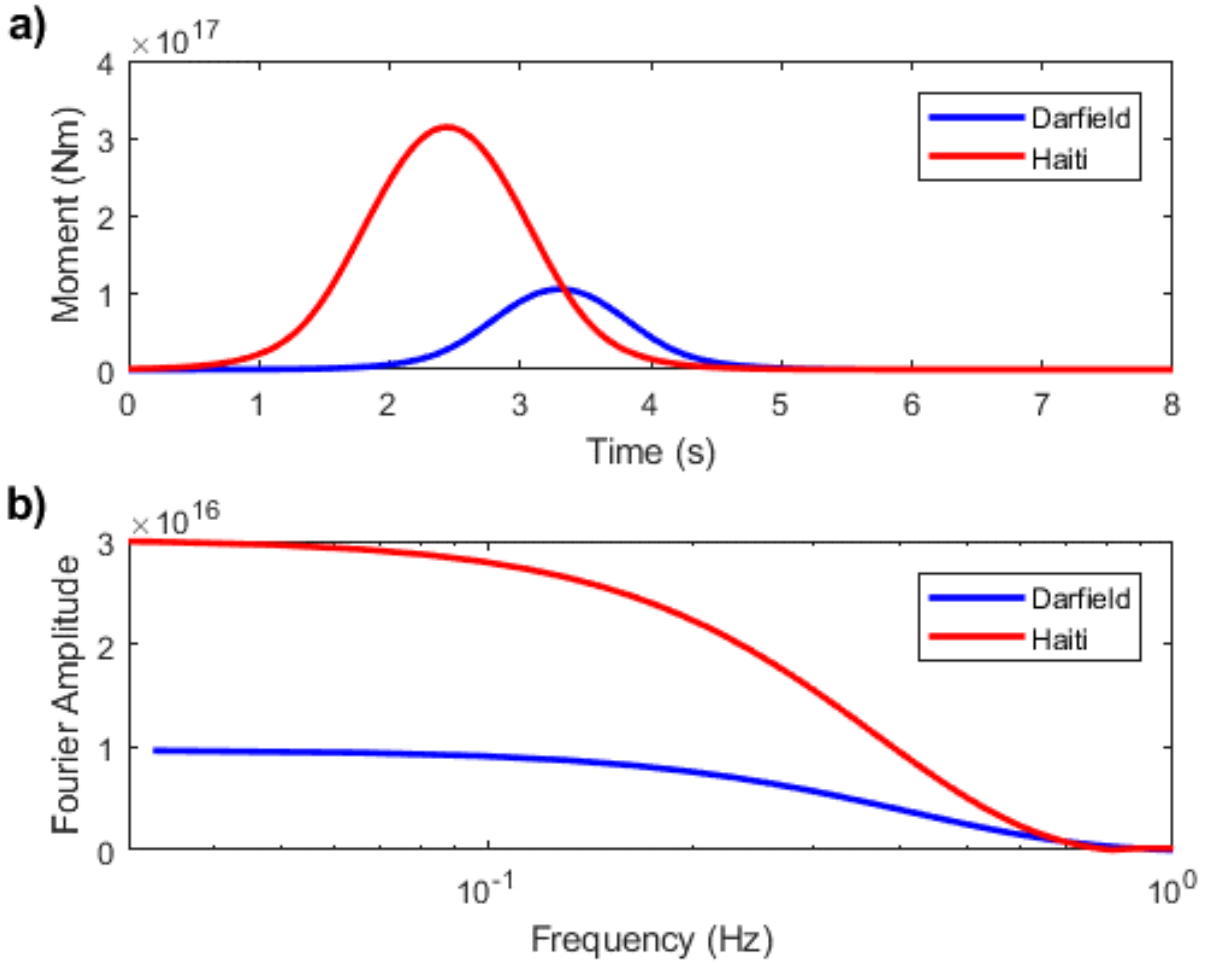

Figure 3.6. (a) Moment rate function of the M_{xx} component. **(b)** Amplitude spectra of moment rate function in a).

3.4 Simulated Finite-Difference Scenarios

24 total FD simulations are performed to examine ground shaking in southern Vancouver Island and Greater Victoria from potential large magnitude LRVFZ rupture scenarios. Previous wave propagation simulations have documented that predicted

ground motions are strongly dependent on rupture length, rupture directivity, and slip distribution (Aagaard et al., 2010b). Ground motions from simulations with varying rise time and rupture speed are less sensitive to these changes (Aagaard et al., 2010a; 2010b).

Each of the two empirical-based **M** ~7 earthquake rupture models are simulated with four different slip distribution patterns (varying the location of maximum slip, rotating the slip distribution pattern), as well as varying the direction of rupture propagation and hypocenter (rupture initiation) location. Four different rupture scenarios of each Darfield and Haiti slip distribution model are generated by reflecting the slip pattern along the x- and/or y- axes of the fault such that patches with the greatest slip occur in the upper west, upper east, lower west, and lower east quadrants of the fault (Figure 3.7). These 4 rotated slip distribution patterns capture changes in slip distribution with depth. The rupture direction is then changed in all four scenarios such that rupture propagates west-to-east or east-to-west to explore the effects of rupture directionality. A uniform 2.5 km/s rupture velocity is used, which is ~80% of the local V_S (Graves and Pitarka, 2004) near the LRVFZ. The hypocentre location (rupture initiation) is also varied from the surface grid corner of each rupture direction (i.e., upper west grid cell for west-to-east rupture propagation) to the location of maximum slip, which is rotating from near surface to depth in the 4 slip models).

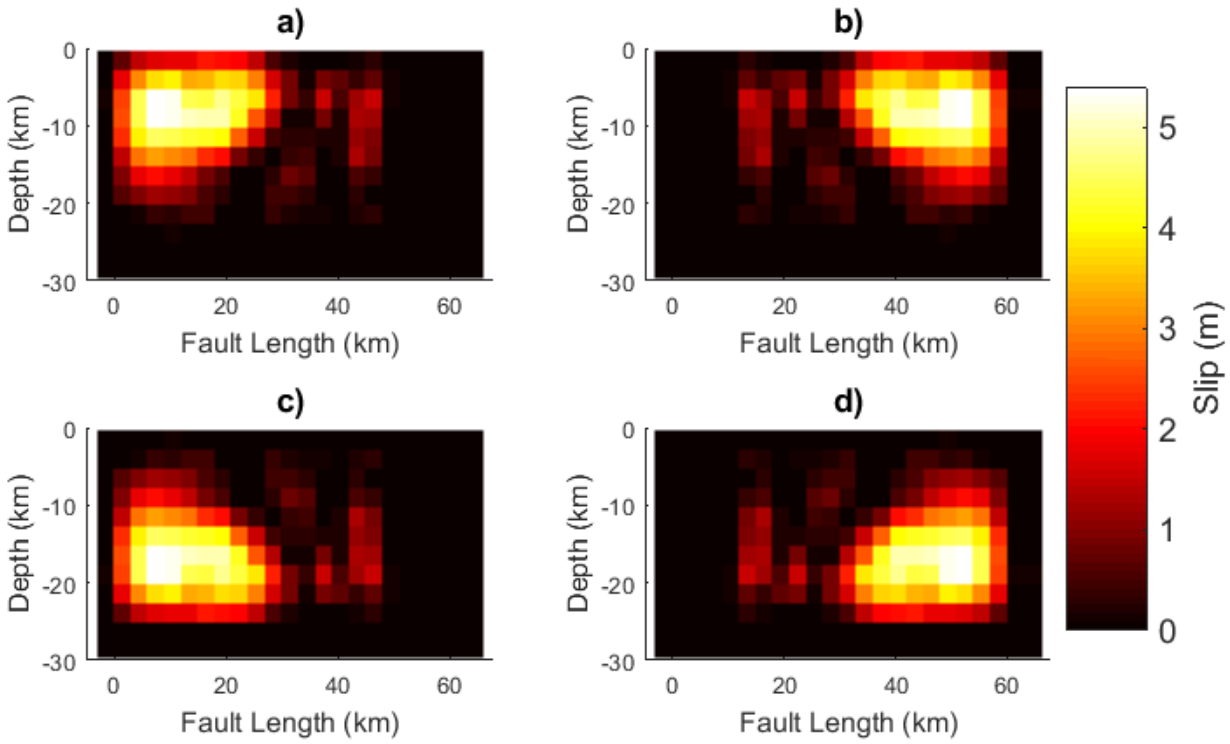

Figure 3.7. Example of how the Haiti slip model is rotated by reflection along the x- and/or y- axes of the fault. Maximum slip is relocated into the **(a)** top west quadrant (original slip model), **(b)** top east quadrant, **(c)** bottom west quadrant, and **(d)** bottom east quadrant.

3.5 Predicted long-period ground motions

To ensure frequencies less than the maximum resolvable frequency (≤ 0.5 Hz) are present in PGV maps and measured waveforms, a lowpass first-order Butterworth filter with a cut off frequency of 0.5 Hz was applied to the input moment tensor and resulting waveforms. The filter was applied once forwards and once backwards to remove high frequency energy with no phase shifting of the waveform. The simulated PGV values in cm/s were converted to MMI estimates using the relation of Worden et al. (2012),

$$\mathrm{MMI} = 2.89 + 3.16 \log(\mathrm{PGV}). \quad (3.5)$$

This relation is based on shallow California earthquakes for use in generating global earthquake USGS ShakeMaps.

3.5.1 Darfield Rupture Scenarios

Figure 3.8 shows predicted ShakeMaps for southern Vancouver Island based on different rupture directions and orientations of the **M** 6.9 Darfield slip distribution model. Consistent in all eight scenarios, areas of greatest ground shaking are focused in the Georgia Strait, Juan de Fuca Strait, and directly over sections of the LRVFZ. High ground motions within the two Straits are related to site amplification effects by the lower velocity sediments (Molnar et al., 2014a; 2014b). Varying the depth of maximum slip yields greater MMI values when source model slip is focused within the upper 10 km of the fault model (Figure 3.8a, b and e, f) compared to slip distributions at greater depths (Figure 3.8c, d and g, h). MMI VIII (very strong shaking) levels are reached in the Georgia Strait and directly above the LRVFZ. Changes in rupture directionality greatly changes the areas where greater ground shaking occurs. With a west to east rupture (Figure 3.8a-d), more ground shaking is observed west of Jordan River and toward the Victoria airport, with moderate shaking (MMI V) extending into the Georgia Strait and as far as Greater Vancouver. East to west rupture scenarios (Figure 3.8e-h) directs greater ground

shaking eastward to Victoria airport and northward towards Nanaimo and northern sections of the Georgia Strait.

Waveforms from the seven selected locations are presented in Figure 3.9. Each waveform was simulated for a total of 70 seconds to ensure that any simulated ground motions from a rupture scenario would fully propagate through southern Vancouver Island. The maximum PGV values from each waveform are listed in Table 3.4. The highest predicted PGV values occur at Jordan River with 17.15 cm/s (MMI VI) from a westward rupture direction and 13.91 cm/s (MMI VII) from an eastward rupture direction. This site also has the highest average ground shaking between all eight Darfield scenarios of 6.79 cm/s (MMI V). Because this location is very close to the surface expression of the LRVFZ, it is expected to receive the highest ground motions. Understanding how high the ground motions could be at this location are of interest due to the presence of two hydroelectric dams at the Diversion and Elliot Lake reservoirs nearby (Morell et al., 2017; 2018).

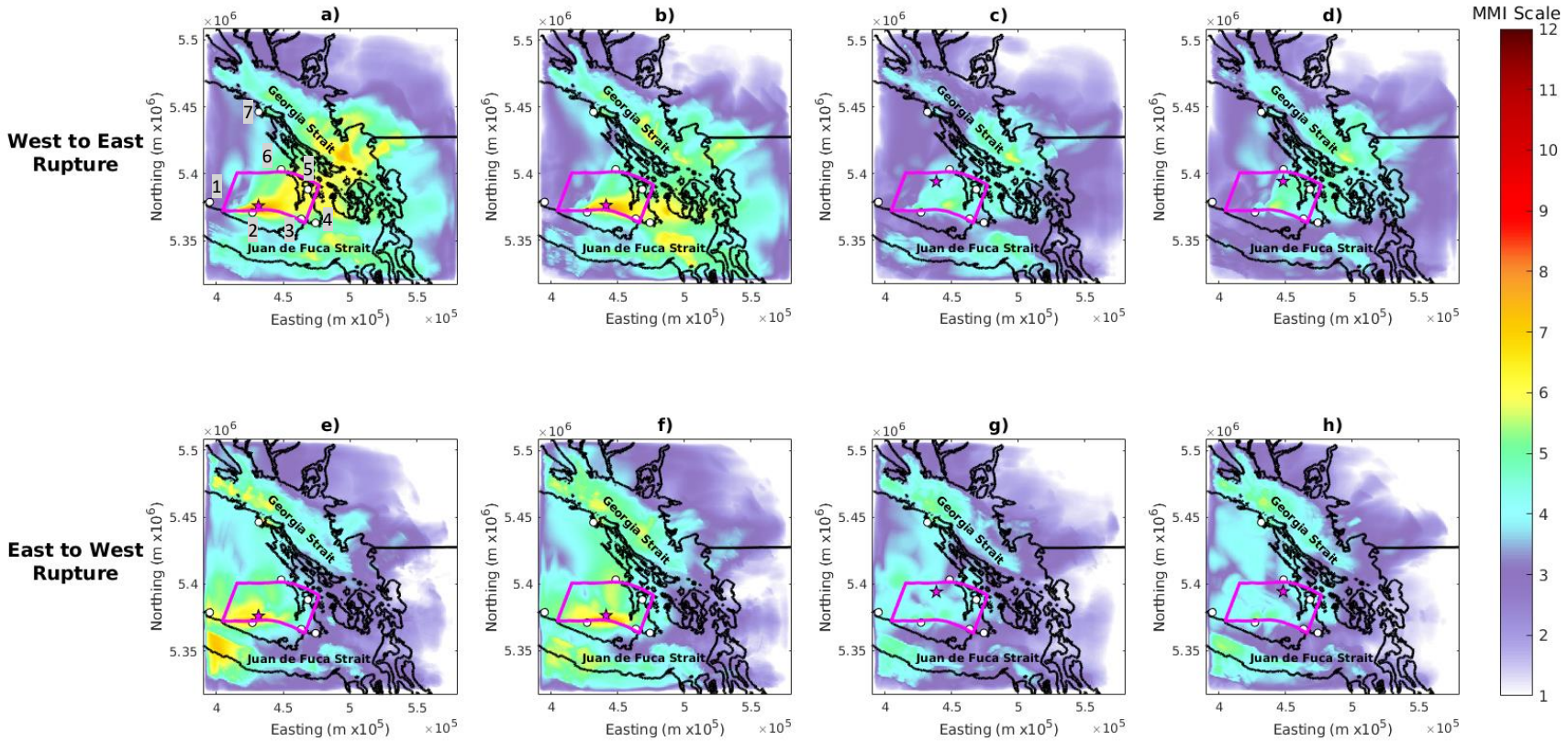

Figure 3.8. Predicted long-period ground motion intensities in southwestern British Columbia from modified **M** 6.9 Darfield scenarios. Each column represents a different location of Darfield source model slip; magenta stars show the locations of maximum slip in the fault model. White dots represent waveform locations, with numbers of the location shown in subplot **(a)**, from Figure 3.1. The magenta box outlines the surface projection of the LRVFZ.

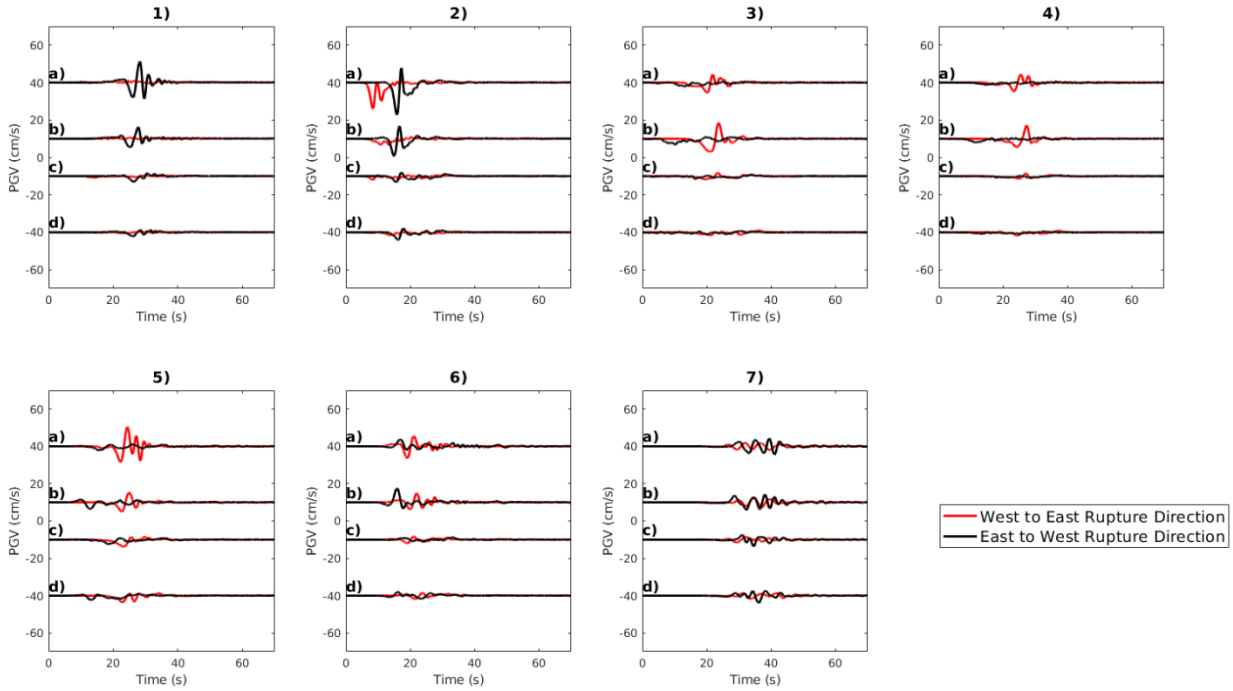

Figure 3.9. Synthetic waveforms extracted at seven locations (see Figure 3.8) from four modified **M** 6.9 Darfield rupture scenarios with maximum slip in **(a)** upper west quadrant, **(b)** upper east quadrant, **(c)** lower west quadrant and **(d)** lower east quadrant.

Table 3.4. Predicted maximum PGV (cm/s) from Darfield Source Models

Location	West to East Rupture (cm/s)				East to West Rupture (cm/s)			
	a)	**b)**	**c)**	**d)**	**e)**	**f)**	**g)**	**h)**
(1) Port Renfrew	1.04	0.78	0.83	0.63	11.26	6.15	2.90	2.18
(2) Jordan River	13.91	3.32	1.87	1.52	17.15	9.29	3.12	4.15
(3) Langford	5.48	8.44	1.73	1.64	2.12	3.17	1.46	1.15
(4) Victoria	4.61	7.01	1.43	1.70	1.20	2.00	0.68	0.84
(5) Victoria Airport	10.33	5.06	3.80	3.51	2.12	3.54	2.32	2.34
(6) Duncan	6.33	4.80	1.98	1.87	3.72	7.49	1.21	1.89
(7) Nanaimo	1.99	2.70	1.50	1.62	4.42	4.15	3.49	3.89

Note: See Figure 3.8 for corresponding scenarios and locations.

Other interesting synthetic waveforms are observed at Victoria Airport (Location 5) and Nanaimo (Location 7) with respect to rupture direction. Noticeable amplification (PGV 10.33 cm/s; MMI VI) that is between 2.04 and 4.87 times greater than any other scenario at Victoria Airport is observed in scenario A with a west to east rupture direction (Figure 3.8a, Figure 3.9, waveform 5a). Looking at the velocity profile at Victoria Airport (Figure 3.4), there is a sharp impedance contrast at a depth of 2.75 km. It is hypothesized that rupture directionality and the location of maximum slip in the source model of scenario A directs larger amplitude waveforms towards the airport which is then amplified by the thicker low velocity sediments at the site. When rupture direction is westward, the northern city of Nanaimo experiences ground motions that are on average 2.05 times greater in simulations with eastward rupture direction, resulting in an average measured PGV of 3.99 cm/s (MMI IV) compared to 1.95 cm/s (MMI III). Nanaimo has a similar velocity profile to Victoria Airport where a sharp impedance contrast at 2.75 km depth would amplify ground motions. This is in addition to the westward rupture direction focusing waveforms north towards Nanaimo compared to eastward ruptures which focus motions away from Nanaimo and more towards Vancouver (Figure 3.8).

3.5.2 Haiti Rupture Scenarios

Figure 3.10 presents predicted ShakeMaps from **M** 7 Haiti- rupture earthquake scenarios. The Haiti source model has a slightly higher seismic moment than Darfield and a greater amount of slip focused into a more concentrated area (Figure 3.6). MMI

values from the **M** 7 Haiti rupture are therefore 1.11 times larger on average than **M** 6.9 Darfield motions between all seven waveform locations. Ground shaking distribution patterns from the Haiti rupture scenarios are generally similar to the Darfield rupture scenarios. An eastward rupture direction focusses ground shaking in the east, towards Vancouver and into the southern section of the Georgia Strait where basin sediments amplify ground motions. In contrast, westward ruptures direct more energy west of Victoria and north towards the northern sections of Georgia Strait and Nanaimo. Greater average ground shaking is observed across the southern section of Vancouver Island. Slip located in the upper west quadrant with an eastward rupture direction (Figure 3.10b) generates the largest ground shaking at Victoria with a PGV of 19.38 cm/s (MMI VI) which is 1.97 to 28.5 times greater than any other Haiti or Darfield rupture scenario.

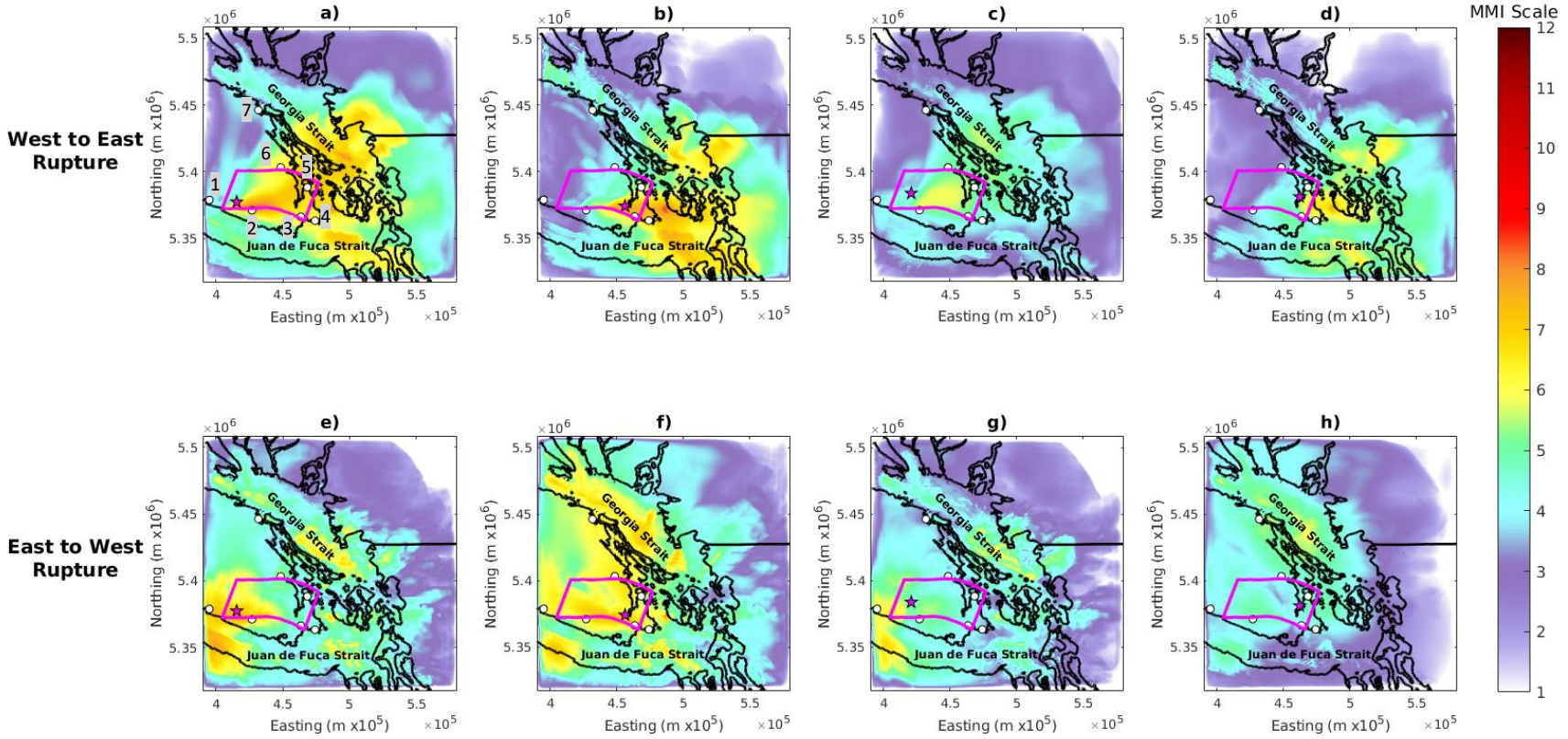

Figure 3.10. Predicted long-period ground motion intensities in southwestern British Columbia from modified **M** 7 Haiti scenarios. Each column represents a different location of Haiti source model slip; magenta stars show the locations of maximum slip in the fault model. White dots represent waveform locations, with numbers of the location shown in subplot **(a)**, from Figure 3.1. The magenta box outlines the surface projection of the LRVFZ.

The largest PGV value predicted by any Haiti scenario is again at Jordan River with a PGV of 25.26 cm/s (Figure 3.10a; Figure 3.11, waveform 2a), correlating to very strong shaking (MMI VII). Jordan River is not the only location to be exposed to very strong shaking (MMI VII) in a Haiti-type rupture. PGV values greater than 19.9 cm/s (MMI VII) are also generated at Victoria airport (Table 3.5). These high predicted motions are due to rupture scenarios with eastward rupture direction and shallow slip.

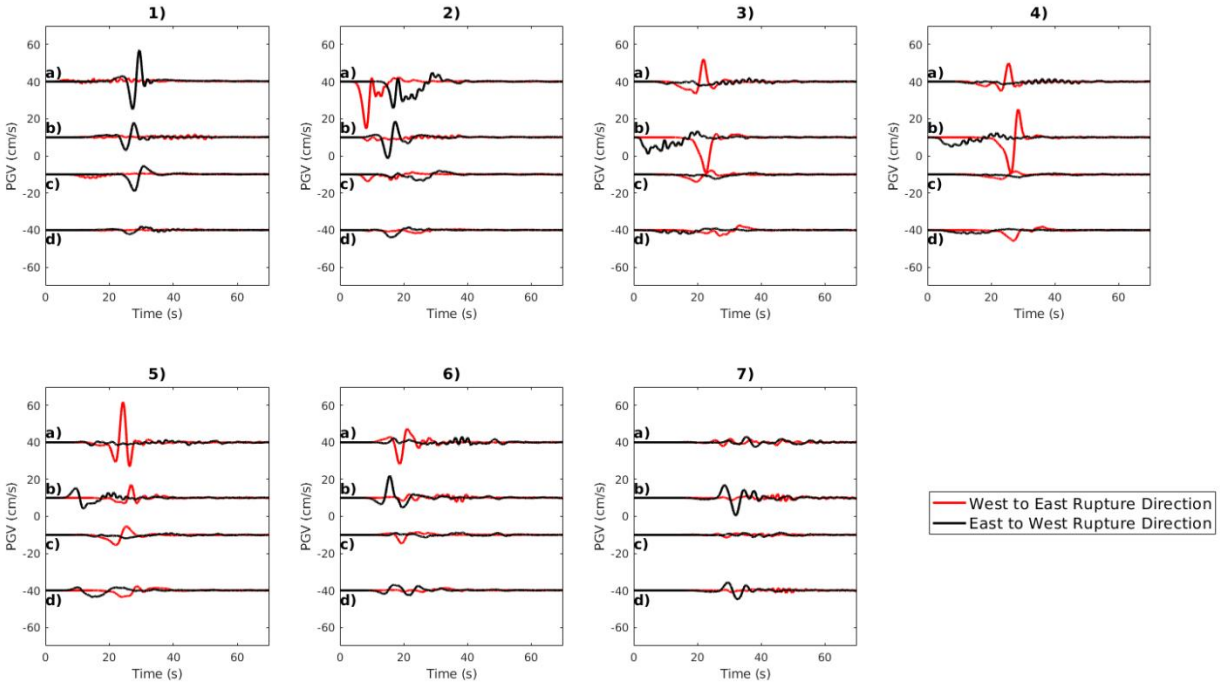

Figure 3.11. Synthetic waveforms extracted at seven locations (see Figure 3.10) from four modified **M** 7 Haiti rupture scenarios with maximum slip in **(a)** upper west quadrant, **(b)** upper east quadrant, **(c)** lower west quadrant and **(d)** lower east quadrant.

Table 3.5. Predicted maximum PGV (cm/s) from Haiti Source Models

Location	West to East Rupture (cm/s)				East to West Rupture (cm/s)			
	a)	**b)**	**c)**	**d)**	**e)**	**f)**	**g)**	**h)**
(1) Port Renfrew	1.86	1.58	2.14	0.65	16.94	7.82	8.92	2.18
(2) Jordan River	25.26	1.91	3.77	1.69	14.34	11.24	3.47	3.88
(3) Langford	12.06	19.18	4.00	3.15	2.20	9.04	2.36	2.07
(4) Victoria	9.86	19.38	2.48	5.74	1.48	5.21	1.6	2.03
(5) Victoria Airport	21.77	7.11	5.47	3.54	1.72	5.82	1.87	3.61
(6) Duncan	11.77	2.20	4.63	1.33	3.02	11.94	1.40	2.94
(7) Nanaimo	2.03	2.19	1.44	1.43	3.03	9.52	1.25	4.76

Note: See Figure 3.10 for corresponding scenarios and locations.

The site effects that are observed at Victoria airport in scenario A of the Darfield rupture are amplified in scenario A of the Haiti rupture. Lower velocity sediments present in the velocity model and the difference in slip between the two ruptures increase ground shaking by 2.11 with Haiti scenario a (Figure 3.10a; Figure 3.11, subplot 5) over Darfield scenario a (Figure 3.8a; Figure 3.9, subplot 5). Scenario B with an eastward rupture direction (Figure 3.10b) increases PGV at both Langford and Victoria by 2.27 and 2.76, respectively, over Darfield (Figure 3.8b). Ground shaking at Nanaimo from an east to west rupture direction that are consistently present in the Darfield scenarios as MMI IV are more varied in the Haiti scenarios; ranging from MMI III to V.

3.5.3 Hypocenter Rupture Scenarios

Figure 3.12 presents predicted ShakeMaps from **M** 6.9 Darfield and **M** 7 Haiti-rupture earthquake scenarios where the hypocenters of each rupture are centered on the

location of maximum slip (termed max-slip hypocentre scenarios) with rupture direction radiating away from the hypocenter. Max-slip hypocentre rupture scenarios increases MMI values from the **M** 6.9 Darfield rupture scenarios (section 3.5.1) and **M** 7 Haiti rupture scenarios (section 3.5.2) on average by 1.12 and 1.22 times, respectfully for all seven measured locations. The change in hypocentre location results in new ground shaking distribution patterns compared to patterns observed with varying rupture directions. Seismic waves radiate away from the hypocenter regardless of the hypocenter location in the upper or lower quadrants of the fault. Shallow max-slip hypocenter scenarios (Figure 3.12a, b, e, and f) focus higher ground motions across southern Vancouver Island and tend to extend further north towards Vancouver and the Georgia Strait. Deep max-slip hypocenter scenarios (Figure 3.12c, d, g, and h) direct higher ground motions towards the Juan de Fuca Strait. These max-slip hypocentre rupture scenarios generate higher ground shaking in Victoria on average with an average PGV of 8.12 cm/s (MMI V). The greatest ground shaking in Victoria occurs from a Haiti rupture scenario where the max-slip hypocenter is located in the upper west quadrant of the fault (Figure 3.12f) with a PGV of 18.81 cm/s (MMI VI).

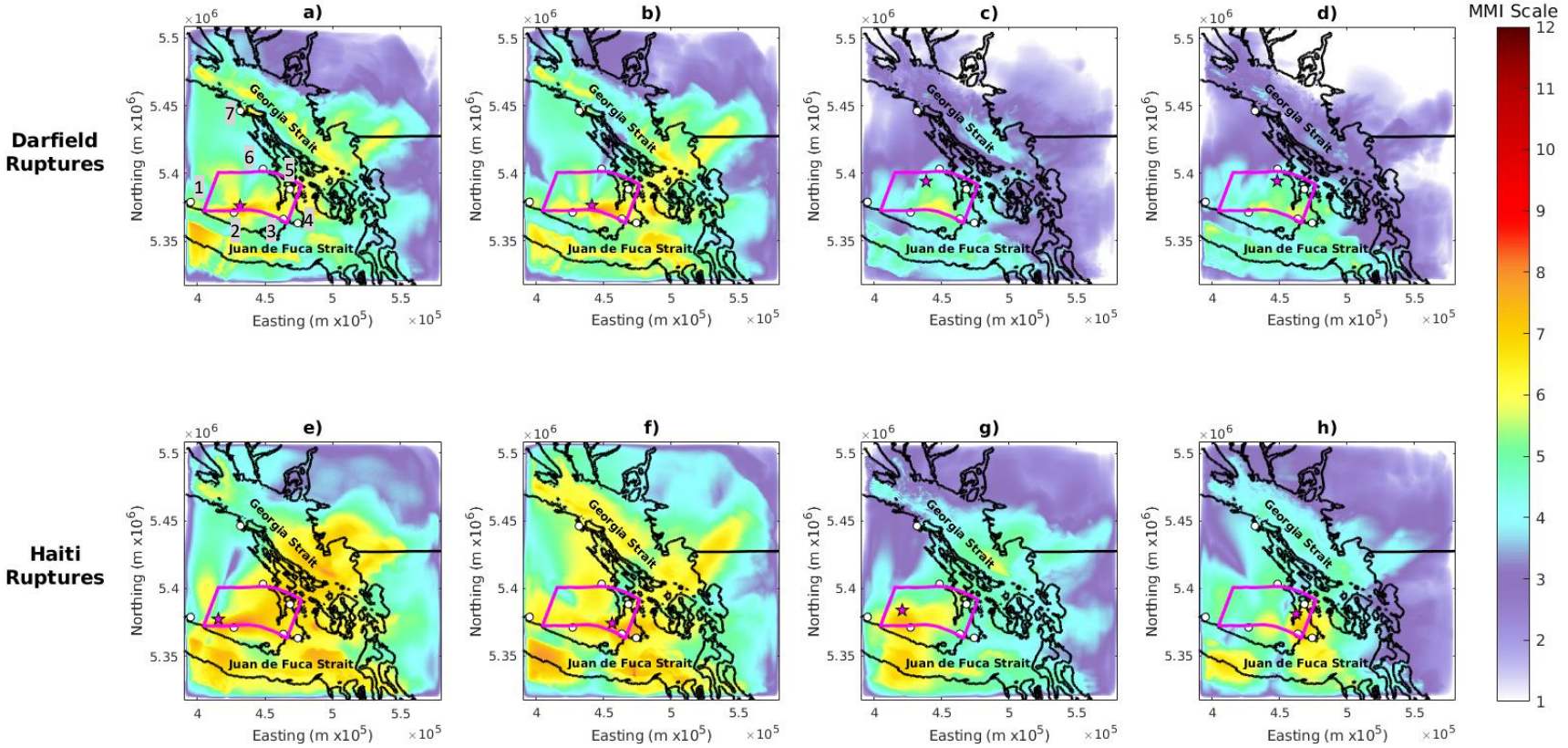

Figure 3.12. Predicted long-period ground motion intensities in southwestern British Columbia from modified **M** 6.9 Darfield (top row) and **M** 7 Haiti (bottom row) rupture scenarios. Each column represents a different hypocenter and maximum slip location of the source models; magenta stars show the locations of hypocenters and maximum slip in the fault models. White dots represent waveform locations, with numbers of the location shown in subplot **(a)**, from Figure 3.1. The magenta box outlines the surface projection of the LRVFZ.

The largest PGV value is at Langford with a PGV of 32.89 cm/s (Figure 3.12f; Figure 3.13, waveform 3b), correlating to very strong shaking (MMI VII). This is the highest predicted ground shaking of all 24 rupture scenarios. This can be attributed to the hypocenter and maximum slip being located very close to the city. Langford is not the only location to be exposed to very strong shaking (MMI VII) due to max-slip hypocentre ruptures. PGV values greater than 19.9 cm/s (MMI VII) are also generated at Jordan River and Victoria airport (Table 3.6). These high predicted motions are due to Haiti-type rupture scenarios.

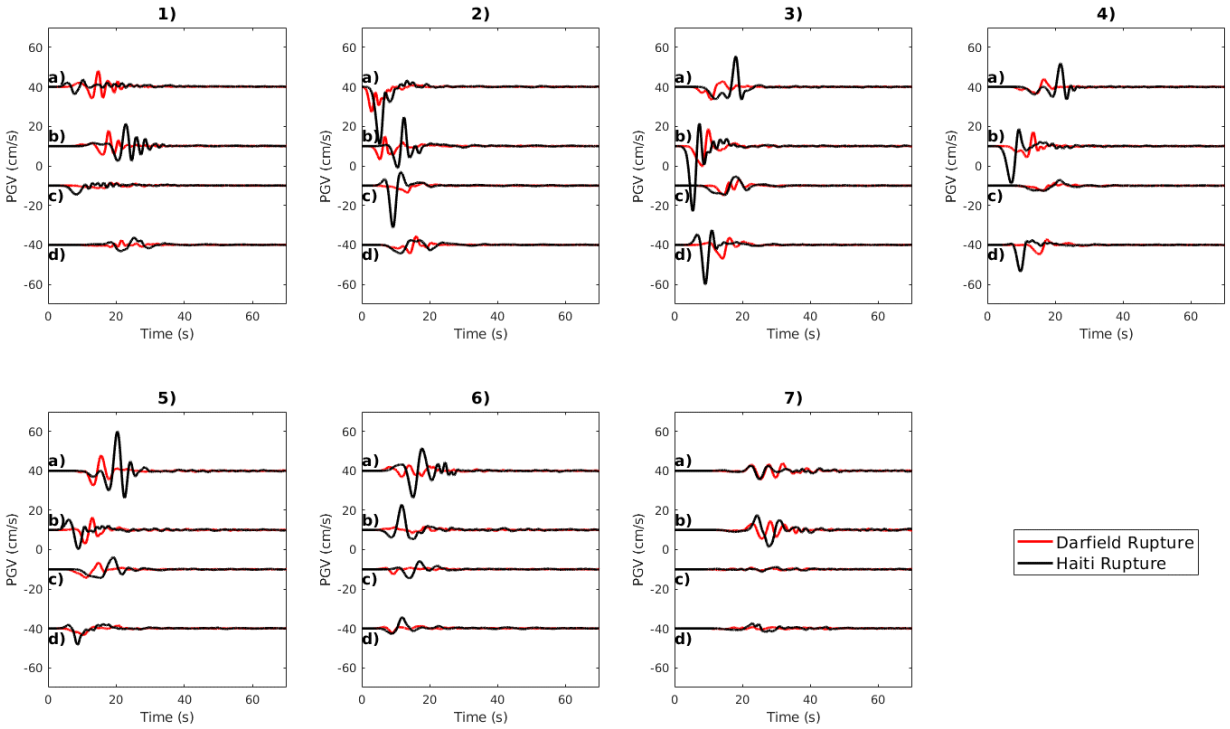

Figure 3.13. Synthetic waveforms extracted at seven locations (see Figure 3.12) from modified **M** 6.9 Darfield and **M** 7 Haiti rupture scenarios with hypocenter and maximum slip in **(a)** upper west quadrant, **(b)** upper east quadrant, **(c)** lower west quadrant and **(d)** lower east quadrant.

Table 3.6. Predicted maximum PGV from Max-Slip Hypocenter Rupture Scenarios

Location	Darfield Rupture (cm/s)				Haiti Rupture (cm/s)			
	a)	**b)**	**c)**	**d)**	**e)**	**f)**	**g)**	**h)**
(1) Port Renfrew	8.01	7.78	1.50	2.37	3.64	11.19	4.46	3.68
(2) Jordan River	12.69	6.73	3.58	4.36	29.08	14.6	21.19	4.27
(3) Langford	6.56	10.23	4.85	6.99	15.43	32.89	4.63	19.96
(4) Victoria	3.89	7.09	2.47	4.64	11.79	18.81	2.84	13.44
(5) Victoria Airport	7.71	6.96	4.19	3.29	19.98	9.64	6.1	8.31
(6) Duncan	3.12	1.63	2.48	2.21	13.57	12.68	4.57	5.62
(7) Nanaimo	4.25	4.47	0.93	0.77	4.31	8.50	1.23	2.53

Note: See Figure 3.12 for corresponding scenarios and locations.

Haiti rupture scenarios generate ground shaking that is on average 1.21 times greater than Darfield rupture scenarios and more locations have ground shaking intensities that are higher than MMI VII. Most notably, the proximity of Langford to the hypocenter in scenario f (Figure 3.12f, Figure 3.13 subplot 3) generated the highest measured ground shaking out of any of the seven measured locations. This was 1.13 times greater than the highest measured value at Jordan River (29.08 cm/s; MMI VII) and 1.64 times greater than any other observed ground shaking at Langford (19.96 cm/s; MMI VII). Rupture scenarios where hypocenter was varied also tended to generate higher ground shaking intensities regardless of the depth of the hypocenter. For example, Haiti-type rupture scenarios d and h from section 3.5.2 have maximum slip located in the same location as scenario h of section 3.5.3, but the rupture direction was changed. These two scenarios only generated a maximum ground shaking value of 3.15 cm/s (MMI IV) for

Langford. However, when the hypocenter is located in the same location as maximum slip, Langford experiences ground shaking with a PGV of 19.96 cm/s (MMI VII) or 6.33 times greater shaking for that location.

3.6 Discussion and Conclusions

We performed low frequency (≤ 0.5 Hz) or long period (≥ 2 sec) 3D wave propagation simulations of potential LRVFZ rupture scenarios using the AWP-ODC FD scheme (version 1.1.2; Olsen, 1994) to examine ground shaking in southern Vancouver Island, including Port Renfrew, Jordan River, Langford, Victoria, the Victoria airport, Duncan, and Nanaimo. The base elastic physical model is a modified version of the Stephenson (2007) Pacific Northwest 3D velocity model by Molnar (2011; Molnar et al., 2014a; 2014b). We modified the slip distribution models of the 2010 **M** 7 Darfield and 2010 **M** 7 Haiti earthquakes to create 24 unique rupture scenarios with varying slip distribution pattern, rupture propagation direction and hypocentre location. These source models were superimposed to be within the bounds of a consistent LRVFZ fault geometry with 66 km length, 30 km width, and 70° NNE dip (Morell et al., 2017; 2018). The suite of source rupture models were generated by transforming the parent slip distributions with reflections along the x- and y- axes to create four rupture models, each with original slip rotated into a different quadrant of the fault. Rupture direction and

hypocenter location were varied such that all four source models for both earthquake scenarios were simulated with rupture starting in the upper west or east corner subfault, or at the location of maximum slip and radiating away from the hypocenter to create the 24 unique scenarios. The LRVFZ has the potential to create very strong shaking (MMI VII) at three of the seven locations on Vancouver Island depending on the rupture direction, slip distribution in the source rupture model, and hypocenter location. When rupture direction was changed, shallower slip distributions (slip concentrated in the upper 10 km) created the greatest ground shaking at surface with eastward ruptures generating higher ground motions within southern parts of the Georgia Strait and Greater Victoria. Westward ruptures generated ground motions with greatest amplitude at Nanaimo and northern parts of the Georgia Strait, and in the western sections of the Juan de Fuca Strait near Port Renfrew. Jordan River, where two hydroelectric dams occur near the fault, is exposed to the highest PGV values with shallow ruptures; averaging ~12 cm/s between the Darfield and Haiti scenarios (MMI VI) and reaching a maximum PGV of ~25 cm/s (MMI VII). In Langford and Victoria, the most populous locations in southern Vancouver Island, shallow ruptures generated maximum PGV of ~19 cm/s, corresponding to MMI VI at which structural damage begins to occur.

When the hypocenter was located at the same location as maximum slip, seismic waves radiate away from the hypocenter. Shallow hypocenters (located in the upper 10 km) for Darfield and Haiti-type ruptures created the greatest ground motions and

focused ground motions north towards Vancouver and the Georgia Strait. When the max-slip hypocenter was located deeper (in the lower 15 km of the fault), large ground motions were reduced and focussed towards the north. Ground shaking intensities were on average 1.11 times greater for Darfield-type rupture scenarios (4.84 cm/s; MMI IV) or 1.22 times greater for Haiti-type rupture scenarios (11.03 cm/s; MMI V). When the hypocenter and maximum slip were located at depths greater than 15 km, significant ground intensities measuring MMI VII were still generated at Jordan River and Langford for Haiti-type rupture scenarios.

Rupture directionality relative to slip location was a controlling parameter to the resulting predicted waveforms at the 7 select locations. If the rupture direction was towards a section of greatest slip on the source model and away from a site, the resulting waveform has minimal amplitude. However, if the rupture direction was towards a section of greatest slip between the hypocenter and the site, the resulting waveform at the site is characterized with a large amplitude pulse.

Recent paleoseismic research (e.g., Morell et al., 2017; 2018) suggests the LRVFZ is an active fault zone. It is important to understand how ground motions are likely to interact in high seismic hazard areas. Future DSHAs for the LRVFZ should implement a wider suite of potential rupture scenarios. Stochastic finite-fault modeling, known as EXSIM software (Motazedian and Atkinson, 2005), produces synthetic earthquake waveforms over the frequency range of engineering interest and is less computationally

expensive, so the number of potential rupture scenarios can be significantly increased. As the extent of the LRVFZ fault geometry becomes more defined, more complex and accurate representations of the fault structure can be developed to examine earthquake ground shaking due to LRVFZ ruptures.

3.7 Data and Resources

Slip models for the 2010 Darfield, New Zealand earthquake and the 2010 Haiti earthquake were obtained from the Finite-Source Rupture Model Database at http://equake-rc.info/SRCMOD/searchmodels/allevents/ (last accessed on September 2018). The model used for the Darfield rupture was taken from the FSP file at http://equake-rc.info/SRCMOD/searchmodels/viewmodel/s2010DARFIE01HAYE/ (created on August 21, 2013) and the model for the Haiti rupture was taken from the FSP file at http://equake-rc.info/SRCMOD/searchmodels/viewmodel/s2010HAITIx02HAYE/ (created on August 20, 2013).

3.8 Acknowledgments

Funding provided by Natural Sciences and Engineering Research Council (NSERC) of Canada and Chaucer Syndicates. We thank Dr. Kim Olsen (San Diego State

University) for providing us with a copy of his AWP-ODC software. All figures produced using Mathworks Matlab® software and ESRI ArcGIS.

3.9 References

Aagaard, B.T., R.W. Graves, D.P. Schwartz, D.A. Ponce, and R.W. Graymer (2010a). Ground-motion modeling of Hayward fault scenario earthquakes, Part I: Construction of the suite of scenarios, *Bull. Seismol. Soc. Am.* **100(6)** 2927–2944.

Aagaard, B.T., R.W. Graves, A. Rodgers, T.M. Brocher, R.W. Simpson, D. Dreger, N.A. Petersson, S.C. Larsen, S. Ma, and R.C. Jachens (2010b). Ground-motion modeling of Hayward fault scenario earthquakes, Part II: Simulation of long-period and broadband ground motions, *Bull. Seismol. Soc. Am.* **100(6)** 2945–2977.

Adams, J.A., and S. Halchuk (2003). Fourth generation seismic hazard maps of Canada: Values for over 650 Canadian localities intended for the 2005 National Building Code of Canada, *Geol. Surv. Canada Open-File Rept. 4459*, 155 pp.

Brocher, T.M. (2007). Key elements of regional seismic velocity models for long period ground motion simulations, *J. Seismol.* doi: 10.1007/s10950-007-9061-3.

Brocher, T.M. (2008). Compressional and shear-wave velocity versus depth relations for common rock types in northern California, *Bull. Seismol. Soc. Am.* **98** 950–968.

Calais, E., A. Freed, G. Mattioli, F. Amelung, S. Jónsson, P. Jansma, S.H. Hong, T. Dixon, C. Prépetit, and R. Momplaisir (2010). Transpressional rupture of an unmapped fault during the 2010 Haiti earthquake, *Nature Geoscience* **3** 794–799. doi: 10.1038/NGEO992.

Cerjan, C., D. Kosloff, R. Kosloff, and M. Reshef (1985). Absorbing boundary conditions for acoustic and elastic wave equations, *Bull. Seismol. Soc. Am.* **67** 1529–1540.

Clayton, R., and B. Engquist (1977). Absorbing boundary conditions for acoustic and elastic wave equations, *Bull. Seismol. Soc. Am.* **67** 1529–1540.

Day, S.M. (1998). Efficient simulation of constant Q using coarse-grained memory variables, *Bull. Seismol. Soc. Am.* **88** 1051–1062.

Day, S.M., and C.R. Bradley (2001). Memory-efficient simulation of anelastic wave propagation, *Bull. Seismol. Soc. Am.* **91** 520–531.

Day, S.M., R. Graves, J. Bielak, D. Dreger, S. Larsen, K.B. Olsen, A. Pitarka, and L. Ramirez-Guzman (2008). Model for basin effects on long-period response spectra in Southern California, *Earthquake Spectra* **24(1)** 257-277.

Earthquake Engineering Research Institute (EERI) (2010). The Mw 7.1 Darfield (Canterbury), New Zealand earthquake of September 4, 2010. *EERI Special Report.*

Eberhard, M.O., S. Baldridge, J. Marshall, W. Mooney, and G.J. Rix (2010). The Mw 7.0 Haiti earthquake of January 12, 2010: USGS/EERI advance reconnaissance team report, *U.S. Geological Survey Open-File Report 2010-1048*

Fairchild, L., and D. Cowan (1982). Structure, petrology, and tectonic history of the Leech River complex northwest of Victoria, Vancouver Island, *Can. J. Earth Sci.* **19** 1817–1835. doi: 10.1139/e82-161.

Frankel, A.D., W. Stephenson, and D. Carver (2009). Sedimentary basin effects in Seattle, Washington: Ground-motion observations and 3D simulations, *Bull. Seismol. Soc. Am.* **99** 1579–1611.

Graves, R.W. (1996). Simulating seismic wave propagation in 3D elastic media using staggered-grid finite differences, *Bull. Seismo. Soc. Am.* **86(4)** 1091-1106.

Graves, R.W., and A. Pitarka (2004). Broadband time history simulation using a hybrid approach, in *Proc. 13th World Conference on Earthquake Engineering*, Vancouver, British Columbia, 1–6 August 2004, Paper 1098.

Groome, W.G., D.J. Thorkelson, R.M. Friedman, J.K. Mortensen, N.W.D. Massey, D.D. Marshall, and P.W. Layer (2003). Magmatic and tectonic history of the Leech River Complex, Vancouver Island, British Columbia: Evidence for ridge-trench intersection and accretion of the Cresent Terrane, *Geol. S. Am. S.* **371**, 327-353.

Kukovica, J., S. Molnar, H. Ghofrani, and K. Assatourians (submitted). Probabilistic seismic hazard analysis of Victoria, British Columbia: Considering an active Leech River fault, *Bull. Seis. Soc. Am*.

Levander, A.R. (1988). Fourth-order finite-difference P-SV seismograms, *Geophysics* **53** 1425–1436.

Moczo, P., J. Kristek, and L. Halada (2000). 3D fourth-order staggered-grid finite-difference schemes: Stability and grid dispersion, *Bull. Seismol. Soc. Am.* **90** 587–603.

Molnar, S. (2011). Predicting earthquake ground shaking due to 1D soil layering and 3D basin structure in SW British Columbia, Canada. *Doctoral dissertation*, Victoria, University of Victoria, British Columbia, Canada.

Molnar, S., J.F. Cassidy, K.B. Olsen, S.E. Dosso, and J. He (2014a). Earthquake ground motion and 3D Georgia Basin amplification in southwest British Columbia: Deep Juan de Fuca plate scenario earthquakes, *Bull. Seis. Soc. Am.* **104** 301-320. doi: 10.1785/0120110277.

Molnar, S., J.F. Cassidy, K.B. Olsen, S.E. Dosso, and J. He (2014b). Earthquake ground motion and 3D Georgia Basin amplification in southwest British Columbia: Shallow blind-thrust scenario earthquakes, *Bull. Seis. Soc. Am.* **104** 321-335. doi: 10.1785/0120130116.

Morell, K., C. Regalla, L. Leonard, C. Amos, and V. Levson (2017). Quaternary rupture of a crustal fault beneath Victoria, British Columbia, Canada, *GSA Today* **27** 1-7. doi: 10.1130/GSATG291A.1.

Morell, K., C. Regalla, C. Amos, S. Bennett, L. Leonard, A. Graham, T. Reedy, V. Levson, A. Telka (2018). Holocene surface rupture history of an active forearc fault redefines seismic hazard in southwestern British Columbia, Canada, *Geophysical Research Letters*. doi: 10.1029/2018gl078711.

Motazedian, D., and G.M. Atkinson (2005). Stochastic finite-fault modeling based on a dynamic corner frequency, *Bull. Seismol. Soc. Am.* **95(3)** 995–1010. doi: 10.1785/0120030207.

Olsen, K.B. (1994) Simulation of three-dimensional wave propagation in the Salt Lake Basin, *Ph.D. Thesis*, Salt Lake City, University of Utah, Utah, 157 pp.

Olsen, K.B. (2000). Site amplification in the Los Angeles basin from three dimensional modeling of ground motion, *Bull. Seismol. Soc. Am.* **90** S77–S94.

Olsen, K.B. (2003). Estimation of Q for long-period (>2 sec) waves in the Los Angeles basin, *Bull. Seismol. Soc. Am*. **93** 627–638.

Potter, S.H., J.S. Becker, D.M. Johnston, and K.P. Rossiter (2015). An overview of the impacts of the 2010-2011 Canterbury earthquakes, *Int. J. Disast. Risk. Re.* **14** 6-14. doi: https://doi.org/10.1016/j.ijdrr.2015.01.014.

Sommerville, P., K. Irikura, R. Graves, S. Sawada, D. Wald, N. Abrahamson, Y. Iwasaki, T. Kagawa, N. Smith, and A. Kowada (1999). Characterizing crustal earthquake slip models for the prediction of strong ground motion, *Seis. Res. Lett.* **70** 59-80.

Stephenson, W.J. (2007). Velocity and density models incorporating the Cascadia subduction zone for 3D earthquake ground motion simulations, version 1.3, *U.S. Geol. Surv. Open-File Rept. 2007-1348*, 24 pp.

Ventura, C.E., and A. Bebamzadeh (2016). Executive summary: Citywide seismic vulnerability assessment of the city of Victoria, *VC Structural Dynamics LTD*.

Worden, C.B., M.C. Gerstenberger, D.A. Rhoades, and D.J. Wald (2012). Probabilistic relationships between ground-motion parameters and modified Mercalli intensity in California, *Bull. Seismol. Soc. Am.* **102** 204–221.

Worden, C.B., and D.J. Wald (2016). ShakeMap 3.5 Manual. *United States Geological Survey.* Released: November 22, 2016.

Zaleski, M.P. (2014). Earthquake loss estimates Greater Victoria, British Columbia, *M.Sc. Thesis*, Vancouver, The University of British Columbia, B.C., Canada.

4 Conclusions

4.1 Summary

The LRF runs across the southern tip of Vancouver Island and is just tens of kilometers from key infrastructure. The steep NE projection of the LRVFZ near Greater Victoria suggests an earthquake along the defined fault zone poses a major seismic hazard. The objective of this thesis is to perform PSHAs and DSHAs with the LRVFZ as an active source zone to determine the impact to earthquake shaking in Victoria and at other seismic risk locations across southern Vancouver Island.

In Chapter 2, we performed PSHAs for Victoria by adding the LRVFZ as an active source zone. We found the new fault source zone contributed significantly at high frequencies (≥ 10 Hz). The LRVFZ contributed similarly to interface and crustal sources in four of the eight (scenarios a, c, f, and h) PSHA calculations. For two of our PSHA calculations (scenarios d and g), the LRVFZ was the greatest contributor for the same ≥ 10 Hz frequency range. The LRVFZ contributes the least to the 2,475 year return period UHS when the simulated seismicity is based on magnitude-frequency statistics from shallow (< 10 km depth) earthquakes of the entire Vancouver Island region. The UHS in Victoria for a 2% probability of exceedance in 50 years significantly increased by a maximum of 23% at 10 Hz frequency from 1064.90 cm/s^2 (1.09 g) to 1312.28 cm/s^2 (1.34 g).

Average PGA of 0.63 ± 0.02 g using fault appropriate GMPEs was an increase of 9% when compared to 2015 NBCC PGA of 0.58 g.

In Chapter 3, we performed DSHAs with low frequency (≤ 0.5 Hz) 3D FD simulations of potential large magnitude LRVFZ ruptures. We modified the slip models of the 2010 **M** 7 Darfield and 2010 **M** 7 Haiti earthquakes to create 8 unique slip distribution models. Rupture direction was changed to simulate eastward and westward ruptures. The hypocenter was then moved over top of the point of maximum slip to create a total of 24 different rupture scenarios. The LRVFZ has the potential to create MMI VII ground motions at Jordan River, Langford, and Victoria Airport. Source models with the greatest slip concentrated shallower in the model (≥ 10 km) generate the greatest ground motions for the entire island. When rupture directionality was changed, the highest MMI values were simulated in Jordan River for shallow slip ruptures, averaging MMI VI for the suite of modified Darfield and Haiti scenarios with a maximum MMI VII. For populous cities of Langford and Victoria, shallow ruptures resulted in a maximum predicted MMI VI.

When the hypocenter occurs at the location of maximum slip, the highest MMI values were calculated at Jordan River and Langford from Haiti-type rupture scenarios, averaging MMI VI. For Langford and Victoria, shallow ruptures of Darfield-type ruptures resulted in maximum predicted MMI V for both locations. Haiti-type ruptures

for Langford and Victoria resulted in maximum predicted MMI of VII and VI, respectively.

Based on the studies performed in Chapters 2 and 3, it is important that city planning in southern Vancouver Island, especially in Greater Victoria, considers the LRVFZ as an active source zone due to calculated very strong (MMI VII) ground shaking in locations of higher seismic risk and greater than 11% increases in the 2,475 year return period UHS of the current 2015 NBCC.

4.2 Future Work

Chapter 2 defined new magnitude-recurrence relations and hybrid characteristic distribution functions for the LRVFZ based on paleoseismic **M** > 6 events along the fault (Morell et al., 2017; 2018). Future PSHA works for the LRF and LRVFZ would therefore benefit from continued monitoring and densifying of local seismic networks around the Leech River Valley to further constrain magnitude recurrence rates. Continued paleoseismic studies would be beneficial to further constrain the fault zones' activity rate. Improved identification of the causative fault from trenching would improve maximum magnitude estimates based on fault geometry. Chapter 3 simulated 3D long-period ground motions based on 24 potential **M** ~7 LRVFZ rupture scenarios. Future DSHAs for the LRVFZ would therefore benefit from studies that encompass more potential rupture

scenarios, implement updated physical structure models, and predict motions over a wider frequency range of engineering interest. As the fault geometry becomes more defined, more complex and accurate representations of the fault structure can be modelled to better understand resulting earthquake ground shaking.

4.3 References

Morell, K., C. Regalla, L. Leonard, C. Amos, and V. Levson (2017). Quaternary rupture of a crustal fault beneath Victoria, British Columbia, Canada, *GSA Today*. **27** 1-7, doi: 10.1130/GSATG291A.1.

Morell, K., C. Regalla, C. Amos, S. Bennett, L. Leonard, A. Graham, T. Reedy, V. Levson, and A. Telka (2018). Holocene surface rupture history of an active forearc fault redefines seismic hazard in southwestern British Columbia, Canada, *Geophysical Research Letters*. doi: 10.1029/2018gl078711.

Curriculum Vitae

Name: Jacob Joseph Kukovica

Post-Secondary Education:

The University of Western Ontario (London, Ontario)
M. Sc. – Geophysics Candidate
2016 – 2019

The University of Western Ontario (London, Ontario)
B. Sc.
2011 – 2016

Honors and Awards:

Seismological Society of America (SSA) Annual Meeting
Student Travel Grant (2017)

The University of Western Ontario
Department of Earth Sciences
Geophysics Travel Grant (2017)

The University of Western Ontario
AER Global Opportunities Award in Environment and Sustainability Studies (2015)

Related Work Experience:

Teaching Assistant
The University of Western Ontario
2016 – 2018

Publications:

Refereed Conference Proceedings

Kukovica, J., Molnar, S., Ghofrani, H., and Assatourians, K. (2018). Impact from a nearby seismically-active fault to seismic hazard in Victoria, Canada. *WIT Transactions on Engineering Sciences*, **121** 173-181, doi: 10.2495/RISK180151, which is superseded by Chapter 2 in this thesis.

Conference Presentations with Published Abstract

Kukovica, J., Molnar, S., Ghofrani, H., and Assatourians, K. (2018). Impact from a nearby seismically-active fault to seismic hazard in Victoria, Canada. *The Wessex Institute - 11th International Conference on Risk Analysis and Hazard Mitigation*, Seville, Spain, June 2018, Oral presentation.

Kukovica, J., J., Molnar, S., and Ghofrani, H. (2018) Deterministic seismic hazard analyses of Victoria, British Columbia, Canada: Considering an active Leech River fault., *Seismological Society of America Annual Meeting*, Miami, Florida, May 2018, Poster presentation.

Kukovica, J., J., Molnar, S., Ghofrani, H., and Assatourians, K. (2017) Probabilistic seismic hazard analysis of Victoria, British Columbia, Canada: Considering an active Leech River fault., *American Geophysical Union Fall Meeting*, New Orleans, Louisiana, December 2017, Poster presentation.